CHARACTERIZATION AND IDENTIFICATION OF HUMAN MESENCHYMAL STEM CELLS AT MOLECULAR LEVEL

A THESIS SUBMITTED TO
THE GRADUATE SCHOOL OF NATURAL AND APPLIED SCIENCES
OF
MIDDLE EAST TECHNICAL UNIVERSITY

BY

CEREN AKSOY

IN PARTIAL FULFILLMENT OF THE REQUIREMENTS
FOR
THE DEGREE DOCTOR OF PHILOSOPHY
IN
BIOTECHNOLOGY

MARCH 2012

Approval of the Thesis

CHARACTERIZATION AND IDENTIFICATION OF HUMAN MESENCHYMAL STEM CELLS AT MOLECULAR LEVEL

submitted by **CEREN AKSOY** in partial fulfillment of the requirements for the degree of **Doctor of Philosophy in Biotechnology Department, Middle East Technical University** by,

Prof. Dr. Canan Özgen _____
Dean, Graduate School of **Natural and Applied Sciences**

Prof. Dr. Nesrin Hasırcı _____
Head of Department, **Biotechnology**

Prof. Dr. Feride Severcan _____
Supervisor, **Biological Sciences Dept., METU**

Examining Committee Members:

Prof. Dr. Ufuk Gündüz _____
Biological Sciences Dept., METU

Prof. Dr. Feride Severcan _____
Biological Sciences Dept., METU

Assoc. Prof. Dr. Ayşen Tezcaner _____
Engineering Sciences Dept., METU

Assoc. Prof. Dr. İhsan Gürsel _____
Molecular Biology and Genetic Dept., Bilkent Univ.

Assoc. Prof. Dr. Ayşen Günel Özcan _____
Faculty of Medicine, Hacettepe Univ.

Date: _____

I hereby declare that all information in this document has been obtained and presented in accordance with academic rules and ethical conduct. I also declare that, as required by these rules and conduct, I have fully cited and referenced all material and results that are not original to this work.

Name, Last name: Ceren Aksoy

Signature :

ABSTRACT

CHARACTERIZATION AND IDENTIFICATION OF HUMAN MESENCHYMAL STEM CELLS AT MOLECULAR LEVEL

Aksoy, Ceren

PhD, Department of Biotechnology

Supervisor: Prof. Dr. Feride Severcan

Co-Supervisor: Prof. Dr. Duygu Uçkan Çetinkaya

March 2012, 154 pages

Bone marrow mesenchymal stem cells (BM-MSCs) are pluripotent cells that can differentiate into a variety of non-hematopoietic tissues. They also maintain healthy heamatopoiesis by providing supportive cellular microenvironment into BM. In this thesis, MSCs were characterized in terms of their morphological, immunophenotypical and differentiation properties. Then, they were examined by attenuated total reflection-Fourier transform infrared (ATR-FTIR) spectroscopy together with hierarchical clustering, and FTIR microspectroscopy.

In the first part of this study, global structural and compositional changes in BM-MSCs during beta thallasemia major (β-TM) were investigated. The significant increase in lipid, protein, glycogen and nucleic acid concentrations in thalassemic MSCs with respect to healthy MSCs were attributed to enhanced cell proliferation and BM activity during ineffective erytropoiesis (IE). MTT assay results reflected

increase in cellular activity of thallasemic BM-MSCs. The significant decreases in the concentrations of the mentioned macromolecules after BM transplantation therapy were interpreted as recovery of IE. Based on these changes, sampling groups were successfully discriminated by using cluster analysis.

In the second part of this study, it was aimed to identify new molecular marker(s) in order to determine the effects of donor age on healthy BM-MSCs. The spectral results reflected that there were significant increases in the concentrations of saturated lipids, proteins, glycogen and nucleic acids in children and adolescent group BM-MSCs when compared with the infants, early and mid adults. These results were interpreted as increased proliferation activity in younger BM-MSCs. The results of MTT assay clarified the increased cellular activity. Spectral data of five different sampling groups was discriminated by hierarchical cluster analysis.

The FTIR microspectroscopic imaging study was also performed in two different parts of the study in order to support the ATR-FTIR spectroscopy results. The FTIR microspectroscopic results were found in agreement with ATR-FTIR spectroscopy results.

Key words: Bone marrow mesenchymal stem cells, bone marrow transplantation, beta thalassemia major, donor age effect, attenuated total reflection- Fourier transform infrared (ATR-FTIR) spectroscopy, Fourier transform infrared (FTIR) microspectroscopy.

ÖZ

İNSAN MEZENKİMAL KÖK HÜCRELERİNİN MOLEKÜLER SEVİYEDE KARAKTERİZASYONU VE TANIMLANMASI

Aksoy, Ceren

Doktora, Biyoteknoloji Bölümü

Tez Yürütücüsü: Prof. Dr. Feride Severcan

Ortak Tez Yürütücüsü: Prof. Dr. Duygu Uçkan Çetinkaya

Mart 2012, 154 sayfa

Kemik iliği mezenkimal kök hücreleri (Kİ-MKH) hematopoetik olmayan, çok sayıda farklı doku hücresine farklılaşabilme özelliği olan hücrelerdir. Bu hücreler kemik iliği mikroçevresi için destek görevi görerek sağlıklı bir hematopoezin devamını sağlarlar. Bu tez kapsamında, Kİ-MKH'leri morfolojik, immunofenotipik ve farklılaşma özellikleri bakımından karakterize edilmişlerdir. Daha sonra attenuated total reflectance-Fourier dönüşüm kızılötesi spektroskopisi (ATR-FTIR), kümeleme analizi ve FTIR mikrospektroskopisi yöntemleri ile incelenmişlerdir.

Çalışmanın ilk kısmında, Kİ-MKH'lerinde beta talasemi major hastalığı süresince meydana gelen genel yapısal ve kompozisyonel değişimler araştırılmıştır. Talasemik Kİ-MKH'lerinde sağlıklı Kİ-MKH'lerine göre lipit, protein, glikojen ve nükleik asit konsantrasyonlarında görülen artışlar inefektif eritropoez (IE) süresince artan hücresel aktivite ve Kİ aktivitesi olarak yorumlanmıştır.

Bahsedilen bu makromoleküllerin konsantrasyonları Kİ nakli sonrasında anlamlı olarak azalmıştır. MTT testi ile talasemik hücrelerdeki hücresel aktivite artışı gösterilmiştir. Bu azalış Kİ nakli sonrasında IE'in iyileşmesi olarak yorumlanmıştır. Bu değişimlere göre örneklem grupları kümeleme analizi ile başarılı bir şekilde birbirlerinden ayrılmışlardır.

Çalışmanın ikinci kısmında donor yaşının sağlıklı Kİ-MKH'leri üzerine etkilerini belirleyebilmek için yeni moleküler belirteçlerin bulunması amaçlanmıştır. Spectral sonuçlar, çocuk ve adolesan çağındaki sağlıklı donörlerin Kİ-MKH'lerinde doymuş lipit, protein, glikojen ve nükleik asitlerin kontsantrasyonlarında bebek, erken yaş ve ileri yaş erişkinlerin Kİ-MKH'lerine göre anlamlı artışlar olduğunu göstermiştir. Bu sonuçlar daha genç yaştaki donörlerden alınan hücrelerde artmış hücresel aktivite olarak yorumlanmıştır ve bu sonuç MTT testi ile doğrulanmıştır. Beş farklı yaş grubuna ait Kİ-MKH'lerin spectral verileri kümeleme analizi ile ayrılmıştır.

FTIR mikrospektroskopik görüntüleme deneyleri ile çalışmanın her iki bölümünden elde edilen ATR-FTIR spektroskopisi sonuçları desteklenmiştir. FTIR mikrospekrospi deneylerinin sonuçları ATR-FTIR spektroskopisi ile aynı yönde çıkmıştır.

Anahtar Kelimeler: Kemik iliği mezenkimal kök hücresi, kemik iliği nakli, beta talasemi major, donör yaşı etkisi, attenuated total reflectance-Fourier dönüşüm kızılötesi spektroskopisi (ATR-FTIR), Fourier dönüşüm kızılötesi spektroskopisi (FTIR) mikrospektroskopi.

To my parents Aliye and Mevlüt Aksoy,

ACKNOWLEDGEMENTS

I would like to express my deepest gratitude to my supervisor Prof. Dr. Feride Severcan for her valuable guidance, continued advice and encouragement throughout this study.

I am also grateful to my co-supervisor Prof. Dr. Duygu Uçkan Çetinkaya for her continuous help, suggestions and support in this study.

I would like to extend my thanks to the members of my thesis follow-up committee Assoc. Prof. Dr. Ayşen Tezcaner and Assoc. Prof. Dr. İhsan Gürsel for their constructive contributions during this study.

I wish to send my special thanks to Fatima Aerts Kaya, Sevil Arslan, Emine Kılıç, and Özlem Küçükbayrak in PEDİSTEM Lab. Group for their friendship and their endless support during experimental period.

My special thanks go to my labmates; Şebnem Garip, Özlem Bozkurt, Nihal Şimşek Özek, Sevgi Türker, Seza Ergün, Damla Güldağ, İlke Şen and Ebru Aras. Thank you for sharing all challenges and all good times for many years. I want to express my special thanks to Nusrettin Güleç for his existence and main motivation in the completion of this study.

I would like to give my deepest thanks to my mother Aliye Aksoy for her endless love and numerous sacrifices in my life.

I am grateful to my brother Taylan Aksoy for his friendship and love during all my life. He has always been my best friend and confidant. Thanks goodness for his existence in my life.

TABLE OF CONTENTS

ABSTRACT iv
ÖZ.....vi
ACKNOWLEDGEMENTS.....ix
TABLE OF CONTENTS.....x
LIST OF TABLES.....xvi
LIST OF FIGURES.....xvii
LIST OF ABBREVIATIONS.....xxi
CHAPTERS
1. INTRODUCTION.....1
1.1 What is Stem Cell ?.....1
1.2 Mesenchymal Stem Cells.....2
1.2.1. Characteristics of Mesenchymal Stem Cells.....3
1.2.1.1. Phenotype of Mesenchymal Stem Cells.....4
1.2.1.2. Production of Cytokines and Growth Factors.....5
1.2.1.3. Differentiation Capacity of Mesenchymal Stem Cells.....5
1.3 Clinical Usage of Mesenchymal Stem Cells.....7
1.4 Mesenchymal Stem Cells as a Main Cellular Component of the Bone Marrow Microenvironment and Hematopoiesis.....7
1.5 What is Thalassemia ?.....8
1.5.1 Beta Thalassemia Major.....10
1.5.2 Ineffective Erythropoiesis.....10
1.5.3 Hematopoietic Stem Cell Transplantation Therapy in Beta Thalassemia Major.....11
1.6 HSC and MSC Interactions in Bone Marrow Microenvironment: Stem Cell Niche.....12

1.7 Aging of Stem Cell Niches and Intrinsic Aging of Mesenchymal Stem Cells.....14
1.8 Optical Spectroscopy.....15
1.8.1 Basis of the Spectroscopy.....15
1.8.2 Infrared Spectroscopy.....19
1.8.2.1 The Fourier Transform Infrared Spectroscopy (FTIR)……..21
1.8.2.1.1 Advantages of FTIR Spectroscopy……..22
1.8.2.1.2 Attenuted Total Reflectance Fourier Transform Infrared (ATR-FTIR) Spectroscopy.....24
1.8.2.2 Fourier Transform Infrared Microspectroscopy.....27
1.8.3 Infrared Spectroscopy in Stem Cell Researches.....29
1.9 Aim of the Study.....31
2. MATERIALS AND METHODS 34
2.1 Materials 34
2.1.1 Chemicals.....34
2.1.2 Mesenchymal Stem Cells and Hematopoietic Stem Cells.....34
2.1.2.1 Sampling Groups.....34
2.1.2.1.1 Study 1.....34
2.1.2.1.2 Study 2.....35
2.2 Methods.....35
2.2.1 Cell Culture Experiments.....35
2.2.1.1 Isolation and Cultivation of Mesenchymal Stem Cells from Human Bone Marrow Samples.....35
2.2.1.2 Freezing and Storage of Bone Marrow Mesenchymal Stem Cells.....36
2.2.1.3 Characterization of Bone Marrow Mesenchymal Stem Cells.....37
2.2.1.3.1 Morphological Assessment……...37
2.2.1.3.2 Differentiation Experiments……..37
2.2.1.3.2.1 Adipogenic Differentiation.....37

2.2.1.3.2.1.1 Oil Red O Staining for Adipogenic Differentiation Assessment....38
2.2.1.3.2.2 Osteogenic Differentiation....38
2.2.1.3.2.2.1 Alizerin Red Staining for Osteogenic Differentiation Assessment....39
2.2.1.3.3 Immunophenotyping of Bone Marrow Mesenchymal Stem Cells by Flow Cytometry 39
2.2.1.3.3.1 Cell Surface Marker Staining....39
2.2.1.3.3.2 Flow Cytometry Analysis....40
2.2.1.4 MTT *(Thiazolyl Blue Tetrazolium Bromide)* Proliferation Assay....40
2.2.1.5 Determination of Erythropoietin (EPO) and Growth Differentiation Factor 15 (GDF 15) Levels in Bone Marrow Plasma Samples....41
2.2.1.6 Analysis of Chimerism by Short Tandem Repeat Polymerase Chain Reaction (STR-PCR) 42
2.2.2 Fourier Transform Infrared (FTIR) Spectroscopy and Microspectroscopy Experiments....43
2.2.2.1 Attenuated Total Reflectance (ATR-FTIR) Spectroscopy Study....43
2.2.2.1.1 Sample Preparation....43
2.2.2.1.2 Data Acquisition and Spectroscopic Measurements....43
2.2.2.1.3 Statistical Analysis....46
2.2.2.1.4 Cluster Analysis....46
2.2.2.2 FTIR Microspectroscopic Study....47
2.2.2.2.1 Slide Preparation....47
2.2.2.2.1.1 Deposition and Fixatition of BM-MSCs on Low-e Microscope Slides....47
2.2.2.2.2 Collection of Visible Images and Spectral Maps....49

2.2.2.2.2.1 Selection of Spectral Images and Preprocessing of Spectral Data.....49
3. RESULTS 51
3.1 Harvesting of Mesenchymal Stem Cells from Bone Marrow Samples by Culturing.....51
3.2 Characterization of Human Bone Marrow Mesenchymal Stem Cells.....54
3.2.1 Flow Cytometry Analysis of CD Marker Expression Profile of Bone Marrow Mesenchymal Stem Cells.....54
3.2.2 Differentiation Analysis of Bone Marrow Mesenchymal Stem Cells.....56
3.2.2.1 Adipogenic Differentiation Analysis.....56
3.2.2.2 Osteogenic Differentiation Analysis.....58
3.3 Results of Chimerism Analysis Following Bone Marrow Transplantation.....60
3.4 FTIR Spectroscopy Results……...61
3.4.1 General FTIR Spectrum and Band Assignments of Thalassemic and Healthy Control Bone Marrow Mesenchymal Stem Cells.....62
3.4.2 Comparison of Spectra of Thalassemic and Healthy Control Bone Marrow Mesenchymal Stem Cells.....65
3.4.2.1 General Information about Numerical Comparisons of the Bands of Thalassemic and Healthy Control Bone Marrow Mesenchymal Stem Cells.....68
3.4.2.2 Detailed Spectral Analysis of Thalassemic and Healthy Control Bone Marrow Mesenchymal Stem Cells.....69
3.4.2.2.1 Comparison of Thalassemic and Healthy Control Bone Marrow Mesenchymal Stem Cells in the 3050-2800 cm^{-1} region.....69

3.4.2.2.2 Comparison of Thalassemic and Healthy Control Bone Marrow Mesenchymal Stem Cells in the 1800-800 cm^{-1} region.....72
3.4.2.3 Cluster Analysis……75
3.4.2.4 FTIR Microspectroscopic Analysis and Comparison of Thalassemic and Healthy Control Bone Marrow Mesenchymal Stem Cells...……..80
3.4.3 Comparison of Spectra of Bone Marrow Mesenchymal Stem Cells from Different Age Groups…...…….85
3.4.3.1 General Information about Numerical Comparisons of the Bands of Bone Marrow Mesenchymal Stem Cells from Different Age Groups……...85
3.4.3.2 Detailed Spectral Analysis of Bone Marrow Mesenchymal Stem Cells from Different Age Groups……...……...85
3.4.3.2.1 Comparison of Bone Marrpw Mesenchymal Stem Cells from Different Age Groups in the 3050-2800 cm^{-1} region.....86
3.4.3.2.2 Comparison of Bone Marrow Mesenchymal Stem Cells from Different Age Groups in the 1800-800 cm^{-1} region.....92
3.4.3.3 Cluster Analysis.....97
3.4.3.4 FTIR Microspectroscopic Analysis and Comparison of Bone Marrow Mesenchymal Stem Cellsfrom Different Age Groups.....101
3.5 MTT *(Thiazolyl Blue Tetrazolium Bromide)* Proliferation Assay.....104
3.6 Erythropoietin (EPO) and Growth Differentiation Factor 15 (GDF 15) Levels in Bone Marrow Plasma Samples.....107
4. DISCUSSION 108
4.1 The Effects of Beta Thalassemia Major on Bone Marrow Mesenchymal Stem Cells.....108

4.2 The Effects of Donor Age on Healthy Bone Marrow Mesenchymal Stem Cells.....119
5. CONCLUSION.....127
REFERENCES.....130
APPENDICES
A. CHEMICALS.....150
CURRICULIUM VITAE.....151

LIST OF TABLES

TABLES

Table 2.1 The integrated spectral regions.....50

Table 3.1 General band assignment of human bone marrow mesenchymal stem cells.....64

Table 3.2 Changes in the wavenumber and area vallues of some infrared bands for the healthy control, pre- and post-transplant BM-MSCs.....70

Table 3.3 Changes in the band area values of the infrared bands for control, pre and post transplant BM-MSCs.....71

Table 3.4 Numerical summary of the detailed differences in the lipid-to-protein ratios of control and thalassemic BM-MSCs spectra.....75

Table 3.5 The band area values of healthy BM-MSCs from five different age groups.....88

Table 3.6 MTT proliferation assay results of thalassemic and healthy control BM-MSCs.....106

Table 3.7 MTT proliferation assay results of P3 BM-MSCs obtained from healthy donors of different age groups.....106

LIST OF FIGURES

FIGURES

Figure 1.1 Mesenchymal stem cells.....3
Figure 1.2 The mesengenic process.....6
Figure 1.3 The structure of hemoglobin.....9
Figure 1.4 Electromagnetic wave.....16
Figure 1.5 Energy level diagram illustrating the ground and first excited electronic energy level.....17
Figure 1.6 The Electromagnetic Spectrum.....19
Figure 1.7 The schematic representation of some molecular vibrations.....20
Figure 1.8 Schematic represantation of a Michelson Interferometer.....22
Figure 1.9 ZnSe Diamond ATR attachment of Perkin Elmer Spectrum 100 FTIR Spectrmeter.....25
Figure 1.10 Schematic representation of ATR top plate…….26
Figure 1.11 Perkin Elmer Spectrum Spotlight 400 imaging FTIR microscope.....28
Figure 2.1 Infrared spectrum of air.....44
Figure 2.2 The ATR FTIR spectrum of PBS buffer solution.....45
Figure 2.3 Inverted ligth microscopy images of MSCs were directly grown on silver coated low-e FTIR microscopy slides.....48
Figure 3.1 Photomicrograph of BM-MNCs in culture flask during their expansion phases to obtain P0 MSCs.....52
Figure 3.2 Healthy BM-MSCs at different passages.....53
Figure 3.3 The FSC/SSC parameters of passage 3 BM-MSCs.....55
Figure 3.4 Surface antigen profile of healthy BM-MSCs at passage 3 55
Figure 3.5 Surface antigen profile of thalassemic BM-MSCs at passage 3.....56

Figure 3.6 Oil Red O staining of thalassemic and healthy control BM-MSCs at the end of 21 days.....57
Figure 3.7 Oil Red O staining of healthy P3 BM-MSCs from five different age groups at the end of 21 days.....58
Figure 3.8 Alizerin Red staining of thalassemic and healthy control BM-MSCs at the end of 21 days.....59
Figure 3.9 Alizarin Red staining of healthy P3 BM-MSCs at the end of 21 days..60
Figure 3.10 The representative average spectra of healthy control, pre-transplant and post-transplant group human bone marrow mesenchymal stem cells in the 3800-800 cm^{-1} region.....63
Figure 3.11 The representative infrared spectra of healthy control, pre-transplant and post-transplant group human bone marrow mesenchymal stem cells in the 3050-2800 cm^{-1} region.....66
Figure 3.12 The represantative infrared spectra of healthy control, pre-transplant and post-transplant group human bone marrow mesenchymal stem cells in the 1800-800 cm^{-1} region.....67
Figure 3.13 Hierarchical cluster analysis of healthy control, pre- and post-transplant group MSCs in the 3050-800 cm^{-1} spectral region.....77
Figure 3.14 Hierarchical cluster analysis of healthy control, pre- and post-transplant group MSCs in the 3050-2800 cm^{-1} spectral region.....78
Figure 3.15 Hierarchical cluster analysis of healthy control, pre and post-transplant group MSCs in the 1800-800 cm^{-1} spectral region.....79
Figure 3.16 Spectral image maps of healthy control, pre- and post-transplant MSCs, which were derived from the peak integrated areas of CH_2 antisymmetric stretching band.....81
Figure 3.17 Spectral image maps of healthy control, pre and post transplant MSCs, which were derived from the peak integrated areas of CH_2 symmetric stretching band.....82

Figure 3.18 Spectral image maps of healthy control, pre and post transplant BM-MSCs. A) Chemical maps were derived from the peak integrated areas of amide I and B) chemical maps were derived from the peak integrated areas of amide II band.....83
Figure 3.19 Spectral image maps of healthy control, pre and post transplant MSCs, which were derived from the peak integrated areas of PO_2^- antisymmetric stretching band.....84
Figure 3.20 The represantative infrared spectra of healthy BM-MSCs from five different age groups in the 3800-800 cm^{-1} region.....87
Figure 3.21 The representative infrared spectra of healthy BM-MSCs from five different age groups in the 3000-2800 cm^{-1} region.....89
Figure 3.22 The represantative infrared spectra of of healthy BM-MSCs from five different age groups in the 1800-800 cm^{-1} region.....93
Figure 3.23 Hierarchical cluster analysis performed on the first-derivative and vector normalized spectra of BM-MSCs of infants, children, adolescents, early and mid adults in the 3000-800 cm^{-1} spectral region.....98
Figure 3.24 Hierarchical cluster analysis performed on the first-derivative and vector normalized spectra of BM-MSCs of infants, children, adolescents, early and mid adults in the 3000-2800 cm^{-1} spectral region.....99
Figure 3.25 Hierarchical cluster analysis performed on the first-derivative and vector normalized spectra of BM-MSCs of infants, children, adolescents, early and mid adults in the 1800-800 cm^{-1} spectral region.....100
Figure 3.26 Spectral image maps of BM-MSCs from five different age groups, which were derived from the peak integrated areas of CH_2 antisymmetric stretching band.....101
Figure 3.27 Spectral image maps of BM-MSCs from five different age groups, which were derived from the peak integrated areas of CH_2 symmetric stretching band.....102

Figure 3.28 Spectral image maps of from five different age groups MSCs, which were derived from the peak integrated areas of amide I band.....103
Figure 3.29 Spectral image maps of from five different age groups BM-MSCs, which were derived from the peak integrated areas of amide II.....103
Figure 3.30 Spectral image maps of from five different age groups BM-MSCs, which were derived from the peak integrated areas of PO_2^- antisymmetric stretching band.....104

LIST OF ABBREVIATIONS

ATR-FTIR	Attenuted Total Reflectance Fourier Transform Infrared
BaF_2	Barium Floride
BM	Bone Marrow
BMT	Bone Marrow Transplantation
BM-MSC	Bone Marrow Mesenchymal Stem Cell
β-TM	Beta Thalassemia Major
CaF_2	Calcium Floride
CD	Cluster of differentiation
CO_2	Carbondioxide
DMEM-LG	Dulbecco's modified Eagle's medium – low glucose
DMSO	Dimethyl sulfoxide
DNA	Deoxyribonucleic Acid
dH_2O	Distilled Water
EDTA	Ethylenediaminetetraacetic acid
EPO	Erythropoietin
ELISA	Enzyme Linked-Immunosorbent Assay
ES	Embryonic stem
FACS	Fluorescene-activated cell sorting
FBS	Fetal Bovine Serum
FITC	Fluorescein isothiocyanate
FTIR	Fourier Transform Infrared
GDF15	Growth Differentiation Factor 15
HSC	Hematopoietic Stem Cell
HCL	Hydrocholoric Acid
HSCT	Hemopoietic Stem Cell Transplantation

IE	Ineffective Erythropoiesis
IR	Infrared
MNC	Mononuclear Cell
MSC	Mesenchymal stem cell
N_2	Nitrogen
PBS	Phosphate buffered saline
PCR	Polymerase Chain Reaction
RT	Room Temperature
SC	Stem Cell
SDS	Sodium Dodesyl Sulphate
STR-PCR	Short Tandem Repeat-Polymerase Chain Reaction
ZnSe	Zinc Selenide

CHAPTER 1

INTRODUCTION

1.1. What is Stem Cell?

Stem cells are unique cells with ability to self-renew for a long time and to give rise to different cell types that make up the tissues and organs of the body. The ability to differentiate into different cell types is called as plasticity. Stem cells may be isolated from embryo, umbilical cord and several adult tissues, and differentiation potention of them varies depending on where they originate from (Kelly, 2007; Panno, 2005).

Embryonic stem (ES) cell is obtained from the inner cell mass of the early (4 to 5 days) embryo called as blastocyst (Figure 1.1) (Chung *et al.*, 2008). ES cells are capable of unlimited number of symmetrical divisions without differention, which means they have long-term self-renewal ability (Kirschstein, 2001). When they are cultured in appropriate media and culture conditions, they can be induced to differentiate selectively into more specialized populations. ES cells are pluripotent and they can differentiate into every cell types in the body. Therefore, they are very attrative candidates for wide range of tissue regeneration and cellular therapies in regenerative medicine (Ami *et al.,* 2008). To date, there has been some success in inducing mouse ES cells to form particular types of cells, such as cardiomyocytes, smooth muscle cells, neuron cells, and hepatocytes (Thumanu *et al.,* 2011).

Adult stem cells are multipotent cells found in a differentiated tissues and organs. They can renew themselves for a long periods of time by making identical copies and they can differentiate into all of the specialized cell types of the tissues from which they originate (Kirschstein, 2001). They exist in various tissues such as blood, bone marrow, cord blood, kidney, adipose tissue, teeth. Adult stem cells are important for homeostatis by keeping the number of stem cells constant and for self renewal of tissues during cellular aging and diseases (Orlic *et al.,* 1999; Perkins, 1998). Adult stem cells can arise from any organ or tissue including hematopoietic or mesenchymal tissues; thus called as hematopoietic stem cells (HSCs) or mesenchymal stem cell (MSC), respectively. HSCs, are obtained from bone marrow, periferal blood, umbical blood, generate all types of blood cells by the process called as hematopoiesis. Another population of adult stem cells is called as mesenchymal stem cells, which can be isolated from many types of tissues and also can be differentiated into mesenchym originated tissues such as adipose tissue, bone tissue and cartilage tissue.

1.2. Mesenchymal Stem Cells

The notion of the mesenchymal stem cells (MSCs) was suggested by Maureen Owen by considering the first experimantal findings about fibroblast-like colony forming cells of bone marrow of Alexander Friendestein and his colleagues in mid 60's. In early 1990's Arnold Caplan proposed that MSCs were fibroblast like adherent cells (Figure 1.1) isolated by fractionation on a density gradient solution ficoll. Especially, in last two decades there was an increasing interest on MSCs studies from different research groups that they were trying to clarify MSCs characteristics to accelerate basic scientific investigations and for further clinical studies of MSCs. In 2000, a report was published by International Society for Cellular Theraphy (ISCT) to define scientifically accurate MSCs identity mainly for laboratory based research purposes by universially accepted standarts.

According to ISCT recommendations; MSCs have to be adherent to plastic surfaces when cultivated in appropriate complete media, they must express CD73, CD90 and CD105 surface antigens while they lack expression of CD34, CD45 and finally they have to have capacity differentiate to osteaoblast, adipocytes and chondroblasts using specific in-vitro inducing media (Horwitz *et al.,* 2005; Dominici *et al.,* 2006).

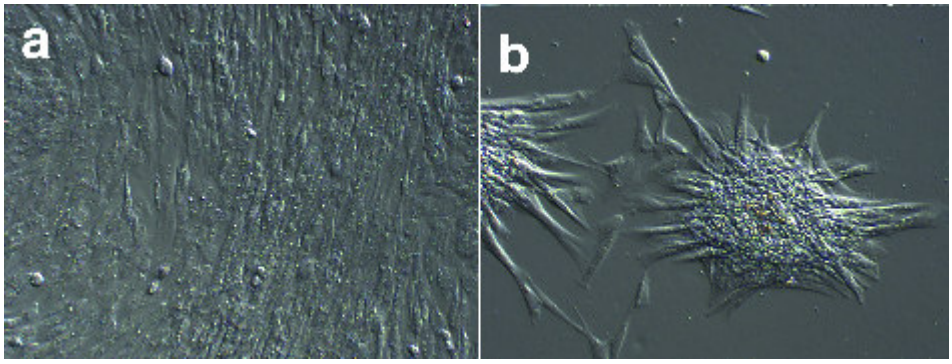

Figure 1.1 Mesenchymal stem cells. "**a)** Monolayer of rapidly expanding adherent spindle-shaped fibroblastoid cells compatible with undifferentiated mesenchymal stem cells (×100) **b)** Cell cluster of rapidly expanding adherent spindle-shaped fibroblastoid cells compatible with undifferentiated mesenchymal stem cell morphology (×100)" (Adopted from Koch *et al.,* 2007 with permission).

1.2.1. Characteristics of Mesenchymal Stem Cells

MSCs which are non-hematopoietic, stromal cells found primarily in bone marrow stroma and other to many human tissues (Jackson *et al., 2007*). MSCs of the bone marrow (BM) provide cellular microenvironment to support maintanance of hematopoietic stem cells's growth and differentiation (Jackson *et al.*, 2007; Kemp

et al., 2005). BM can be collected from posterior iliac crests of pelvis and then mononuclear cells (MNCs) are harvested from BM with a density gradient isolation procedure with ficoll (Pittenger *et al.,* 1999). A small fraction of (0,01-0,0001 %) isolated MNCs adhere to the plastic surfaces in culture and expand as fibroblast like cells that are considered as the primary ex-vivo source of mesenchymal progenitor cells (Pittenger *et al.*, 1999; Minguell *et al.*, 2001; Jackson *et al.,* 2007).

1.2.1.1. Phenotype of Mesenchymal Stem Cells

There is a considerable interest on definition of MSC phenotype to be able to accomplish characterization, purification and further analysis of MSCs. Recent studies has shown the availibility of an expression of several cell surface antigens and monoclonal antibodies in BM-MSCs (Aerts, 2004; Dennis and Caplan, 2004). Human MSCs don't express main hematopoietic antigens called as CD14, CD34 and CD45 (Baksh *et al.,* 2004). The monoclonal antibodies SH2, SH3 and SH4 are raised against human MSCs (Barry, 2003). SH2 antibody binds an epitope on endoglin (CD105, a receptor for tranforming growth factor βI and βIII). SH3 and SH4 antibodies recognize different region of antigenic epitopes on the membrane bound ecto-5-nucleotidase that known as CD73 surface antigen expressed by MSCs. The SB10 antibody reacts with activated leukocyte-cell adhesion molecule (ALCAM; CD166). The monoclonal antibody Stro1 is specific for clonogenic BM stem cell progenitors in human bone marrow. In order to characterize phenotype of MSCs and to enrich MSCs from mixed cell population, the combination of antibodies have to be used (Aerts, 2004; Kemp *et al.,* 2005). MSCs also express cell adhesion molecules like ICAM-1, integrin α4, α5 and β1, αvβ3 and αvβ5 and CD44H. MSCs express extracellular matrix molecules such as collagen fibronectin, laminin, and proteoglycans which clarify and strengthen the

suggestion about an important and dynamic role of MSCs in the BM during development of stromal marrow microenvironment. The several counter receptors required for cell-matrix and cell-to-cell direct interactions are also expressed by MSCs (Minguell *et al.*, 2001).

1.2.1.2. Production of Cytokines and Growth Factors

MSCs, which have capabilities of self-renewal and differentiation into different lineages of mesenchym tissues, need secretion and regulation of specific growth factors, cytokines and chemokines in a lineage or stage specific manner (Dormady *et al.*, 2001). The variability of secretion profile of MSCs provide therapeutic effects of them (Zhukareva *et al.*, 2010). BM-MSCs produce an extended profile of growth factors and cytokines, which have significant role in the regulation of hematopoiesis (Majumdar *et al.*, 2000). Primary stromal cell cultures or in stromal cell lines secrete Granulocyte-Colony Stimulating Factor (G-CSF), GM-CSF, M-CSF, Interleukin-1 (IL-1), IL-3, IL-6, IL-7, IL-8, IL-11, IL-12, IL-14, IL-15, LIF, fibroblast growth factor (FGF), stem cell factor (SCF), Flt-3 ligand (FL), and tumor necrosis factor (TNF) (Dormady *et al.*, 2001; Majumdar *et al.*, 1998; Harneysworth *et al.*, 1996; Thalmeier *et al.*, 1996).

1.2.1.3. Differentiation Capacity of Mesenchymal Stem Cells

Differentiation ability of bone marrow mesenchymal stem cells into osteocytes was firstly discovered by Friedenstein *et al.*, 1966. Then Pittenger *et al.*, 1999 mentioned about differentiation potential of human mesenchymal stem cells into lineages of mesenchymal tissues, like bone, cartilage, fat, tendon, muscle and marrow stroma. However; recent studies have shown that bone marrow mesenchymal stem cells (BM-MSCs) have multilineage differentiation capacity with their differentiation into mesodermal and non-mesodermal cell lineages (Yan

et al., 2010). As it is seen in Figure 1.2, BM-MSCs can differentiate into not only osteocytes, adipocytes, chondrocytes but also myocytes, cardiomyocytes, fibroblasts myofibroblasts, epithelial cells and neurons (Liu *et al.*, 2009). Miyogenic differentiation of MSCs was determined by myotube formation (Beier *et al.*, 2010; Yan *et al.*, 2010) and induction and differentiation of BMMSCs into cardiomyocyte-like cells. The in-vitro differentiation of BM-MSCs into neuron-like cells was explained by not only expression of neuron phenotype and membrane channel protein including Nav1.6, Kv1.2, Kv1.3 and Cav1.2 but also exhibited functional ion currents (Zeng *et al.*, 2011). BM-MSCs have also capacity to differentiate into renal (Asanuma *et al.*, 2010) of kidney and also hepatic cells of liver (Mohsin *et al.*, 2011).

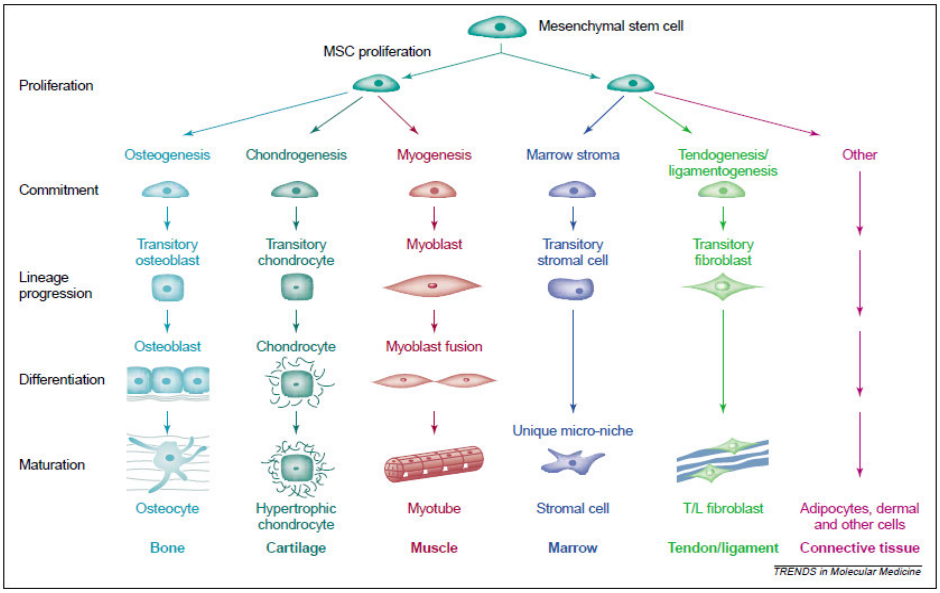

Figure 1.2 "The mesengenic process. The stepwise cellular transition from the putative mesenchymal stem cell (MSC) to highly differentiated phenotypes are depicted schematically" (Adopted from Caplan, 2009 with permission).

1.3. Clinical Usage of Mesenchymal Stem Cells

Human MSCs with their multilineage differentiation ability and self renewal capacity have great potential as a source of cells for cellular therapies in regenerative medicine and for tissue engineering approaches (Baksh *et al.*, 2004). Autologous or allogenic stem cells may be transplanted into patients during stem cell therapy, therefore; the use of MSCs in clinical applications requires standardization and quality control of each step from isolation to transplantation (Wagner *et al.*, 2010). BM-MSCs provide housing for HSCs and enhance their engraftment after HSC transplantation (Lazarus *et al.*, 2005) which has been used for some years in the treatment of leukemia and other cancers (Tabbara *et al.*, 2002). MSCs carry the potential for use in treatment of injury in different diseases including cardiovascular repair, coronary artery disease (Stamm *et al.*, 2003), treatment of lung fibrosis, spinal cord injury and bone and cartilage repair (Barry, 2003). Implemantation of stem cells with the ability to differentiate into neurons and neural stem cells in an adult rat model of spinal cord injury resulted in long-term functional healing (Teng *et al.,* 2002). It was shown in rat models that MSCs may be useful in the treatment of stroke, traumatic injury and Parkinson's Disease. MSCs can also be used in the area of orthopedic medicine for the repair of segmental bone defects (Quarto *et al.*, 2001) and craniotomy defects (Krebsbach *et al.,* 1998), and for repair of focal defects in articular cartilage (Ponticiello *et al.*, 2002) and tendon (Young *et al.*, 1998).

1.4. Mesenchymal Stem Cells as a Main Cellular Component of the Bone Marrow Microenvironment and Hematopoiesis

The bone marrow microenvironment contains both mesenchymal and hematopoietic stem cells. This microenvironment is the main site of hematopoiesis during the development of any types of blood cells (Gordon, 2010). The other cell

types such as osteoblasts, adipocytes and endothelial cells have an important roles throughout the regulation of normal and malignant mechanisms in hematopoiesis (Walkley, 2011). “It has been well established that some hematopoietic diseases can dramatically affect the composition or function of certain cell types of the BM microenvironment, and that this in turn may further contribute to the severity of the hematopoietic disease” (Askmyr *et al.*, 2011). “Thalassemia represents an extreme example of chronic anemia associated with changes in the bone marrow microenvironment” (Walkley, 2011).

1.5. What is Thalassemia?

Thalassemia is an inherited blood disorder. The defect in the globin gene causes unsufficient production of hemoglobin molecule that leads to anemia as a result of excessive destruction of red blood cells. Hemoglobin which is an oxygen carrying, tetrameric, globular protein composed of four globin chains. The most well known adult hemoglobin molecule is called as Hemoglobin A consisting of 2β and 2α globin chains (Figure 1.3). Thalassemia results from a genetic mutation in alpha or beta globin molecule that causes non or reduced production of mutated globin chain while unmutated globin chain accumulates in red blood cells (Lanzkowsky, 2000).

Thalassemias are characterized according to type of deficient globin chain. The missing or mutated alpha genes related with the absence or reduced synthesis of alpha (α) globin protein that give the name to the disease as alpha thalassemia. If similar genetic defect affects the genes of beta (β) globin protein, the disease is called as beta thalassemia (Mader, 1997). Alpha thalassemias are observed commonly in people from South Asia, Malaysia, and Southern China, while beta thalassemias generally are seen in people from Mediterranean origin, Africa and

other Asia countries. Thalassemia has been started to be seen since ten years in America, because of the huge migration potential of America (Loukopoulos *et al.*, 1991).

The severity of disease is defined according to the number of mutated genes in globin protein. If inherited defective gene(s) comes from both mother and father, the disease called as thalassemia major. However, thalassemia minor occurs when the defective gene(s) comes from only one parent. People who have thalassemia minor become a carrier of the disease, however they usually do not have disease symptoms (Lanzkowsky, 2000).

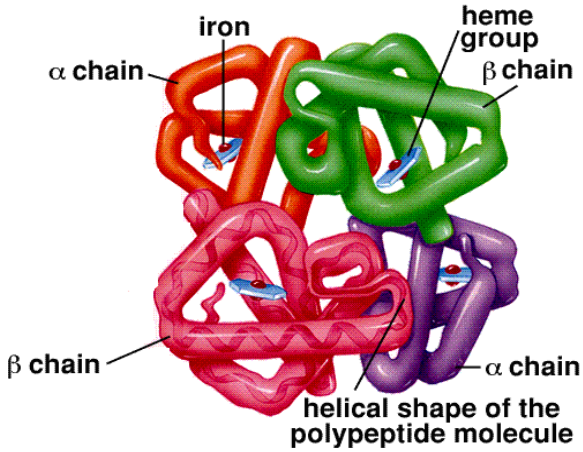

Figure 1.3 The structure of hemoglobin (Adopted from Mader, 1997 with permission).

1.5.1. Beta Thalassemia Major

Beta thalassemia is an autosomal recessive blood disease with diminished production of hemoglobin that leads to hemolytic anemia. In order to make sufficient beta globin chains, two genes are required. If one or both of these genes are mutated beta thalassemia occurs. The severity of beta thalassemia and resulting anemia depends on the number of genes that are affected from mutations. If one gene is abnormal, the disease is known as beta thalassemia trait that is associated with reduced beta globin chain which does not cause great problem in the normal functioning of hemoglobin molecule. When two genes are mutated the more severe form of beta thalassemia which is called as beta thalassemia major (β-TM) or Cooley's anemia are seen. The severe decrease or complete lack of beta globin synthesis prevents the production of Hemoglobin A that causes life-threatening anemia after three months of age. Survival of patients with this severe anemia depends on lifelong regular blood transfusions that lead iron accumulation in vital organs of the body such as liver and heart (Olivieri, 1999; Lanzkowsky, 2000; Birgens and Ljung, 2007).

1.5.2. Ineffective Erythropoiesis

The inbalanced synthesis of β-globin chains leads to accumulation of excess α-globin chains in red blood cells. The aggregation of α-globin chains produces precipitates that cause cell hemolysis by destroying red cell membranes and results with destruction of erythroid precursors in bone marrow termed. This is called as ineffective erythropoiesis (IE). In thalassemia, IE is characterized by apoptosis and limited differentiation of erythroid cells. Overall erythropoiesis in BM and spleen increases impressively during ineffective erythropoiesis conditions. However, such an increased erythropoietic activity can not prevent intramedullary and intrasplenic

death of erythroid precursors. This condition is often coupled with a dramatic expansion of the bone marrow to get rid of exarcerbation of deep anemia and iron accumulation (Melchiori *et al.*, 2010). Changes of oxygen tension occur in tissues due to anemia which is associated with a rise in erythropoietin (EPO) level in order to compansate for anemia. EPO serves as the main regulator of all stages of erythroid differentiation, proliferation, and maturation during profound anemia (Fang *et al.*, 2007). Increased EPO levels drive an uncontrolled expansion of erythroid precursors with an enhanced proliferative and survival capacity. However, these cells fail to differentiate into mature red blood cells, therefore severe anemia can not be ameliorated by excess production of erythroid precursors in bone marrow which leads ineffective erythropoiesis (Libani *et al.*, 2008). GDF15 is a protein of transforming growth factor-β (TGF-β) superfamily which is involved in several processes like cell differentiation, development and apoptosis (Whitman *et al.*, 1998). Since the expression of GDF15 is generally associated with apoptosis, serum GDF15 levels increases in many types of hematological diseases associated with ineffective erythropoiesis such as thalassemia (Tanno *et al.*, 2010). Imbalance in the production of α- and β-globin chains cause apoptosis of erythroblasts during which severe ineffective erythropoiesis and extreme bone marrow expansion are combined as a result of anemia (Schrier *et al.*, 2002). Meanwhile, GDF15 is overexpressed and secreted from erythroblast as a member of bone morphogenic protein family, also contributes to the severe bone abnormalities of thalassemia. Therefore, elevated GDF15 levels in serums of β-thalassemia patients is used as a biomarker of the disease (Tanno *et al.*, 2007).

1.5.3. Hematopoietic Stem Cell Transplantation Therapy in Beta Thalassemia Major

The standard blood transfusion therapy in order to sustain life of thalassemic patients causes development of splenomegaly and also dramatic iron overload in

tissues. Excessive iron accumulates in vital organs like liver, heart, endocrine glands. Therefore; iron overload is one of the major reason of death in thalassemia patients. (Melchiori *et al.*, 2010). In order to improve the quality of life of thalassemic patients and to prevent undesired effects of iron accumulation, iron chelation therapies are applied. Aggressive blood transfusions and iron chelation are expensive and life-long therapies with significant morbidity Allogeneic hematopoietic stem cell transplantation (HSCT) from an HLA-compatible family donor has been accepted as the most effective therapy of thalassemia major since 30 years (Aggarwal *et al.*, 2003). HSCT in thalassemia major replaces IE with an effective allogeneic hematopoietic cell substitute to obtain permanent, effective healing of the hemolytic anemia (Angelucci and Baronciani, 2008)

Chimerism analysis after bone marrow transplantation (BMT) is used to determine genotypic origin of bone marrow cells. It has been shown that full donor chimerism is usually achieved in hematopoetic cells after transplantation. However, BM-MSCs remain of host origin post-transplant (Rieger *et al*., 2009; Bartsch *et al.,* 2005) The normal MSC content of bone marrow is about 0.01 to 0.05% of mononuclear cells (Minguell *et al.*, 2001). The limited MSCs content of bone marrow could explain why after bone marrow transplantation, MSC of donor origin could not be detected.

1.6. HSC and MSC Interactions in Bone Marrow Microenvironment: Stem Cell Niche

Stem cells (SCs) are located in highly regulated, complex and multifactorial microenvironment defined as niche. A stem cell niche is required for the maintenance of balance between self-renewal and differentiation. There is constant dialog between SCs, non-SCs, an extra cellular matrix and molecular signals in the niche to control stimuli for differentiation and self-renewal (Becerra *et al.*, 2011;

Mitsiadis *et al.*, 2007). The control and regulation of SCs and interactions with their niche are important in terms of cell therapy and regenerative medicine for gaining of basic understanding of stem cell applications into clinical medicine (Becerra *et al.*, 2011).

Hematopoietic stem cells are localized in two different niches in the bone marrow. The locations are called as an "endosteal niche" and a "perivascular niche" (Mitsiadis *et al.*, 2007). Interaction between HSCs and their niches provide maintanance and balance for their differentiation, self-renewal and quiescence. Therefore, the location of HSCs are determined according to the their lineages and hierarchical positioning. While undifferentiated HSCs are mainly found in the endosteal region, hematopoietic progenitors are generally located in central (vascular) bone marrow regions (Kiel and Morrison, 2006).

Hematopoietic stem cell transplantation has gained great importance for the treatment of hematologic malignancies and non-malignant disorders. Several research groups have focused on ex vivo expansion of HSCs in order to improve the clinical outcome of autologous and allogeneic HSC transplantation (Jing *et al.*, 2010). In this context, understanding of factors contributing the maintanace of HSCs in their niches has been recently investigated and the existing studies showed that MSCs facilitate HSCs maintenance through the secretion of soluble factors and cell-cell contact (Wagner *et al.*, 2007). Therefore; investigation of interactions between HSCs with MSCs will provide an information in order to understand in-vivo regulation of hematopoietic stem cells and to design stem cell based cellular therapies (Purton and Scadden, 2011).

1.7. Aging of Stem Cell Niches and Intrinsic Aging of Mesenchymal Stem Cells

Adult stem cells in specific organ systems are required for the maintenance and repair of these organs throughout adult life. This funcion of stem cells is regulated by molecular signaling to ensure proper cellular, tissue and organ homeostasis, but how this coordination changes with aging is mostly unknown (Drummond-Barbosa, 2008). The reciprocal interactions between stem cell aging on tissue homeostasis and aged cellular microenvironment on stem cells will be critical to the success of any therapeutic application of stem cells in the emerging field of regenerative medicine (Rando, 2006; Drummond-Barbosa, 2008; Greco and Rameshwar, 2008).

The process of MSC aging is important because of their role in tissue regeneration and repair. For the success of clinical application and for desired therapeutic outcome, the impact of aging on stem cells have to be understood (Wilson *et al.*, 2010). Existing studies have focused on the effect of aging on the differentiation ability or the changes in the number of MSCs. Some, but not all studies showed that aging reduces osteogenesis, chondrogenesis and adipogenesis (Moerman *et al.*, 2004; Zheng *et al.*, 2007; Tokalov *et al.*, 2007) and they also showed decreases in the number of MSCs in the bone marrows of rodents, monkeys and humans. Recent studies in the literature observed that MSCs of older donors showed decreased proliferation potential and increased senescence when compared with the cells of younger donors (Vacek, 2000; Stenderup *et al.*, 2003; Baxter *et al.*, 2004; Mareschi *et al.*, 2006).

Recent studies suggested that aging can be related with decrease in the number and function of stem cells. However, causal relationships is largely unknown. In other words, there are some questions to be answered; does aging lead to decline in stem

cell number or does stem cell decline lead to aging? Despite available information, little is known about how and why MSCs age in vivo. The effects of donor age in regenerative medicine and in-vivo use for damage healing has not been investigated well. It is thougth that donor age can be effective parameter to obtain most efficient recovery. Stem cells can differentiate into many different cell types and the determining of molecular changes depending on the donor age in the stem cells have great importance in terms of regenerative medicine to select donor for therapeutic purposes. These recent knowledge will contribute development of in vitro conditions for stem cell based clinical applications. Characterization of interactions of cellular, biochemical and molecular interactions between MSCs and their microenvironment will contribute to understand in vitro control of them.

1.8. Optical Spectroscopy

1.8.1. Basis of the Spectroscopy

A spatially-varying electric field generates time-varying magnetic field which oscillate mutually perpendicular in a single plane to form electromagnetic radiation. Figure 1.4 shows these fields as a sine wave with their direction of propagation (Stuart, 1997).

The interaction between electromagnetic radiation and matter redirect radiation between energy levels of the atoms or molecules. This interaction can be in various manners like absorbtion, scattering, reflection, emission etc. When the light is absorbed, chemical bonds vibrate and intermolecular distance of two or more atoms changes. This is called as vibrational energy which is resulted from excitation of an atom to an upper energy level in accordance with the wavelength of the light (Freifelder, 1982). An excited atom or molecule can have any one of a set of unique amounts of energy which are called as the energy levels of the

molecule. The energy levels are usually described by an energy level diagram shown in Figure 1.5.

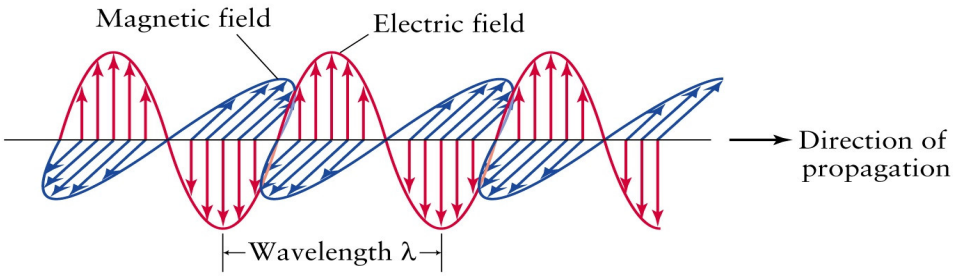

Figure 1.4 Electromagnetic wave

The total energy of a molecule is composed of several distinct reservoirs of energy as it is given by the following equation (Campbell and Dwek, 1984).

$$E_{total}=E_{translation}+E_{rotation}+E_{vibration}+E_{electronic}+E_{electronicspinorientation}+E_{nuclearspin\ orientation}$$

In this equation, each E that is represented by its subscript reflects the appropriate energy level. The separations between the neighboring energy levels corresponding to $E_{rotation}$, $E_{vibration}$ and $E_{electronic}$ are associated with the microwave, infrared and ultraviolet-visible regions of the electromagnetic spectrum, respectively (Campbell and Dwek, 1984).

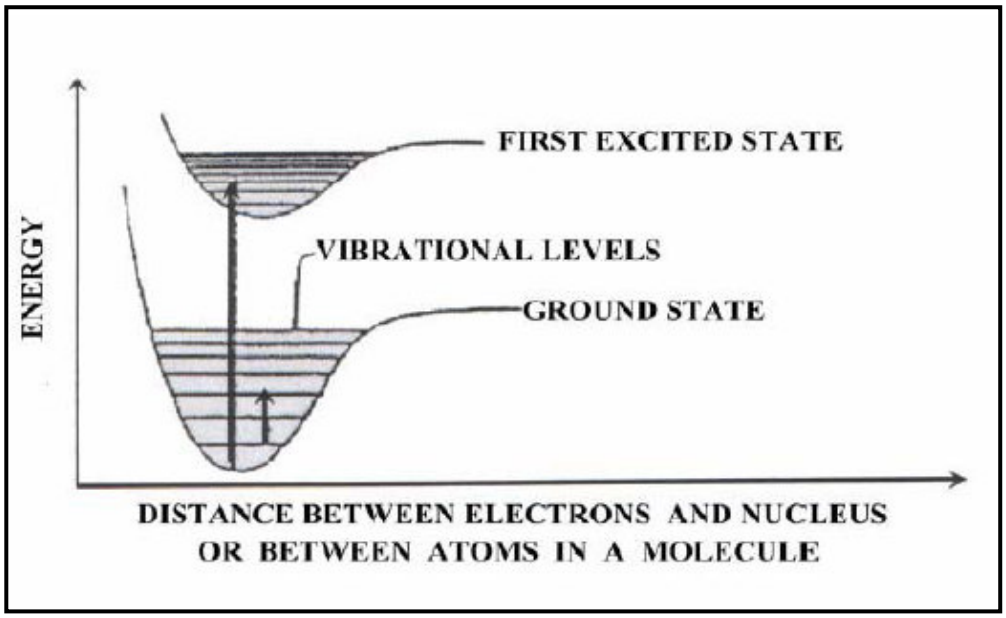

Figure 1.5 "Energy level diagram illustrating the ground and first excited electronic energy level. Vibrational energy levels are represented as parallel lines superimposed on the electronic levels. The long arrows show a possible electronic transition from the ground state to the first excited state while the short arrow represents a vibrational transition within the ground electronic state" (Freifelder, 1982).

When the specific vibration with an equal frequency of IR radiation moves on the molecule, the molecule absorbs the energy of radiation by transitions induced between different energy states of the molecules in the sample. Absorption is most probable when the energy level separation matches the energy of the incident radiation as indicated below,

$$\Delta E = h\nu$$

where ΔE is the dispertion between the energy states of sample, ν is the frequency of the applied radiation and h is Planck's constant ($h = 6.6 \times 10^{-34}$ joule second),

$$c = \lambda \nu$$

c is the speed ($3.0x10^8$ ms^{-1}) and λ is the wavelength of light. From these two equations we can derive wavenumber, which is presented by ν, reciprocal with the wavelength (λ). Wavenumber means the number of waves per unit length, so it is directly proportional to frequency, as well as the energy of the IR absorption. Wavenumber is defined as in the below interconvertion;

$$\overline{\nu} = \text{wavenumber} = (1/\lambda) \text{ [has a unit of } cm^{-1}]$$

Thus, IR absorption positions are shown with wavenumbers ($\overline{\nu}$) or wavelengths (λ). In contrast, wavelengths are inversely proportional to frequencies and their associated energy.

$$E = h\nu = h\,c\,(1/\lambda) = hc\overline{\nu},$$

The study of interaction of electromagnetic radiation with matter is called as spectroscopy. Spectrum is defined by a plot of the energy absorbed (E =hν) as a function of wavelength or more commonly frequency. The electromagnetic spectrum ranges from the shorter wavelengths (including gamma and x-rays) to the longer wavelengths (including microwaves and broadcast radio waves) (Figure 1.6). Light can interact with sample with some form of electromagnetic radiation like scattering, absorption, or emission. The determination of radiation in terms of some measured parameters and the interpretation of these measured parameters generates the basis of spectroscopic techniques.

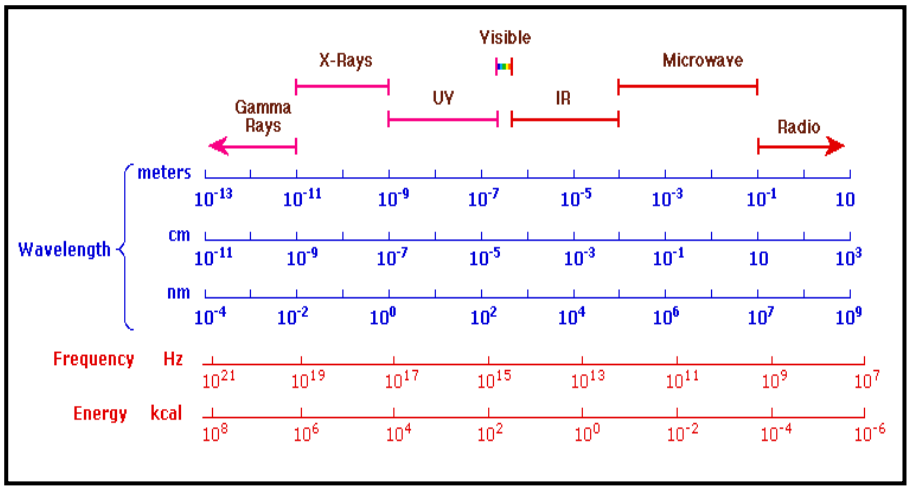

Figure 1.6 The Electromagnetic Spectrum

1.8.2. Infrared Spectroscopy

The region between 14.000 cm^{-1} and 4 cm^{-1} of the electromagnetic spectrum is called as infrared region which is divided three sub-regions as near-infrared region (14.000 cm^{-1} to 4.000 cm^{-1}), mid-infrared region (4.000 cm^{-1} to 400 cm^{-1}) and far-infrared region (400 cm^{-1} to 4 cm^{-1}). The infrared applications related with biological samples use mid infrared region of the electromagnetic spectrum. The IR spectroscopy works on the basis of determination of the chemical functional groups in the sample according to their unique absorbtion charactheristics. Therefore, the infrared spectrum can be used as a fingerprint for identification of unknown molecule by comparing it with known reference spectra (Hsu, 1997).

The molecular atoms oscillate constantly around average positions. The chemical bonds and the intramolecular distance between two or more atoms changes when the IR radiation is absorbed by the molecule. When the change in the dipole

moment, which occurs during charge separation across the bond, is accompanied by the vibration, the molecule can absorb IR radiation. The oscillations of the atoms can be defined in terms of two types of molecular vibrations as stretching and bending. Stretching is a symmetric or antisymmetric rhythmical movement along the bond axis. The bending vibration occurs when the bond angle change. These motions are also called as scissoring, wagging, rocking, and twisting (Figure 1.7).

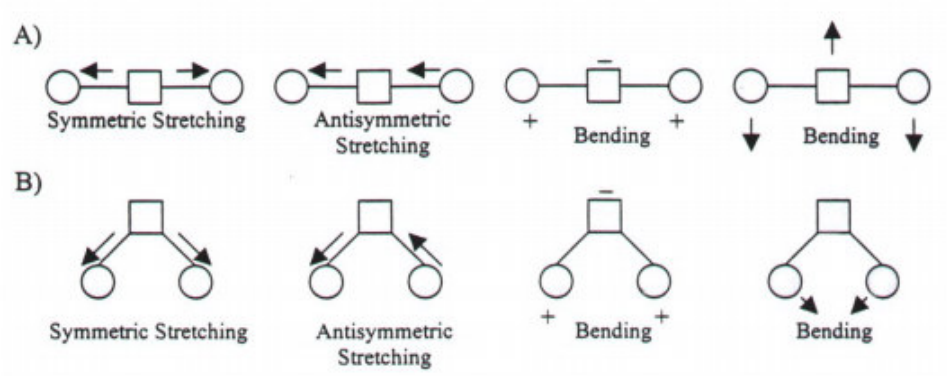

Figure 1.7 "The schematic representation of some molecular vibrations in linear triatomic molecules (A) and non-linear triatomic molecules (B). (+) and (–) symbols represent atomic displacement out of page plane" (Arrondo et al., 1993).

The infrared spectroscopy is a useful chemical analytical method, because each different material has a unique chemical structure and therefore each molecule has a different wavenumber which is correlated with its chemical structure. This means that two compounds create different infrared spectrum like their chemical fingerprints. This makes infrared spectroscopy available for identification of

unknown materials, determination of quality or consistency of a sample and determination of the amount of components in a mixture, ect.

1.8.2.1. The Fourier Transform Infrared Spectroscopy (FTIR)

Fourier transform infrared (FTIR) spectroscopy has found increasing interest by the invention of Michelson interferometer (Figure 1.8) since early eighties. Michelson interferometer produces an interferogram by spliting an electromagnetic radiation between two directions and then by recombining the intensity variation which can be determined as a function of the path difference between them. The interferometer contains two orthogonal mirrors: one movable and the other fixed. The light passes through a beam splitter, which sends the light in two directions at right angles. One beam goes to a stationary mirror then back to the beam splitter. The other beam goes to a moving mirror. The motion of the mirror makes the total path length variable versus that taken by the stationary-mirror beam. When the two meet up again at the beam splitter, they recombine, and the difference in path length creates constructive and destructive interference, which is called as an interferogram. The recombined beam passes through the sample. The sample absorbs all the different wavelength characteristics of its spectrum. The detector now reports variation in energy absorbed or transmitted versus time for all wavelengths simultaneously. A laser beam is superimposed to provide a reference for the instrument operation.

Energy versus time is an odd way to record a spectrum until it is recognized the relationship between time and frequency was recognized: they are reciprocal. A mathematical function called Fourier transform allows us to convert an intensity-versus-time spectrum into an intensity-versus-frequency spectrum. The spectrometer computer is able to deconvolute (Fourier Transform) all the

individual cosine waves that contribute to the interferogram and so produce a plot of intensity against wavelength (cm^{-1}), or more usually frequency (cm^{-1}).

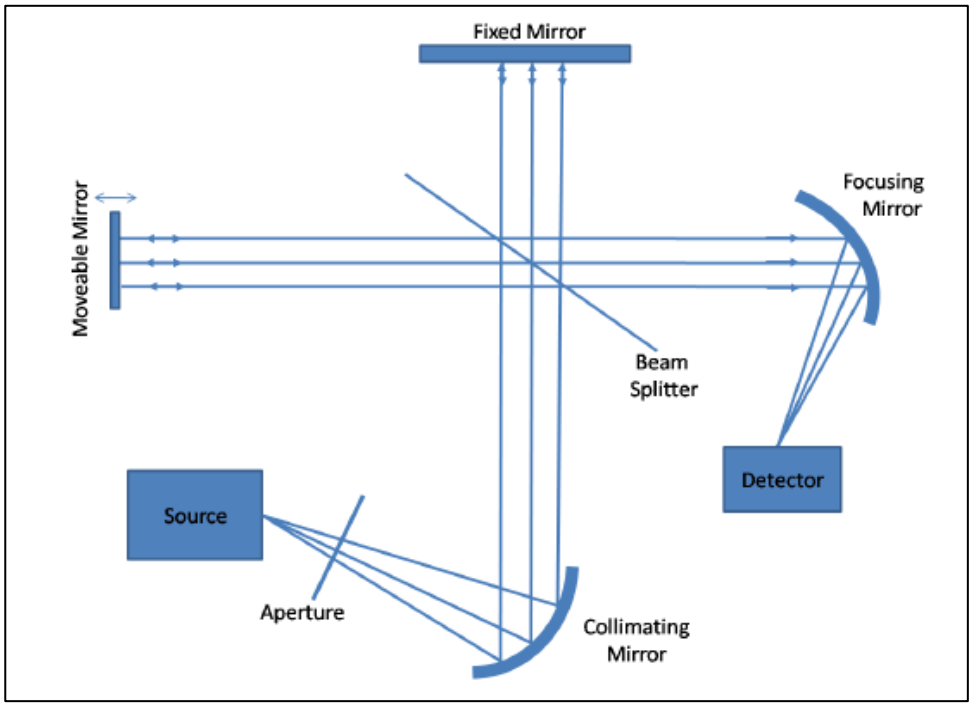

Figure 1.8 Schematic representation of a Michelson Interferometer.

1.8.2.1.1. Advantages of FTIR Spectroscopy

- It is rapid and sensitive technique which enables to make measurements within seconds and reduce the noise levels (Hsu, 1997).

- FTIR spectrometers are self-calibrating and never need to be calibrated externally (Rigas *et al.*, 1990)
- It is a non-invasive and non-destructive technique (Melin *et al.*, 2000; Severcan *et al.*, 1999; Cakmak *et al.*, 2003).
- It is a low cost technique.
- FTIR can analyze small quantities of samples (Mendelsohn *et al.*, 1986).
- It can be applied to any kind of materials in different physical states such as solutions, viscous liquids, suspensions, inhomogeneous solids or powders (Colthup *et al.*, 1975).
- It gives valuable information about the biological samples by detecting changes in the functional groups belonging to the tissue components such as lipids, proteins, carbohydrates and nucleic acids, simultaneously (Kneipp *et al.*, 2000; Bozkurt *et al.*, 2007; Garip *et al.*, 2007).
- The specific computer based softwares for FTIR spectrometers enable to make data storage and data processing (Yono *et al.*, 1996; Ci *et al.*, 1999). Digital substraction is used to obtain good difference spectra especially for infrared spectra of aqueous solutions (Campbell and Dwek, 1984).
- The shifts in the band frequencies and changes in the bandwidth, and band area/intensity values provide valuable informations that are correlated with the alterations in the structure and composition of macromolecules. These informations can be used as a diagnostic tool for the analysis of cell components, tissue sections, biofluids and so on. So that, FTIR spectroscopy has become mostly preferable method for biomedical diagnosis, recently (Liu *et al.*, 1996; Yano *et al.*, 1996; Schultz *et al.*, 1998; Ci *et al.*, 1999; Dicko *et al.*, 1999; Severcan *et al.*, 2000; Toyran *et al.*, 2004; Akkas *et al.*, 2007a; Akkas *et al.*, 2007b; Szczerbowska-Boruchowska *et al.*, 2007).

- Recently, FTIR spectroscopy has become a promising tool in biomedicine for diagnosis and discrimination of characteristic molecular changes between normal and disease states, especially in different cancer types (Argov et al., 2002; Babrah *et al.,* 2009). This technique is also used in the analysis of cytotoxic effects of radiation in radiobiology, taxonomical stuies in microbiology (Dogan *et al.*, 2007; Garip *et al.*, 2007) and plant studies (Gorgulu et.al., 2007), the discrimination of drug resistant and drug sensitive cancer cells, the examination of apoptosis (Gaigneaux *et al.,* 2006; Sahu *et al.*, 2006) and the determination of stem cell differentiation into adipogenic, osteogenic and neurogenic cells (Aksoy et.al., 2012; Tanthanuch *et al.,* 2010; Downes *et al.,* 2010; Ishii *et al.*, 2007).

1.8.2.1.2. Attenuated Total Reflectance Fourier Transform Infrared (ATR-FTIR) Spectroscopy

ATR-FTIR spectroscopy works on the basis of total internal reflection phenomenon. When the infrared beam, which is directed onto an optically dense crystal with a high refractive index, passes through an ATR crystal at a certain angle, it is internally reflected that causes creation of evanescent wave protruding only a few micrometers beyond the surface of ATR crystal. If the refractive index of sample be slower than that of the crystal, the light will be transmitted rather than internal reflectance. Although the extention of the evenescent wave depends on the type of crystals being used, the wave can protrude maximum between 0.5 μ -5 μ beyond the surface of the crystal into the sample. There are many kinds of materials used for ATR crystal such as diamond, amorphous material transmitting IR (AMTIR), germanium and silicon, however; the mostly used one is zinc selenide (ZnSe). ZnSe which is water resistant, cost effective and easly cleanable material for ATR. The distance that the wave extends from the crystal surface is

about 1.66 μm for ZnSe ATR crystal. The radiation that penetrates a fraction of a wavelength beyond the surface of the crystal enters the sample that is placed on its surface and therefore, there must be complete contact between sample and crystal surface (Figure 1.9 and Figure 1.10) (Perkin Elmer Life Sciences, 2005; Kazarian *et al.,* 2006).

Figure 1.9 ZnSe Diamond ATR attachment of Perkin Elmer Spectrum 100 FTIR spectrometer.

ATR is very applicable technique to different kinds of samples. A solid sample can be directly placed on ATR crystal with a pressure to obtain best contact for reliable FTIR spectra, while aqueous samples can be placed on crystal with a volume of a few microliters appropriate with their concentration. However cells are deposited onto crystal by evaporating the cell suspension buffer by nitrogen flux to obtain cell film (Peak, 2004). In the cell studies absolute absorbance can change as a

results of variation in the cell density, because the distribution of cells on the ATR crystal can not be adjusted accurately during cell film preparation. Therefore, absolute absorbance variation is usually corrected by the scaling of all spectra to be compared. The usual scaling criteria is the setting of the maximum absorbance of Amide I peak to 1 (Gaigneaux *et al.,* 2006) Attenuated Total Reflection (ATR) mode of FTIR spectroscopy has wide range of application area like discrimination of normal and disease states (Bozkurt *et al.,* 2010; Khanmohammadi *et al.,* 2007), biodiagnostics and cell line classification (Ozek et.al., 2010; Gaigneaux *et al.,* 2006), investigation of cellular activation (Timlin et.al., 2009), characterization of stem cells in disease and healthy states (Aksoy C et.al., 2012), fingerprinting of microorganisms (Winder *et al.,* 2004) and detection of microbial products (Bullen *et al.,* 2008; Leitermann *et al.,* 2008), structural analysis of proteins (Goldberg and Chaffotte, 2005).

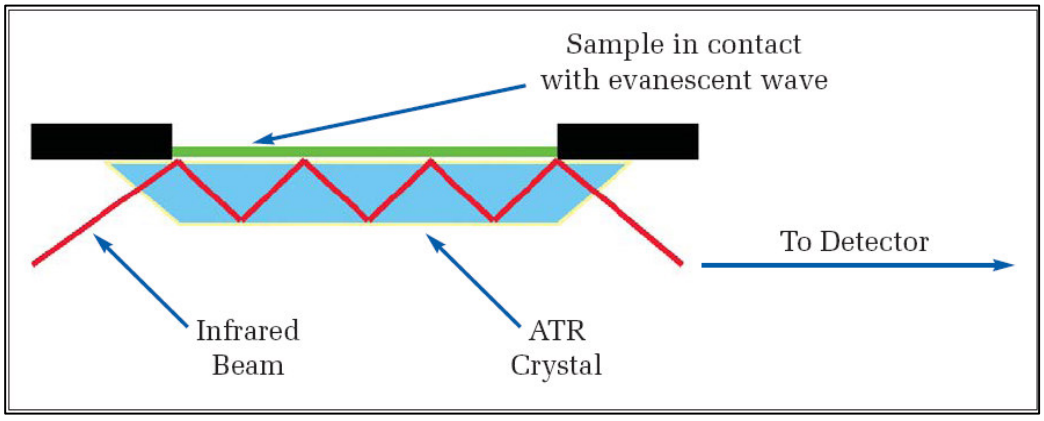

Figure 1.10 Schematic representation of ATR top plate (Perkin Elmer TCH material)

1.8.2.2. Fourier Transform Infrared Microspectroscopy

Fourier transform infrared (FTIR) microspectroscopy can be defined as a combination of an infrared spectroscopy with a microscope (Figure 1.11). FTIR microspectroscopy allows the detection of chemical species from a spatial region by combining spatial specificity with information on its chemical constitution. "The integration of a microscope into the FTIR spectrometer enables it to be used in an imaging mode to create micron-scale chemical maps of a multicomposite sample like single cell. This can be achieved by using a single point detector with an adjustable sampling aperture to define an area on the cell from which the spectral data can be acquired. The cell is then moved in small increments that complement the sampling aperture size, with an IR spectrum recorded at each increment, resulting in the IR chemical map. Thus, the lateral resolution of the IR map is defined by the sampling aperture size" (Gazi *et al*., 2005). Compared to standart methods of histology, cytology and biomedical microscopy, IR spectral imaging offer the adventage of probing biochemical nature of cells with minimal sample preparation and without the use of dyes, stains and flourescent agents (Bechtel *et al.,* 2009; Diem *et al.,* 2004; Romeo *et al.,* 2008).

IR microspectroscopy of biological systems is a developing area to investigate cells in different stages such as their growth cycles (Matthaus *et al.,* 2006), cancerous states (Dukor, 2002), contaminated states with pathogens (Erukhimovitch *et al.,* 2003). IR microspectroscopy applications can be performed in transmission or reflection mode according to the optical properties of the sample (Bechtel *et al.,* 2009). In transmission mode, sample or substrate are placed on an IR transparent microscope slides such as barium floride (BaF_2), calcium floride (CaF_2), ZnSe glass slides. In reflection mode measurements gold or silver coated substrates are used. In recent studies "low-e slides" of Kevley Technologies are used in transflection measurement. Low-e slides, coated with this silver tin oxide

(Ag/SnO_2), are made of glass and they are similar dimension to traditional glass microscope slides. The slides are chemically inert and nearly transparent to visible ligth; however, mid infrared radiation is almost completely reflected. The ligth beam passes through the sample to the substrate, reflects off the silver surface, and passes through the sample a second time (Romeo *et al.,* 2008). Sample preparation for microspectroscopic investigation of individual cells is composed of several steps as attachement of cells onto microscopic slides, fixatition of cells on slide, washing of fixed cells and drying. These steps were expressed as in methodology chapter.

Figure 1.11 Perkin Elmer Spectrum Spotlight 400 imaging FTIR microscope.

1.8.3. Infrared Spectroscopy in Stem Cell Researches

Over the last few years, there has been increased interest of biomedical applications of stem cells in therapeutic and regenerative medicine because of their significant role in tissue renewal and homeostasis with their unique capacity to differentiate into cell types. Such an inceasing interest on the therapeutic usage of stem cells, bring with its challenges, that have to be addressed before cell-based clinical applications, such as isolation, identification, purification and enrichment of stem cells (Pijanka *et al.,* 2010; Chan *et al.,* 2009). Identification of purity and differentiation stages of stem cells are greatest challanges of stem cell biology and regenerative medicine. The existing methods to carefully monitor and characterize the stem cells have some unwanted effects on the properties of stem cells and these methods also do not provide real-time information about cellular conditions. These challanges enforces the usage of non-destructive, rapid, sensitive, high quality, label-free, cheep and innovative chemical monitoring methods. Commonly used biological assays for stem cell analyses like fixation, staining and drying do not provide real time information and destroy cellular characteristics (Konorov *et al.,* 2011). Therefore, the development of new methods that are available to collect real-time biochemical information about living stem cells is important for clinical studies in regenerative medicine (Moody *et al.,* 2010). Some spectroscopic methods can be successfully used to characterize the biochemical make-up of intact live stem cells in non-destructively and label-free manner (Pijanka *et al.,* 2010; Konorov *et al.,* 2011). IR spectroscopy is complementary, label-free, non-invasive and non-destructive vibrational spectroscopic techniques in which the optical signals is generated intrinsically from the sample to obtain information about relative concentrations and structure of macromolecules such as protein, lipids, carbohydrates and nucleic acids (Krafft *et al.,* 2006; Diem *et al.,* 2008). IR spectroscopy is very attractive method because of its great potential to identify similarities and differences between stem cell populations and stem cell lineages,

and the level of maturation and differentiation of stem cells, by determining their unique optical markers (Chan *et al.,* 2009).

Cells and tissues give complex infrared spectra with their complex biological nature. The infrared spectrum of cells and biological tissues is composed of summation of proteins, lipids, carbohydrates, sugars and nucleic acid contributions. Each component is assigned with a characteristic absorbtions in the mid-infrared region (4000–400 cm^{-1}). The bands observed in within the 3000–2800 cm^{-1} region are resulted from the symmetric and antisymmetric stretching vibrations of CH_2 (2852 and 2922 cm^{-1}) and CH_3 (2874 and 2956 cm^{-1}), respectively (Mantsch, 1984; Severcan *et al.,* 2000; Severcan *et al.,* 2003, Cakmak *et al.,* 2006). The strong absorbtion band located 1735 cm^{-1} is associated with the C=O stretching vibration of ester groups. The frequency of this band is strongly affected by hydration (Melin *et al.*, 2000; Cakmak *et al.*, 2003; Severcan *et al.*, 2003). The most intense absorption bands are observed in 1800-800 cm^{-1} region. The band at 1650 cm^{-1} is attributed mainly from the C=O stretching vibration of the amide C=O group and is termed as the amide I band. The frequency of this band can be used detailed analysis of conformation of the protein secondary structure. Another amide mode of protein spectra is the amide II absorption band that is located between 1500–1560 cm^{-1} is associated with the N– H bending vibrations and the C–N stretching vibrations of proteins. Additional bands which are found at 1580 and 1400 cm^{-1} are assigned to the COO^- symmetric and antisymmetric stretching vibrations, respectively. These absorptions are related with the amino acids aspartate and glutamate (Manoharan *et al.,* 1993, Haris and Severcan, 1999). Small numbers of very weak bands are observed between 1500–1250 cm^{-1} region. The most distinct band is located at 1452 cm^{-1} which is characteristic of the CH_2 bending vibration (Cakmak *et al.,* 2003; Di Giambattista *et al.,* 2011) and COO^- symmetric stretching vibrations of fatty acid and amino acid side chains, at around 1400 cm^{-1} (Peuchant *et al.,* 2008; Cakmak *et al.,* 2006;

Melchiori *et al.,* 2010). There are two intense bands due to the symmetric and antisymmetric vibrational modes of phosphate groups (PO_2^-), respectively. These are associated with the phosphodiester linkages of the polynucleotide chain and are assigned to symmetric (1085 cm^{-1}) and antisymmetric (1225 cm^{-1}) phosphate stretches. The frequency of these bands can provide information into head-group hydration (Rigas *et al.,* 1990; Wong *et al.,* 1991; Wang *et al.,* 1997; Cakmak *et al.*, 2003). Carbohydrates give rise to strong bands between 1200 and 1000 cm^{-1}. The band at 1152 cm^{-1} is due to stretching mode of the CO-O-C groups present in glycogen and nucleic acids (Rigas *et al.*, 1990; Cakmak *et al.*, 2003). The bands at 1025 and 1045 cm^{-1} are attributed to the vibrational frequency of CH_2OH groups and the C-O stretching frequencies coupled with C-O bending frequencies of the C-OH groups of carbohydrates (including glucose, fructose, glycogen, etc.) (Parker, 1971). The main absorption bands found within mammalian cells and tissues are displayed in band assignment table (Table 3.1).

1.9. Aim of the Study

Stem cell studies hold enormous potential for development of new therapies. Investigation of stem cells in normal developmental and physiological state as well as in pathological conditions may lead to understanding of disease pathogenesis and development of cellular therapies.

Bone marrow mesenchymal stem cells (BM-MSCs), which are the main cellular components of the bone marrow (BM), have been deeply investigated in order to clarify their significant contributions to heamatopoietic stem cells (HSCs) and organ transplantation because of their intrinsic ability to differentiate into functional cell types and immunsuppressive properties. BM-MSCs provide a supportive microenvironment for maintanance of healthy heamatopoiesis. Their contributions in the prevention of bone marrow rejection by supporting and

enhancing engraftment potential of newly developing hematopoiesis is very important that raises the question what type of cellular interaction is available in bone marrow microenvironment. The specific microenvironment in which HSCs interact with MSCs is called as stem cell niche that is important for heamatopoietic regeneration including erythropoiesis. BM-MSCs both provide the supportive microenvironmental niche for hematopoietic stem cells (HSCs) and facilitate HSC maintenance by secreting soluble factors and direct cell-to-cell contact.

Beta thalassemia is a genetic based hematological disease resulting from lack or reduced synthesis of β-globin chains in hemoglobin because of partial or total mutations in the genes of these chains. The defect in hemoglobin cause deep anemic symptoms that leads to increased but non effective erythropoietic activity in bone marrow that is called as ineffective erythropoiesis. How cell-to-cell interactions between hematopoietic cells and BM-MSCs are effected during genetic based beta-thalassemia major (β-TM) disease condition have not been investigated yet. Within this context, in the first part of the study we aimed to investigate the molecular changes of BM-MSCs in β-TM disease pathology by FTIR spectroscopy and microspectroscopy. We hypothesized that hematopoietic defect in β-TM may induce changes in morphological, proliferative, differentiative and molecular properties of BM-MSCs as a result of cellular interactions between defective HSCs and healthy BM-MSCs.

In the second part of the study we aimed to investigate the molecular level effects of donor age on BM-MSCs properties by means of FTIR spectroscopy and microspectroscopy. A complete characterization of the cellular, biochemical, and molecular interactions of MSCs with their niche components is needed to understand how these cells can be optimally regulated in vitro. Therefore; understanding the effect of donor age on efficiency of tissue homeostasis, disease

recovery and the success of therapeutic application has to be answered. In this context, we hyphothesized that infrared spectroscopy can be used as a new, non-destructive research method that enables real-time chemical monitoring, high-quality data collection with less experimental complexity to identify novel molecular marker(s) that reflects the stem cell aging.

CHAPTER 2

MATERIALS and METHODS

2.1. Materials

2.1.1. Chemicals

The list of used and their suppliers are given in Appendix A.

2.1.2. Mesenchymal Stem Cells and Hematopoietic Stem Cells

Human bone marrow aspirates (3-5 ml) which were obtained from posterior iliac crest of healthy bone marrow donors and patients with thalassemia major were used as a source of BM-MSCs and HSCs. All samples were taken after signing of informed consent that were prepared according to procedures approved by the ethics commitee of the Hacettepe Univesity Childrens Hospital, BMT Unit Ankara, Turkey.

2.1.2.1. Sampling Groups

2.1.2.1.1. Study 1

Human BM-MSCs were isolated from bone marrow samples of β-TM patients before and after their BMT therapy. The aged matched healthy mesenchymal stem

cells were used as a control. The groups that were used to obtain BM-MSCs during this part of the study were ordered in below.

Control Group (n=5): Aged matched healthy bone marrow donors.
Pre-Transplant Group (n=5): Patients before BMT therapy.
Post-Transplant Group (n=5): Same patients after BMT therapy.

2.1.2.1.2. Study 2

Human BM-MSCs of healthy donors from different ages were used in the second part of the thesis study. The BM-MSCs were grouped according to human life cycle and development stages. The groups that were used to obtain BM-MSCs during this part of the study were ordered in below.

Infants: Ages were between 0-3 (n=5)
Children: Ages were between >3-12 (n=5)
Adolescents: Ages were between >12-19 (n=5)
Early Adults: Ages were between >19-35 (n=5)
Mid-Adults: Ages were between >35-50 (n=5)

2.2. Methods

2.2.1. Cell Culture Experiments

2.2.1.1. Isolation and Cultivation of Mesencyhmal Stem Cells from Human Bone Marrow Samples

Bone marrow aspirates (3-5 ml) were diluted in an equal volume of 0,9% phosphate buffer solution (PBS) (Sigma, USA). They were subjected to

fractionation on a density gradient solution Ficoll (1.077 g/l; Biochrom AG, Berlin, Germany) to obtain mononuclear cells (MNCs). MNCs were then washed twice with PBS and cultivated in complete medium contaning Dulbeco's Modified Eagle Medium-Low Glucose (DMEM-LG; Biochrom AG, Berlin, Germany), 10% (vol/vol) Fetal Bovine Serum (FBS; Biochrom AG, Berlin, Germany), 1% (vol/vol) L-glutamine (0.584 g/l; Biochrom AG, Berlin, Germany), 1% (vol/vol) penicillin (100 units/ml) and streptomycin (100 g/ml) (Biochrom AG, Berlin, Germany), 0,1% (vol/vol) Leukemia Inhibitory Factor (LIF) (0,5 μg/ml in 1% BSA solution; Invitrogen) at 37°C in a 5% CO_2 environment to obtain primary BM-MSCs culture. After 24 hours non-adherent mononuclear cells were discarded and adherent primary MSCs called as passage 0 MSCs, were expanded by replacing culture medium twice a week. After the cells reached 80% confluency in 2 weeks, they were detached with 3ml 0.25% Trypsin + 1mM EDTA in PBS for 10 mins. The trypsinization was blocked with 10% FBS supplemented cmplete medium and then the cells were washed with PBS once and harvested with centrifugation at 1500 rpm for 5 minutes by using Eppendorf International 5810 centrifuge. $3x10^5$ viable cells were plated per T75 culture flask for following passages. The cells were counted by Thoma Lam after mixing with trypan blue by considering their viability. All detailed investigations in scope thesis study were perfomed by using passage 3 BM-MSCs.

2.2.1.2. Freezing and Storage of Bone Marrow Mesenchymal Stem Cells

The cells were stored at -196°C in liquid nitrogen cooled special tank to use during thesis study. The cells were firstly suspended in freezing medium containing 10% (vol/vol) DiMethylSulfoxide (DMSO, Applichem, Germany) suplemented with 20% (vol/vol) FBS and 70% (vol/vol) DMEM-LG on ice. Then the cell suspension was aliquoted into cryovials (Greiner Bio-One) as $1x10^6$ MSCs/ 1 ml/ tube on ice.

Cryovials were placed in a Mr. Frosty freezing container (Nalgene Labware, Rochester, NY, http://www.nalgenunc.com) for 24 hours at -80^{o}C. After Mr. Frosty was stored at -80°C overnight, cryotubes were transferred to -196°C liquid nitrogen tank for long term preservation.

2.2.1.3. Characterization of Bone Marrow Mesenchymal Stem Cells

2.2.1.3.1. Morphological Assessment

BM-MSCs was evaluated in terms of their adherence onto the plastic surface of culture flask and fibroblast like morphology under inverted light microscopy.

2.2.1.3.2. Differentiation Experiments

Healthy and thalassemic BM-MSCs were induced for osteogenic and adipogenic differentiation by cultivating them into the special differentiation mediums during 21 days.

2.2.1.3.2.1. Adipogenic Differentiation

After harvesting trypsinized BM-MSC (at P2) by centrifugation at 1500 rpm for 5 mins by using Eppendorf International 5810 centrifuge, the trypsinization was blocked with 10% FBS supplemented complete medium and then cells were washed with PBS once and harvested with centrifugation by using Eppendorf International 5810 centrifuge at 1500 rpm for 5 minutes into cells. The washed cells were seeded in 6-well plates at a density of $25x10^3$ cells/well. The cells were expanded in complete medium until 90-100% conflueny. Then medium was removed and replaced with adipogenic induction medium including DMEM-LG (Biological Industries, Israil), 10% of Fetal Bovine Serum (FBS) (Gibco, USA),

1μM dexamethasone (Sigma, USA), 60 μM indomethacine (Sigma, USA), 500 μM IBMX (Sigma, USA) and 5 μg/ml insulin (Sigma, USA). The induction medium of wells was replenished every 3 days and also adipogenesis was followed by microscopic investigation during 21 days period. Meanwhile, the cells in control well were cultured for 21 days in low glucose DMEM with 10% FBS. At the end of differentiation period cells were stained with Oil Red O (Sigma,USA) to visualize adipogenic differentiation.

2.2.1.3.2.1.1. Oil Red O Staining for Adipogenic Differentiation Assessment

At specified time points, adipogenic induction media was aspirated and the wells were washed with PBS buffer. The fixation of cells was done in 10% formol (Sigma, USA) for 20 mins at RT. After fixation, cells in each well were stained with 500 μl Oil Red O solution (Sigma, USA) by incubating at RT for 10 mins. At the end of 10 mins, the Oil Red O Solution was aspirated and cells were rinsed gently with for dH_2O two times. For picture capturing (Olympus, Japan), 1-2 ml dH_2O was added into the wells. Then cells were rinsed and incubated for 1 hour with %2 igepal/isopropanol (v/v) (Sigma-Aldrich, USA; DOP Organik Kimya Sanayi, Turkey) for quantitative analysis of lipid droplets.

2.2.1.3.2.2. Osteogenic Differentiation

After harvesting trypsinized passage 2 BM-MSC by centrifugation at 1500 rpm (Eppendorf International 5810) for 5 mins, cells were washed with PBS and then seeded in 6-well plates at a density of $12.5x10^3$ cells/well. Cells were expanded in complete medium until 60-70% conflueny. Then medium was removed and replaced with osteogenic induction medium consisting DMEM-LG (Biological Industries, Israil), 10% of Fetal Bovine Serum (FBS) (Gibco, USA), 100 nM dexamethasone (Sigma, USA), 10 mM beta glycerophosphate (Sigma, USA) and

0.2 mM ascorbic acid (Sigma, USA). Meanwhile, the cells in control wells were cultured for 21 days in low glucose DMEM with 10% FBS. The induction medium of wells was replenished every 3 days and also osteogenesis was followed by microscopic investigation during 21 days period. At the end of differentiation period cells were stained with Alizerin Red Stain (Sigma,USA) to visualize osteogenic differentiation.

2.2.1.3.2.2.1. Alizerin Red Staining for Osteogenic Differentiation Assessment

At specified time points, osteogenic induction media was aspirated and the wells were gently washed with PBS buffer. The fixation of cells was done in 10% formol (Sigma, USA) for 20 mins at RT. After washing with dH_2O, Alizarin Red solution (Sigma,USA) was left at room temperature in wells for 10 minutes. At the end of 10 mins, the stain was aspirated and cells were gently washed with dH_2O for 3 times to remove any nonspecific staining. Then 1-2 ml distilled water was added to each well for imaging of stained area by microscopically (Olympus, Japan).

2.2.1.3.3. Immunophenotyping of Bone Marrow Mesenchymal Stem Cells by Flow Cytometry

2.2.1.3.3.1. Cell Surface Marker Staining

The analysis of cell surface markers were studied by passage 3 BM-MSCs. The cells in T75 flasks were washed with PBS buffer for once and then trypsinized at 37°C for 10 mins. The trypsinization was blocked with 10% FBS supplemented with complete medium and then washed with PBS once and harvested with centrifugation at 1500 rpm (Eppendorf International 5810) for 5 minutes into the falcon tubes.

Previously, trypsinized passage 3 BM-MSCs were separated into different flow cytometry tubes in 2ml PBS buffer at a density of $2x10^5$ cells/tube for specific cell surface marker staining. After centrifugation at 1500 rpm for 5 mins supernatant was removed and cell pellet was distributed by finger tapping. 100 µl PBS-BSA-Na Azide and CD34 (BD Biosciences, USA), CD45 (BD Biosciences, USA), CD73 (BD Biosciences, USA), CD90 (BD Biosciences, USA), CD105 (E-Bioscience, USA), CD133 (E-Bioscience), antibodies were added homogenized cell pellet and then tubes were incubated +4°C for 30 min by covering thinfoil. At the end of 30 mins incubation in dark, cells were washed twice with 2 ml PBS-BSA-Na Azide and centrifuged at 1500 rpm (Eppendorf International 5810) for 10 minutes. Finally, cells were resuspended in 200 µl PBS-BSA-Na Azide in FACS tubes and analyzed in FACS Aria (Becton, Dickinson Biosciences, USA).

2.2.1.3.3.2. Flow Cytometry Analysis

The analysis of cells was done according to 10.000 event count with the FACS Aria (Beckon Dickinson Biosciences, USA). The channel choice, gating and compensation adjustments were done related to sample and staining properties.The analysis of acquired data was carried out using BD FACSDiva Software v6.1.2 (Becton, Dickinson Biosciences, USA).

2.2.1.4. MTT *(Thiazolyl Blue Tetrazolium Bromide)* Proliferation Assay

Passage 2 BM-MSCs were trypsinized and the trypsinization was blocked with 1 complete medium. After the cells were washed with PBS once and harvested with centrifugation at 1500 rpm (Eppendorf International 5810) for 5 minutes into falcon tubes, they were seeded in a 96-well plates at a density of $1x10^4$ cells/well in 200 µl complete medium. Cultured cells were expanded in 5% CO_2 incubator at 37ºC to obtain passage 3 BM-MSCs which were used in MTT assay. One set of

wells with MTT and complete medium without cells were used as a blank control. 20 µl MTT (5mg/ml in PBS) (Thiazolyl Blue Tetrazolium Bromide, Sigma-Aldrich,USA) solution was added to each well at day 1, 3, 5, 7, 9 and 11 of culturing. After addition of MTT 96-well plate was covered with thinfoil and incubated for 4 hours at 37ºC in 5% CO_2 incubator in dark. After incubation period was completed in dark side, the black formazan crystals were observed by inverted ligth microscope at the bottom of the wells. Once the incubation time was ceased, 100 µl sodium dodesyl sulphate (SDS) (Sigma-Aldrich,USA) was put into each well and then incubated at room temperature for 24 hours by covering the plate thinfoil. SDS which is defined as MTT solvent dissolves formazan cystals, producing a purple solution. At the end of incubation time, the absorbance of each well was measured at 620 nm using ELISA reader (Tecan Systems Inc., San Jose, CA, USA).

2.2.1.5. Determination of Eythropoietin (EPO) and Growth Differentiation Factor 15 (GDF 15) Levels in Bone Marrow Plasma Samples

Bone marrow samples of thalassemic patients and healthy donors were collected into heparin anticoagulant containing tubes. The tubes were centrifuges at 2500 rpm (Eppendorf International 5810) for 15 minutes to obtain BM plasma samples. Quantification of EPO and GDF15 levels of BM plasma samples was performed by ELISA assays for human EPO (Quantikine IVD, R&D Systems, Minneapolis, USA) and for human GDF 15 (Quantikine IVD, R&D Systems, Minneapolis, USA) according to the instruction manual of manufacturer's. While BM plasma samples were used immediately in ELISA assays, remaining plasma samples were stored at -20 ºC by aliquoting.

2.2.1.6. Analysis of Chimerism by Short Tandem Repeat Polymerase Chain Reaction (STR-PCR)

Genomic DNAs were extracted from recipient and donor BM-MSCs samples using MagNA Pure Systems (Roche) according to the manufacturer's recommendation. AmpFlSTR Identifiler amplification kit (Applied Biosystems) was used to perform STR-PCR. The kit amplifies 15 loci (CSF1P0, D7S820, D8S1179, D21S11, D2S1338, D3S1358, D13S317, D16S539, TH01, D1S51, D19S433, TPOX, vWA, D5S818, FGA and Amelogenin in a single tube and provides loci consistent with major world-wide STR databasing standards. PCR was performed using 1 ng of genomic DNA in a final reaction volume of 15 µl as suggested by the manufacturer. The PCR cycle conditions were: 95°C for 11 min, followed by 28 cycles with 94°C for 1 min, 59°C for 1 min and 72°C for 1 min. The final elongation step was 60 min at 60°C. The PCR products were analyzed with an ABI PRISM 310 DNA sequencer and GeneScan Analysis software (Applied Biosystems) as described in the the instruction manual of manufacturer's. Percentage donor chimerism was assumed from the peak area contributed by one heterozygous allele, visible distinct in the mixed profile, was identical to that area contributing to a mix ture of donor and recipient. Chimerism analysis was perfomed in DNA Analysis Laboratory of Hacettepe University Faculity of Medicine Department of Pediatric Hematology as a procurement of services.

2.2.2. Fourier Transform Infrared (FTIR) Spectroscopy and Microspectroscopy Experiments

2.2.2.1. Attenuated Total Reflectance (ATR-FTIR) Spectroscopy Study

2.2.2.1.1. Sample Preparation

In ATR-FTIR spectroscopy measurements, $2x10^6$ BM-MSCs at passage 3 were used. MSCs cells harvested by 5 mins centrifugation at 1500 rpm (Eppendorf International 5810) after 10 mins trypsin (0.25% Trypsin+1Mm EDTA) treatment at 37°C in a 5% CO_2 environment. Then cell pellet was washed twice with 1ml 0.9% PBS solution to remove all groving media. The cell pellet was re-suspended in 10 µl 0.9% PBS buffer and then cell suspension was deposited on Diamond/ZnSe (Di/ZnSe) crystal plate of the Universal ATR unit of the FTIR spectrometer by rapidly evaporating using mild N_2 flux during 30 mins to obtain a homogenous film of entire cells on ATR crystal.

2.2.2.1.2. Data Acquisition and Spectroscopic Measurements

Infrared spectra were obtained by scanning the prepared homogenous BM-MSCs film on Diamond/ZnSe (Di/ZnSe) crystal plate of the Universal ATR of Spectrum 100 FTIR spectrometer in the one-bounce ATR mode (Perkin-Elmer Inc., Norwalk, CT, USA). The spectra were recorded in the 4000-650 cm^{-1} region at room temperature. A total of 100 scans were taken for each interferogram at 4 cm^{-1} resolution. The spectrum of atmospheric water vapor and carbondioxide interference were recorded as background and then subtracted automatically using the Spectrum One Software program. Figure 2.1 shows the infrared spectrum of air. In order to prevent the contribution from the inorganic phosphate in PBS, 10

µl PBS buffer was first dried with nitrogen (N_2) flux during 30 minutes and the buffer spectrum was subtracted from the cell spectra. Figure 2.2 shows the infrared spectra of the PBS buffer. Recording and analysis of the spectral data were performed using the Spectrum One Software from Perkin Elmer.

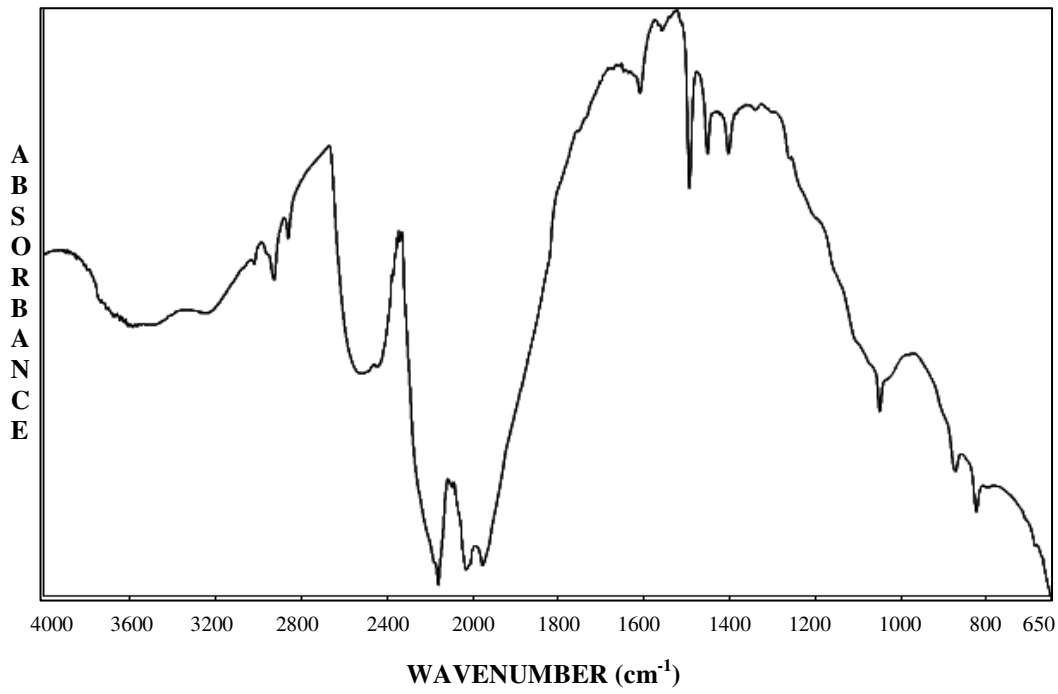

Figure 2.1 Infrared spectrum of air.

Before the spectral analysis are performed, according to the requirements of analysis technique, some preprocessing steps are applied to the spectral data sets to make the spectra comparible. By these preprocessing approaches the number of variables can either be reduced to prevent overfitting. Baseline correction, which is

mainly used to get rid of a sloping and curving baseline, is a wavelength-dependent intercept and unique for each sample spectrum (Franke, 2006). The detailed data analysis and accurate determination of the variations in band area values original base-line corrected spectrum was considered, while the band positions (frequency values) were measured according to the center of weight of the peaks from raw spectral data. All these mentioned quantitative analysis were performed on non-normalized but pre-processed average spectra. However, by the purpose of visual presentation of the differences, the average spectra of sampling groups were normalized with respect to the specific bands and information about the intensity of the spectrum is completely eliminated (Kramer, 1998).

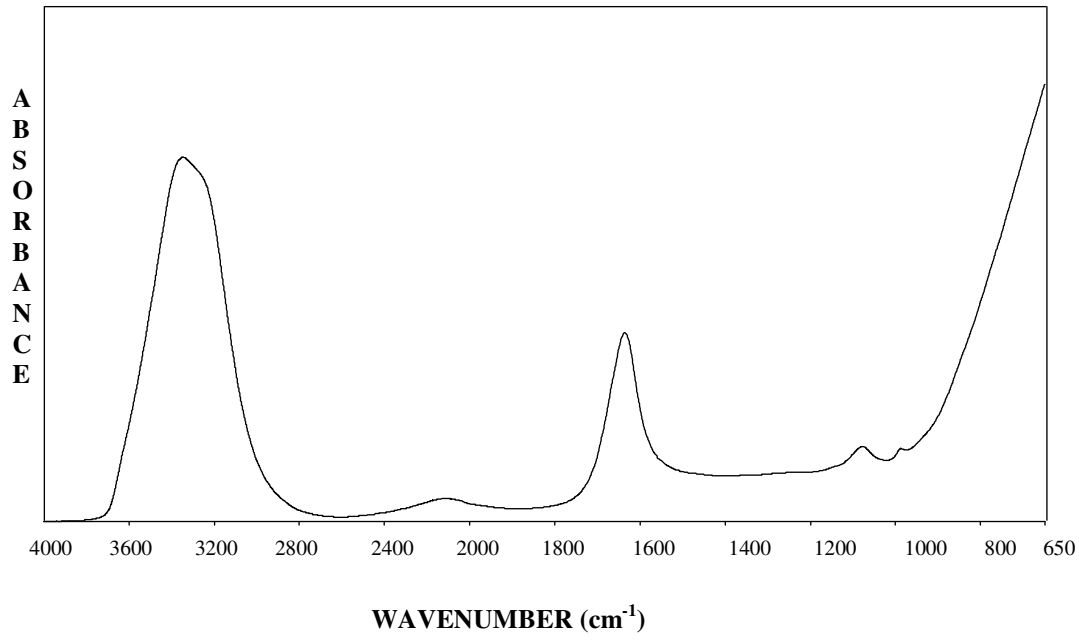

Figure 2.2 The ATR FTIR spectrum of PBS buffer solution.

2.2.2.1.3. Statistical Analysis

The results of spectral measurements were expressed as "mean ± standard error" values. The spectra were analyzed by using different spectral parameters like band frequencies, band widths and band areas. As first, the data were evaluated by normality test to decide whether the parametric or non-parametric statistical test to be used. Since the data showed normal distribution, they were compared to each other by using One Way Anova and Tukey Multiple Comparison Test by considering their statistical significances in terms of $p<0.05$, $p<0.01$, $p<0.001$.

2.2.2.1.4. Cluster Analysis

It was applied to find out spectral relationships among sampling groups that were investigated in the study. The first derivativative, vector normalized spectra were used in the cluster analysis by using OPUS 5.5 software (Bruker Optic, GmbH) in order to distinguish control and thalassemic MSCs, and also to distinguish MSCs belonging to different age groups. Cluster analysis is separated the spectra of samples according to their spectral similarities and differences. The result of the analysis are represented in the form a dendrogram. The change in variances between the spectra of samples is represented by heterogeneity values. Higher heterogeneity in between the clusters demonstrates higher differences among analyzed groups. Pearson's correlation coefficients were used to measure the distances between the pairs of spectra. Ward's algorithm was used to construct dendograms for hierarchical clustering. The details of the calculation and algorithm can be found in Severcan *et al.*, 2010.

2.2.2.2. FTIR Microspectroscopic Study

2.2.2.2.1. Slide Preparation

2.2.2.2.1.1. Deposition and Fixatition of BM-MSCs on Low-e Microscope Slides

Passage 3 BM-MSCs were trypsinized and after the tryspsin was blocked with 10% FBS collected with centrifugation at 1500 rpm (Eppendorf International 5810) for 5 mins, the cell washed with PBS once and then the two final washings were performed with serum physiologic solution to remove salt crystals. The cell pellet was dissolved in 1mL of culture medium and BM-MSCs were counted with thoma lam by using trypan blue. 25.000 MSCs were placed on silver (Ag/SnO_2) coated low-e microscope slides and they were grown on at 37ºC in a 5% CO_2 environment by overnigth cultivation. At the end of cultivation time, MSCs on low-e microscope slide were fixed by 10% formalin for 10 minutes. In order to remove excess formalin, slides were washed with serum physiologic solution and then they were kept in dry environment to evaporate excess solution at room temperature for at least 1 hour.

Fixation is a major issue after cells are deposited onto microscope slides. Air drying is a mild form of fixation and for further fixation some chemicals such as ethonol, methanol, acetone and formalin are used. Ethanol and methanol cause minor spectral changes because of removal of phospholipids and minor changes are observered in the main protein bands amide I and amide II (Romeo *et al.*, 2008). Acetone fixation decreases cell volume, breaks hydrogen bonds and causes coagulation of water-soluble proteins and the destruction of cellular organelles (Hasting *et al.*, 2008). Therefore, buffered formalin that preserves lipids and has little impact on carbohydrates is generally used for fixation of cells that will be

used in IR microscopy. 10% buffered solution of formaldehyde, is called as formalin, preserves protein secondary structure of cells and it does not harm the spectra of cells (Romeo *et al.*, 2006). After fixation, cells have to be washed with deionized water or physiological saline solution (0.9 % NaCl) in order to prevent hemolysis. Then they have to be dried very quickly under a stream of dry and compressed air. The attachement of cells to the slide is so strong that they can be fixed onto the slide by chemically without dislodging them (Romeo *et al.*, 2006; Romeo *et al.*, 2008).

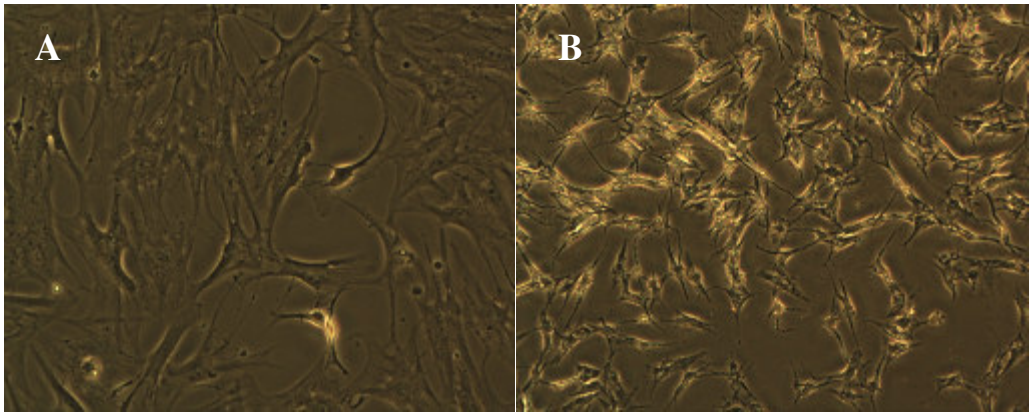

Figure 2.3 Inverted ligth microscopy images of BM-MSCs that were directly grown on silver coated low-e FTIR microscopy slides. **A)** Before formalin fixation. **B)** After formalin fixation.

The low-e MirrIR slides are coated with Ag/SnO_2 layer which provide reflectance property of slides. Infrared beam is reflected by Ag/SnO_2 layer through a thin sample. Since the low-e slides are transparent in the visible region, before IR

imaging of cells samples can be examined by light microscope as it can be seen from Figure 2.3.

2.2.2.2.2. Collection of Visible Images and Spectral Maps

Perkin Elmer FTIR microscope coupled with Perkin Elmer Spotlight 400 software was used to map MSCs samples on slides. The microscope is equipped with a liquid nitrogen cooled MCT detector and a CCD camera to provide an optical image of the area under interrogation. An aperture size of 6.25μm X 6.25μm was used to obtain spectra from confluent monolayers. IR image maps were collected in the reflection mode through the spectral range between 4000-700 cm^{-1} with a 4 cm^{-1} resolution and 32 scan numbers. Background spectra were collected from a separate piece of blank MirrIR low-e slide. At least 3 spectra were acquired from each sample.

2.2.2.2.2.1. Selection of Spectral Images and Preprocessing of Spectral Data

ISys software (Spectral Dimensions, Olney, MD, USA) was used to analyze the conventional FTIR microspectroscopic data. ISys programme uses image files with the .spf extention, however; Perkin Elmer FTIR microscope coupled with Perkin Elmer Spotlight 400 software provides image files with .fsm extention. Therefore, at the beginnig of image data analysis with ISys software, the .fsm extended files were translated to .spf extended ones. Whole baseline correction were performed between 3800-800 cm^{-1} region. Then spectral masking was applied for analysis by using ISys software to get rid of the contributions from the surface around the cellular regions by marking the cells. The chemical maps were constructed for each group by taking area of specifically selected spectral bands arisen from lipids, proteins and nucleic acids. The integrated spectral regions for

the infrared bands that were used to determine distribution of functional groups were presented in Table 2.1.

Table 2.1 The integrated spectral regions

Infrared Band	**Integrated Spectral Range (cm^{-1})**
CH_2 antisymmetric stretching	2944-2880
CH_2 symmetric stretching	2864-2862
Amide I	1712-1534
Amide II	1534-1480
PO_2^- antisymmetric stretching	1272-1184

CHAPTER 3

RESULTS

Bone marrow mesenchymal stem cells (BM-MSCs) are found in BM microenvironment with other cells like hematopoietic stem cells as a main cellular supportive component. Therefore, prior to experiments BM-MSCs have to be isolated from bone marrow samples and then they have to be characterized. BM-MSCs were characterized by their adherence to plastic surface of culture flask and their fibroblast like morphology under inverted light microscope according to the rules of ISCT (International Society for Cellular Therapy) (Horwitz *et.al.*, 2005; Dominici *et.al.*, 2006). These cells have to be evaluated for their expression of CD73, CD90 and CD105 surface antigens and their capacity to differentiate into at least osteoblasts and adipocytes by standard differentiation inducing media (Dominici *et.al.*, 2006) in order to be defined as MSCs. BM-MSCs that were used in the thesis study were characterized first in terms of their morphological, immunophenotypical and differentiation properties and then used in other experimental parts of the study.

3.1. Harvesting of Mesenchymal Stem Cells from Bone Marrow Samples by Culturing

As first, bone marrow MNCs were isolated from bone marrow aspirates by ficoll extraction method as stated in section 2.2.1.1. Then, MNCs were seeded in plastic culture flasks to obtain MSCs. At the first day of culturing of MNCs, hematopoietic progenitor cells and erythrocytes were observed as unattached

bright cells in flask. Culture media was aspirated and replenished with fresh media during two weeks to remove these concomitant cell types. While these contaminating cells were eliminated with the media replenishment, BM-MSCs were obtained by their plastic adherence property. These BM-MSCs were called as passage 0 (P0) cells (Figure 3.1).

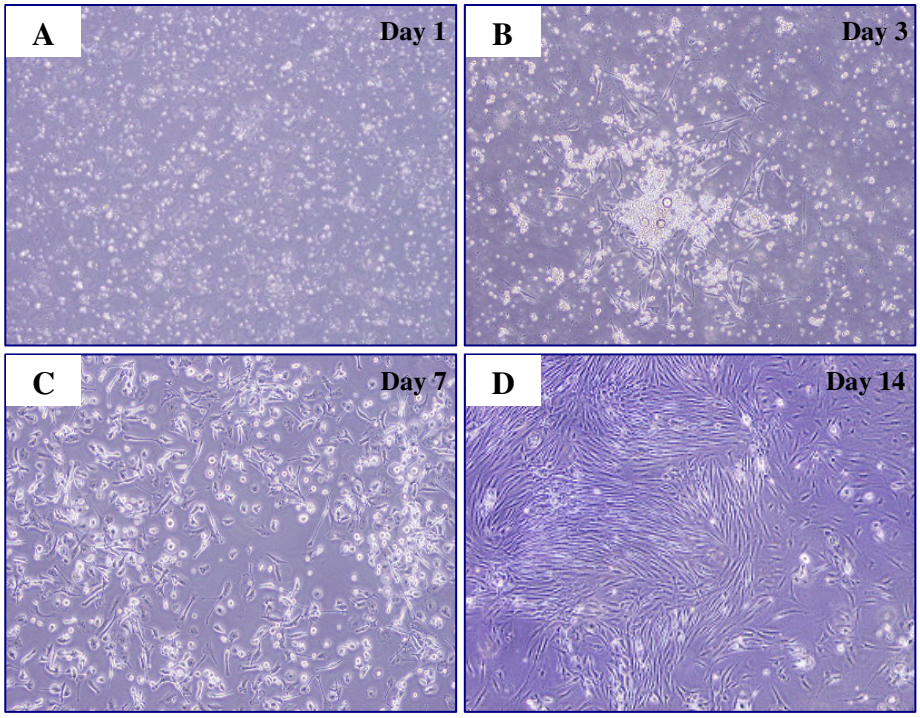

Figure 3.1 Photomicrograph of healthy BM-MNCs in culture flask during their expansion phases to obtain P0 MSCs. **A)** MNCs after 24 hours, **B)** Newly formed fibroblast like MSCs around erythropoietic colony, **C)** Fibroblast like MSCs and brigth hematopoietic cells, **D)** Confluent MSCs colony.(Mag = 10X)

Further passaging was performed to obtain pure P3 BM-MSCs that were used in other experiments during the thesis study. In Figure 3.2, P1, P2 and P3 (passage number will be stated as P1, P2, e.g.) BM-MSCs populations could be observed. As can be seen from the Figure 3.2, while shiny hematopoietic cells were available in P1, they disappeared during proceeding passages.

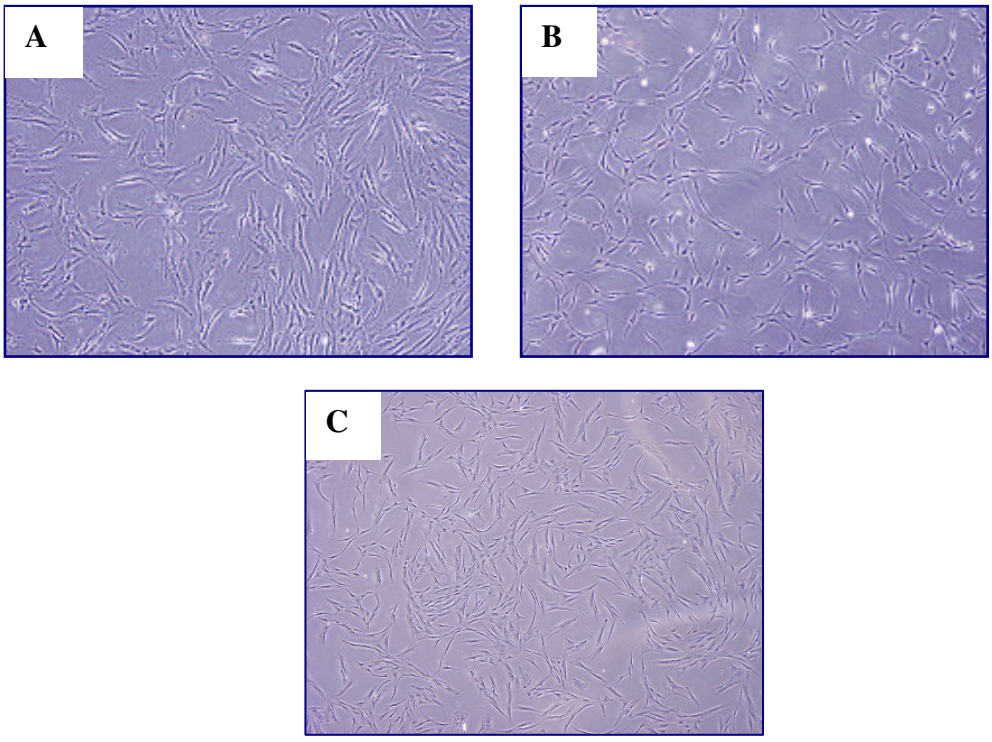

Figure 3.2 Healthy BM-MSCs at different passages. **A)** P1 MSCs with several round and shiny hematopoietic cells, **B)** P2 MSCs, **C)** P3 MSCs. (Mag = 10X)

3.2. Characterization of Human Bone Marrow Mesenchymal Stem Cells

Bone marrow mesenchymal stem cells from healthy and thalassemic bone marrow samples were isolated and characterized as mentioned in sections 2.2.1.1 and 2.2.1.3. After BM-MSCs were isolated by their adherence to plastic surface of culture flask and their morphological characterization was performed by inverted light microscopy. They were also analyzed in terms of their expression of BM-MSCs's surface markers by flow cytometry.

3.2.1. Flow Cytometry Analysis of CD Marker Expression Profile of Bone Marrow Mesenchymal Stem Cells

In the late passages, the genes that are involved in cell cycle, DNA replication and DNA repair are significantly down-regulated (Wagner *et al.*, 2010). Passaging over and over can affect stem cell like potential of MSCs that they can loose their stemness properties (Yu *et al.,* 2010), while early passages contain contaminating cells which decrease purity of MSC population. Therefore, both in the first and the second part of the thesis BM-MSCs were used in P3.

Passage 3 BM-MSCs, which were used in the present study, were evaluated for their expression of MSCs surface antigens CD105, CD73, CD90, CD34, CD45. Both thalassemic and healthy BM-MSCs were positive for CD105, CD73 and CD90 antigens in ≥95%, while they showed lack of expression for heamatopoietic markers CD45, CD34, as stated in the definitions of ISCT for MSCs (Dominici *et al.,* 2006). There was no difference in the levels of expressions of BM-MSCs specific surface antigens between P3 thalassemic and their healthy control BM-MSCs (Figures 3.3, 3.4 and 3.5).

In the scope of second part of the thesis, P3 BM-MSCs obtained from different age donors showed same expression profile for surface antigens CD105, CD73, CD90, CD34, CD45. They expressed CD105, CD73 and CD90, while they did not show any expression for CD34 and CD45.

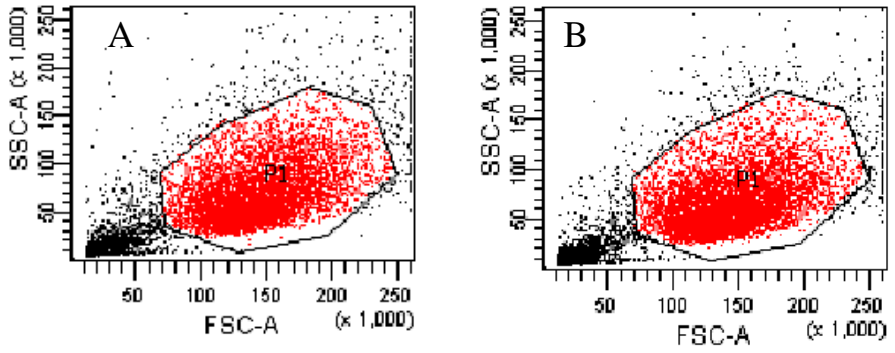

Figure 3.3 The FSC/SSC parameters of passage 3 BM-MSCs **A)** Healthy BM-MSCs; **B)** Thalassemic BM-MSCs.

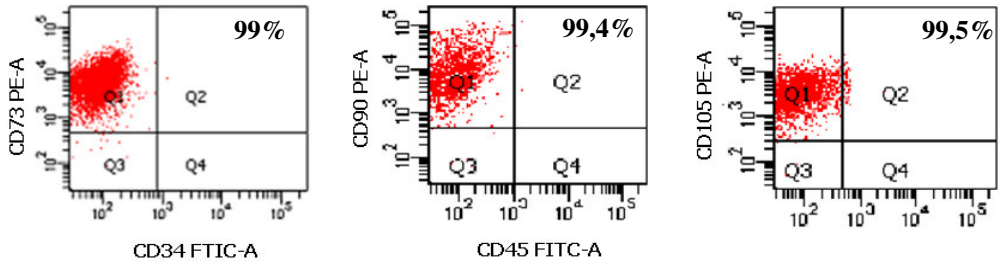

Figure 3.4 Surface antigen profile of healthy BM-MSCs at passage 3.

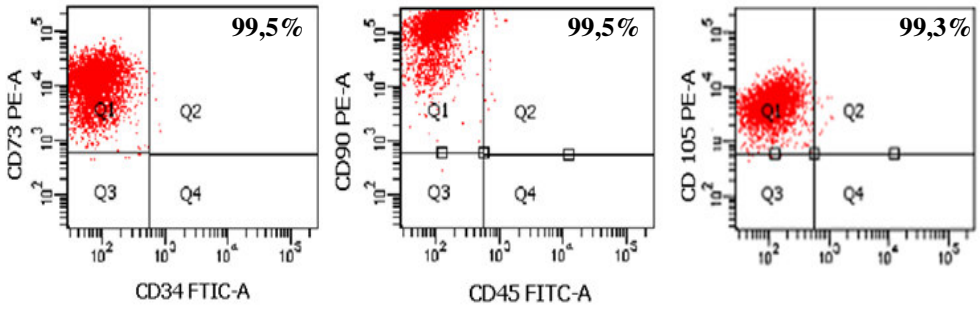

Figure 3.5 Surface antigen profile of thalassemic BM-MSCs at passage 3.

3.2.2. Differentiation Analysis of Bone Marrow Mesenchymal Stem Cells

Healthy and thalassemic BM-MSCs, which were cultivated till P3 in six well culture dishes, were investigated in terms of their adipogenic and osteogenic differentiation potentials.

3.2.2.1. Adipogenic Differentiation Analysis

Mesenchymal stem cells can be differentiated into different lineages by using selective induction media supplemented with specific compounds at specific concentrations.

In the first part of the thesis study, adipogenic differentiation potentials of P3 thalassemic BM-MSCs before and after bone marrow transplantation therapy (BMT) and their healthy controls were examined by using specific adipogenic induction media. Adipocyte conversion of BM-MSCs by incubating with selective media takes 21 days. By the 6^{th} day of an induction, shiny lipid droplets started to be observed in the BM-MSCs. Throughout the induction period, the lipid droplets

became larger and increased in number. At the end of induction period, they filled the cytoplasm and Oil Red O staining were perfomed to evaluate adipocyte differentiation. Morphological assessment of induced cells was performed under inverted light microscope. Figure 3.6 shows adipogenic differentiation results of thalassemic BM-MSCs before and after BMT therapy and healthy control BM-MSCs. There was no morphological difference for the adipogenic differentiation of healthy and thalassemic BM-MSCs. In the second part of the study adipogenic differentiation potentials of healthy BM-MSCs that were obtained from volunteer BM donors in different ages were compared. The results showed that BM-MSCs of younger and older donor groups differentiated into adipocytes (Figure 3.7).

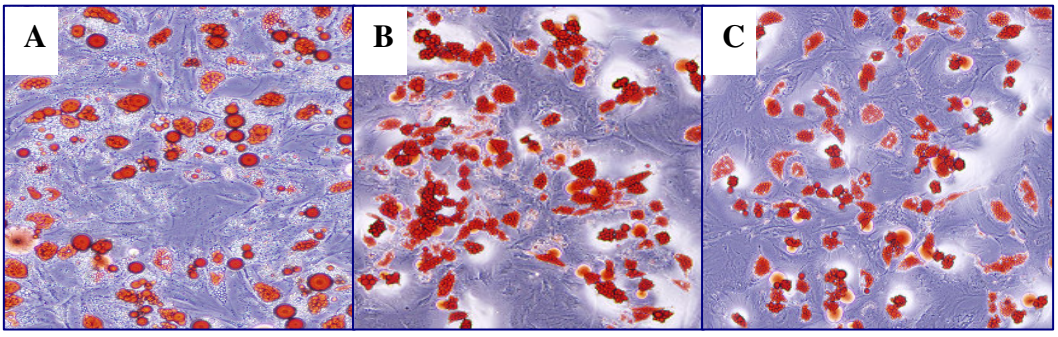

Figure 3.6 Oil Red O staining of thalassemic and healthy control BM-MSCs at the end of 21 days. **A)** Healthy BM-MSCs, **B)** Thalassemic MSCs before transplantation, **C)** Thalassemic MSCs after transplantation. (Mag = 20X)

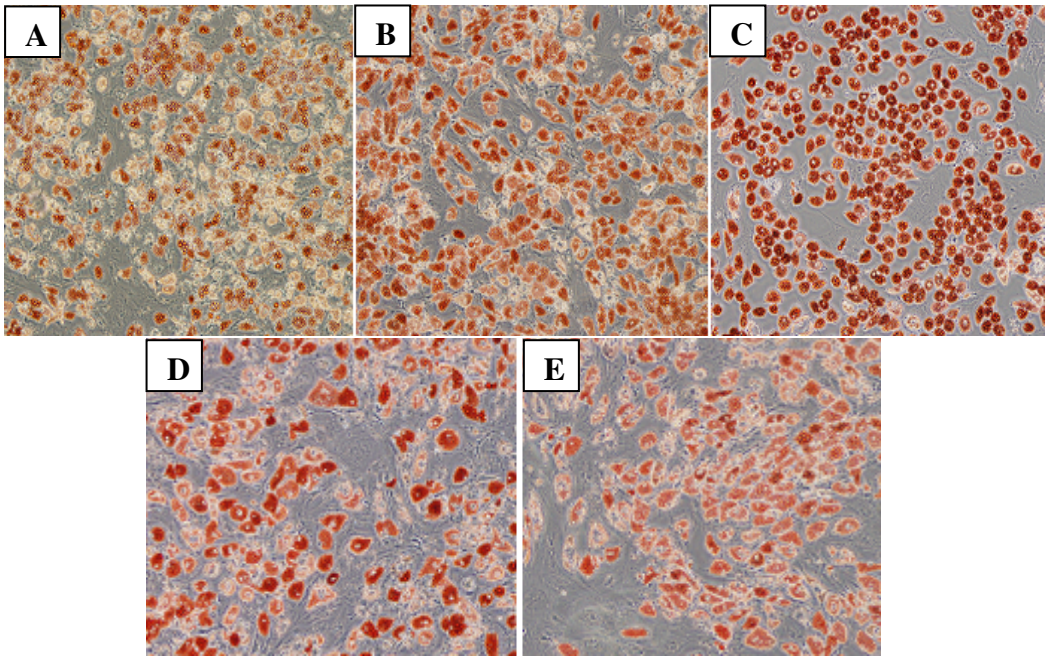

Figure 3.7 Oil Red O staining of healthy P3 BM-MSCs at the end of 21 days **A)** Infants MSCs, **B)** children MSCs, **C)** adolescents MSCs, **D)** early adults MSCs, **E)** mid adults MSCs. (Mag = 20X)

3.2.2.2. Osteogenic Differentiation Analysis

In the first and the second part of the thesis study, BM-MSCs were induced by using specific induction media for osteogenic differentiation during 21 days. By the 7th day of induction, fibroblast like morphology of BM-MSCs started to change and they became larger, dark-colored calcium deposition was observed in cells. As the induction period continued, the number of amorphous calcium deposition increased and filled up the cell cytoplasm. At the end of induction period, calcium deposition in differentiated cells were observed by Alizerin Red staining as black crystals under inverted light microscope as an indicator of osteogenic

differentiation. The osteogenic differentiation results of thalassemic BM-MSCs before and after BMT therapy with their healthy control BM-MSCs are shown in Figure 3.8. The osteogenic differentiation of BM-MSCs that was obtained from different aged healthy donors is presented in Figure 3.9.

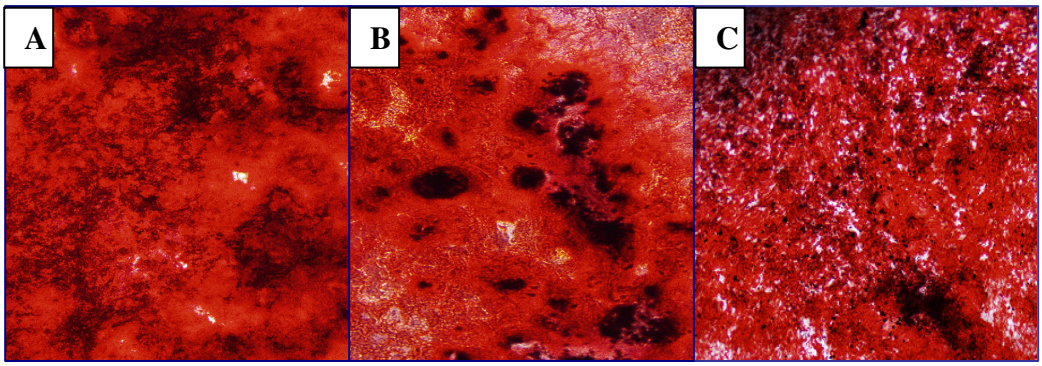

Figure 3.8 Alizerin Red staining of thalassemic and healthy control BM-MSCs at the end of 21 days **A)** Healthy MSCs, **B)** Thalassemic MSCs before transplantation, **C)** Thalassemic MSCs after transplantation. (Mag = 20X)

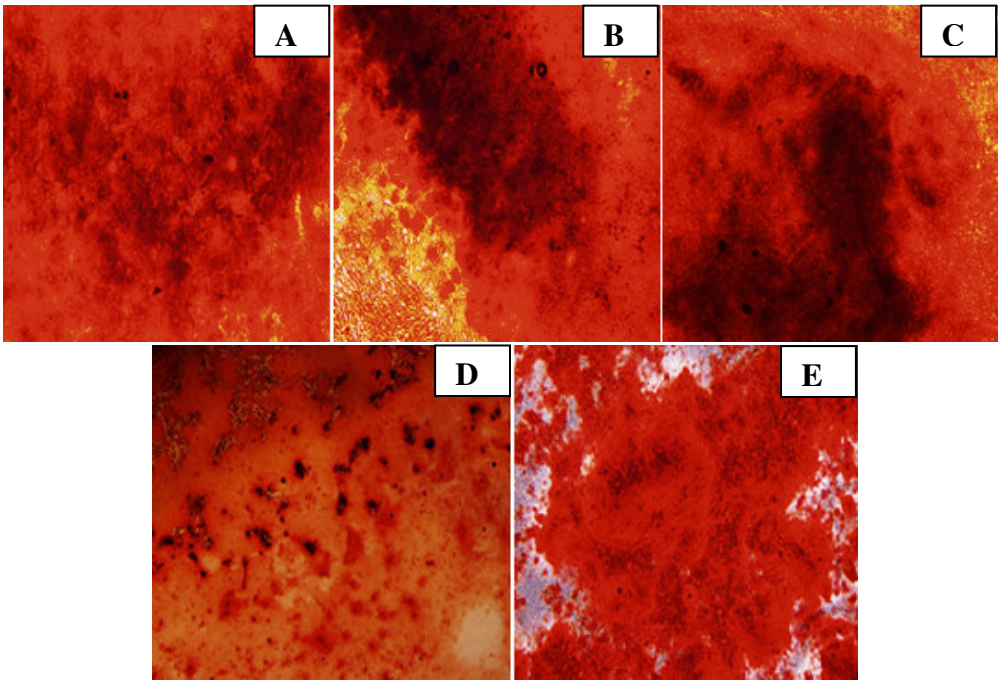

Figure 3.9 Alizarin Red staining of healthy P3 BM-MSCs at the end of 21 days. **A)** Infants MSCs, **B)** children MSCs, **C)** adolescents MSCs, **D)** early adults MSCs, **E)** mid adults MSCs. (Mag = 20X)

3.3. Results of Chimerism Analysis Following Bone Marrow Transplantation

In the present study, chimerism analysis was performed by amplifying 15 STR loci in genomic DNA to determine whether BM-MSCs were of recipient or donor origin after bone marrow transplantation (BMT) therapy. STR-PCR is based on the amplification of tetranucleotide STR loci by PCR. Post-transplant DNAs of BM-MSCs of our all 5 patients were obtained between +25 and +35 days after transplantation and they were used in chimerism test by comparing pre-transplant DNA of patients and DNA of donors. Our chimerism results showed that after BMT bone marrow MSCs were of patient origin while while complete donor type

hematopoietic engraftment was present in all patients. The results of chimerism analysis revealed that BM-MSCs were of 100% patient origin while there were between 95% and 99% donor type HSCs engraftment in their bone marrows.

3.4. FTIR Spectroscopy Results

The thesis study was aimed to investigate molecular level differences or similarities in human BM-MSCs during human aging periods and thalassemia disease states. The FTIR spectrum of BM-MSCs represents many different functional groups belonging to many different macromolecules.

Fourier-transform infrared (FT-IR) spectroscopic approach is very convenient to obtain quantitative and structural information about biological samples. The specific groups of atoms in the system are defined by specific infrared absorption bands that are assigned to specific vibrational modes of particular functional groups in molecule (Steele, 1971).

Attenuated Total Reflection (ATR) mode of FTIR spectroscopy does not require detailed sample preparation procedure (Kazarian *et al.*, 2006; Perkin Elmer Life and Analytical Sciences, 2005). ATR-FTIR is based on the total reflection phenomenon. When the radiation beam passes through an ATR crystal, it is internally reflected that causes creation of evanescent wave protruding only a few micrometers beyond the surface of ATR crystal. The distance that the wave extends from the crystal surface is about 1,66 μm for ZnSe diamond ATR crystal. The radiation that penetrates a fraction of a wavelength beyond the surface of the crystal enters the sample that is placed on its surface (Perkin Elmer Life and Analytical Sciences, 2005). A solid sample can be directly placed on ATR crystal by applying a pressure to obtain best contact for realible FTIR spectra, however; cells are deposited onto crystal by evaporating the cell suspension buffer to form

cell film. When the infrared beam reflected through the ATR crystal, the sample absorbs a part of the radiation as a result of an interaction and the sample interface produces an absorbance spectrum (Kazarian *et al.,* 2006; Gaigneaux *et al.,* 2006).

3.4.1. General FTIR Spectrum and Band Assignments of Thalassemic and Healthy Control Bone Marrow Mesenchymal Stem Cells

Figure 3.10 shows the averaged representative infrared spectrum of thalassemic and healthy control BM-MSCs in the 3800-800 cm^{-1} region. The wavenumber (frequency) values of the bands at peak positions were used to assign the bands. The main bands are labelled with numbers in the figure and specific assignments of these spectral bands for BM-MSCs are listed in Table 3.1.

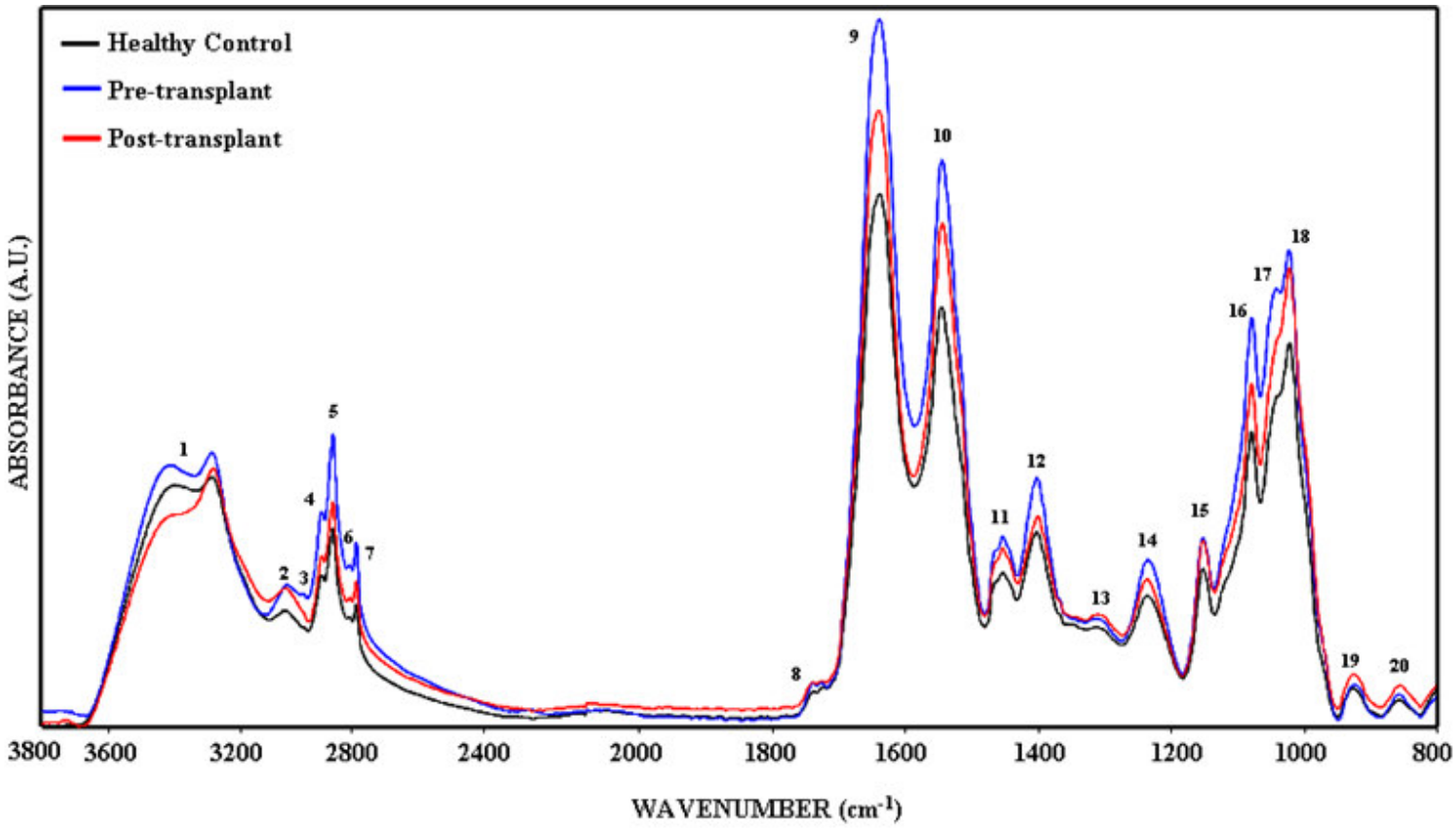

Figure 3.10 The representative average spectra of healthy control (**black line**), pre-transplant (**blue line**) and post-transplant (**red line**) group human bone marrow mesenchymal stem cells in the 3800-800 cm^{-1} region. (The spectra were normalized with respect to the amide A band located at 3330 cm^{-1}).

Table 3.1 General band assignment of human bone marrow mesenchymal stem cells.

Peak No	Wavenumber (cm^{-1})	Definition of the sprectral assignments
1	3330	**Amide A:** N-H and O-H stretching vibrations of polysaccharides, proteins
2	3065	**Amide B:** N-H vibrations of proteins
3	3015	**Olefinic =CH stretching:** unsaturated lipids, cholesterol esters
4	2957	**CH_3 antisymmetric stretching:** lipids, protein side chains, wih some contribution from carbohydrates and nucleic acids
5	2924	**CH_2 antisymmetric stretching:** mainly lipids, with the little contribution from proteins, carbohydrates, nucleic acids
6	2873	**CH_3 symmetric stretching:** protein side chains, lipids, with some contribution from carbohydrates and nucleic acids
7	2852	**CH_2 symmetric stretching:** mainly lipids, with the little contribution from proteins, carbohydrates, nucleic acids
8	1740	**C=O stretching vibrations** of triglycerides, cholesterol esters
9	1639	**Amide I:** C=O stretching vibrations of proteins
10	1545	**Amide II:** N-H bending and C-N stretching vibrations of
11	1453	**CH_2 bending vibrations** of lipids
12	1402	**COO^- symmetric stretching:** fatty acid side chains
13	1310	**Peptide side chain vibrations**
14	1234	**PO^-_2 antisymmetric stretching:** fully hydrogen bonded: mainly nucleic acids with the little contribution from phospholipids
15	1152	**CO-O-C antisymmetric strectching vibraitions** of glycogen and nucleic acid ribose
16	1080	**PO^-_2 symmetric stretching:** nucleic acids and phospholipids; C-O stretching: glycogen,polysaccharides, glycolipids
17	1045	**CO stretching vibrations** of carbohydrates, glycogen; deoxyribose/ribose of nucleic acids
18	1025	**Mainly from glycogen**
19	925	**Sugar vibrations** in backbone of DNA-Z form
20	855	Vibrations in N-type sugars in nucleic acid backbone

3.4.2. Comparison of Spectra of Thalassemic and Healthy Control Bone Marrow Mesenchymal Stem Cells

In the first part of the thesis study, the differences in the structure and the function of macromolecular components of healthy control BM-MSCs and thalassemic BM-MSCs before and after BMT therapy were investigated by FTIR spectroscopy and microspectroscopy. FTIR spectra of all samples were collected in 4000-650 cm^{-1} frequency region. A detailed spectral analysis was performed in two separate regions, namely 3050-2800 cm^{-1}, 1800-800 cm^{-1} (Figure 3.11 and Figure 3.12). As seen from these figures, thalassemic and healthy control BM-MSCs spectra substantially differ in band positions, band heights and band widths. The details of these differences between thalassemic and control BM-MSCs were discussed in Chapter 4 more specifically.

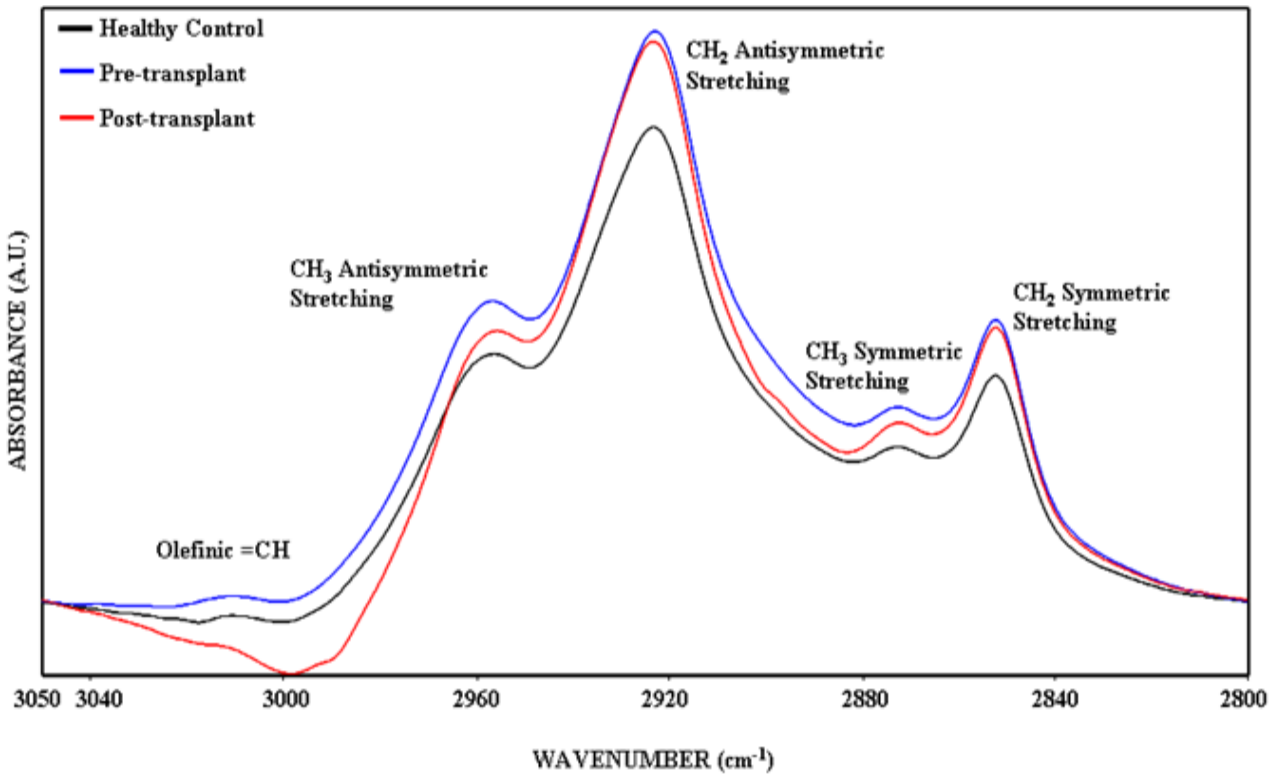

Figure 3.11 The representative infrared spectra of healthy control (**black line**), pre-transplant (**blue line**) and post-transplant (**red line**) group human bone marrow mesenchymal stem cells in the 3050-2800 cm^{-1} region. (The deconvolved spectra were normalized with respect to the amide A band).

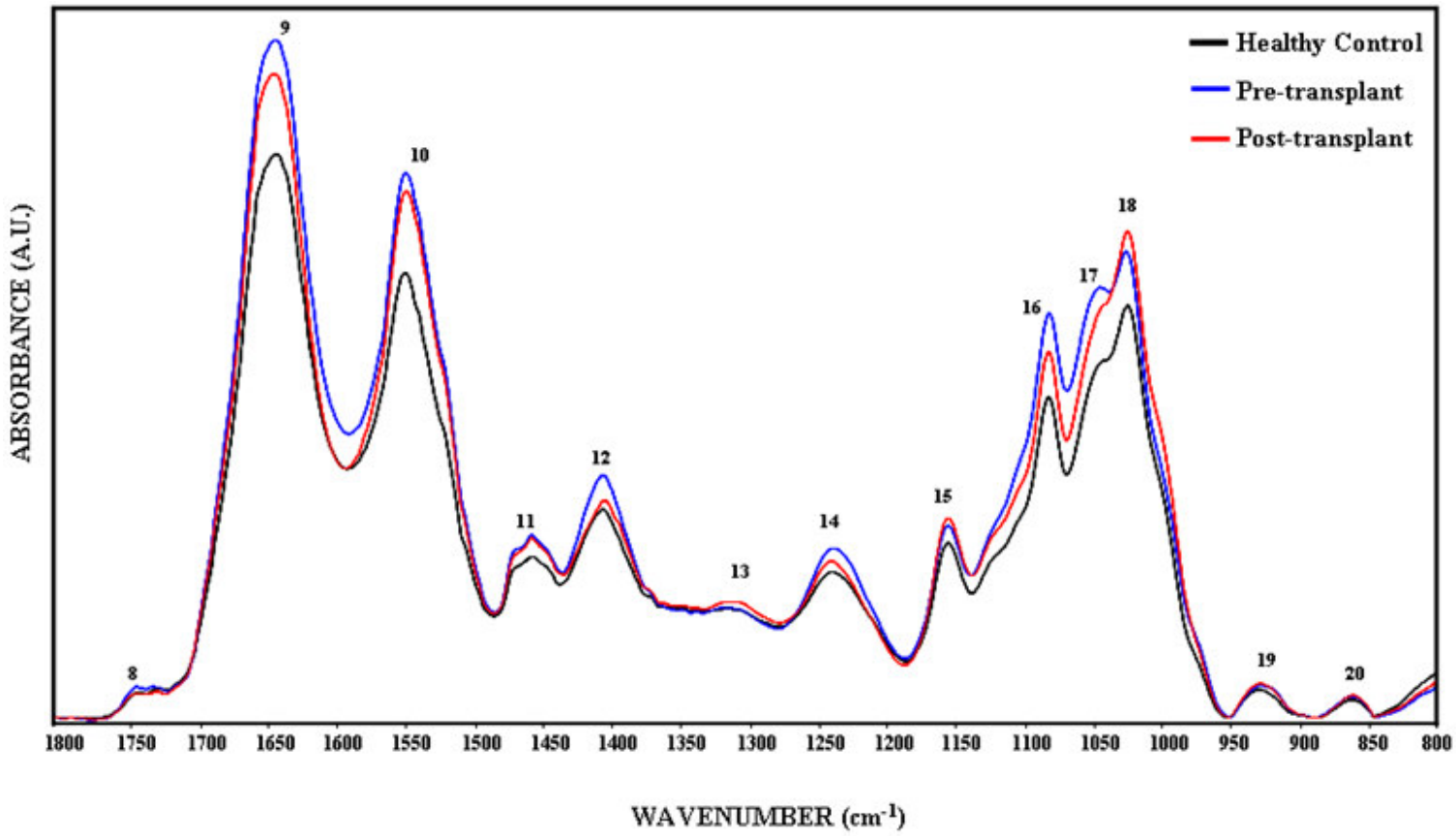

Figure 3.12 The represantative infrared spectra of healthy control (**black line**), pre-transplant (**blue line**) and post-transplant (**red line**) group human bone marrow mesenchymal stem cells in the 1800-800 cm^{-1} region. (The spectra were normalized with respect to the amide A band).

3.4.2.1. General Information about Numerical Comparisons of the Bands of Thalassemic and Healthy Control Bone Marrow Mesenchymal Stem Cells

The spectrum of each sample was analyzed using Spectrum 100 Software by considering different spectral parameters such as band frequencies, band widths and band areas. The shift in the wavenumber (frequency) value of the spectral band at peak position gives information about the structure/conformation and intermolecular interactions (Jackson *et al.,* 1997; 1999; Toyran *et al.,* 2003), while the area under the bands reflects the concentration of the related molecules (Freifelder, 1982; Toyran and Severcan, 2003; *Toyran et al.,* 2004). The band area and band wavenumber values were expressed in terms of "means and standard errors". The baseline-corrected average spectra of each sample group were used to perform accurate measurements of the spectral parameters. However, all spectra represented in the figures were normalized with respect to the amide A band centered at around 3330 cm^{-1} for illustrative purposes. Then the data were evaluated by normality test in order to decide whether the parametric or non-parametric statistical test to be used for an evaluation of statistical significancy. Since in the present study, the data showed normal distribution; spectral measurements were compared to each other by using One Way Anova and Tukey Multiple Comparison Post Test. Statistical significances were conveyed in terms of $p<0.05$, $p<0.01$, $p<0.001$. The changes in wavenumber and band area values are given in Table 3.2 and in Table 3.3, respectively.

3.4.2.2. Detailed Spectral Analysis of Thalassemic and Healthy Control Bone Marrow Mesenchymal Stem Cells

3.4.2.2.1. Comparison of Thalassemic and Healthy Control Bone Marrow Mesenchymal Stem Cells in the 3050-2800 cm^{-1} region

The deconvolved and normalized averaged representative infrared spectra of thalassemic and control BM-MSCs in the 3050-2800 cm^{-1} region are shown in Figure 3.11. The spectra were normalized with respect to the amide A band located at around 3360 cm^{-1}. The 3050-2800 cm^{-1} region contains some important bands. The band centered at 3015 cm^{-1} attributes C-H stretching mode vibrations of the H-C=C-H groups. This olefinic C-H stretching band is used to determine the level of unsaturation of phospholipid acyl chains (Takahaski *et al.,* 1991; Melin *et al.,* 2000; Liu *et al.,* 2002; Severcan *et al.*, 2005). As given in Table 3.3, there was a significant increase in the area of this band in pre-transplant group BM-MSCs (0.658±0.02) ($p<0.01$) with respect to the value of healthy control BM-MSCs (0.506±0.02). The area of this band was significantly lower in post-transplant group (0.538±0.02) ($p<0.01$) when compared to pre-transplant group (0.658±0.02).

The other bands located at 2957 cm^{-1}, 2924 cm^{-1}, 2873 cm^{-1} and 2852 cm^{-1}, belongs to CH_3 and CH_2 antisymmetrical, and CH_3 and CH_2 symmetrical vibrations, respectively (Melin *et al.*, 2000; Chang and Tanaka, 2002; Cakmak *et al.*, 2003; Severcan *et al.*, 2003; Cakmak *et al.,* 2006). The CH_3 antisymmetric, the CH_2 antisymmetric and the CH_2 symmetric stretching bands originate mainly from lipids, the CH_3 symmetric stretching band originates mainly from proteins (Mantsch, 1984; Severcan *et al.*, 2000; Severcan *et al.*, 2003; Cakmak *et al.*, 2006). As seen in Table 3.3, the area of CH_3 antisymmetric, CH_2 antisymmetric and CH_2 symmetric stretching bands significantly ($p<0.05$) increased in pre-transplant thalassemic BM-MSCs with respect to the control ones. However, after

BMT therapy we observed tendency to decrease in the area of these bands according to pre-transplant BM-MSCs.

The shifts in the wavenumber values of the CH_3 and CH_2 antisymmetric, CH_2 symmetric stretching bands are related to the order/disorder states of membrane lipids (Toyran *et al.,* 2004; Umemura *et al.,* 2000). The changes in the frequency values of the band at 2957 cm^{-1} provides structural information about deep interior part of the membrane (Mantsch, 1984; Severcan *et al.*, 1997). The wavenumber of this band tended to decrease both in pre (2957.194±0.173) and post-transplant (2957.228±0.156) BM-MSCs with respect to the healthy controls BM-MSCs (2957.428±0.124). The peak positions of CH_2 antisymmetric and symmetric stretching bands determine degree of conformational order/disorder of the membrane structures and give information about the average trans/gauche isomerization of membrane fatty acids (Mantsch, 1984; Severcan *et al.*, 1997; Bizeau *et al.*, 2000). The reduction in CH_2 antisymmetric stretching band frequency was significant in pre-transplant group (2923.88±0.144) ($p<0.05$) when compared with healthy control group (2924.68±0.342). The frequency of the CH_2 symmetric stretching band shifted to a lower values for the pre- and post-transplant groups according to the control group (Table 3.2).

Table 3.2 Changes in the wavenumber values of some infrared bands for the healthy control, pre and post-transplant BM-MSCs. The values were shown as 'mean ± standard error' for each group. The degree of significance was denoted as: *$p<0.05$ with respect to the healthy control group.

	Healthy Control (n=5)	**Pre-Transplant (n=5)**	**Post-Transplant (n=5)**
Wavenumber (cm^{-1})	**Band wavenumber**		
2957	2957.428±0.124	2957.194±0.173	2957.228±0.156
2924	2924.684±0.342	2923.88±0.144*↓	2924.316±0.122
2852	2853.022±0.376	2852.514±0.034	2852.718±0.087

Table 3.3 Changes in the band area values of the infrared bands for control, pre and post transplant BM-MSCs. The values were shown as 'mean ± standard error' for each group. The degree of significance was denoted as *p<0.05, **p<0.01, ***p<0.001 according to the healthy control group and †p<0.05, ††p<0.01 according to the pre-transplant group.

		Band Area		
Band No	**Band Wavenumber (cm-1)**	**Healthy Control (n=5)**	**Pre-Transplant Group (n=5)**	**Post-Transplant Group (n=5)**
3	**3015**	0.506±0.02	0.658±0.02 **↑	0.538±0.02 ††↓
4	**2957**	1.522±0.097	1.958±0.074 *↑	1.766±0.123
5	**2924**	2.510±0.09	3.172±0.118 *↑	2.890±0.177
6	**2873**	0.334±0.01	0.424±0.016*↑	0.38±0.026
7	**2852**	0.586 ±0.042	0.746±0.033 *↑	0.654±0.045
8	**1740**	0.40±0.01	0.48±0.01 *↑	0.41±0.02 †↓
9	**1639**	17.371±0.456	19.22±0.366 *↑	18.71±0.577
10	**1545**	7.158±0.339	11.78±0.759 ***↑	10.07±0.484 **↑
11	**1453**	1.584±0.108	2.606±0.124 ***↑	2.382±0.189 **↑
12	**1402**	2.064±0.084	3.792±0.284 ***↑	3.37±0.221 **↑
13	**1310**	1.234±0.042	2.294±0.227 **↑	1.898±0.178 *↑
14	**1234**	1.904±0.173	3.704±0.286 **↑	3.29±0.359 *↑
15	**1152**	0.634±0.114	1.996±0.141 ***↑	1,99±0.151 ***↑
16	**1080**	1.452±0.066	3.107±0.046 ***↑	2.852±0.092 ***↑ †↓
17	**1045**	1.594±0.132	3.616±0.126 ***↑	2.938±0.114***↑ ††↓
18	**1025**	1.594±0.109	3.77±0.203 ***↑	3.728±0.241 ***↑
19	**925**	0.142±0.016	0.276±0.03 **↑	0.242±0.027 *↑
20	**855**	0.068±0.004	0.094±0.017	0.088±0.008

3.4.2.2.2. Comparison of Thalassemic and Healthy Control Bone Marrow Mesenchymal Stem Cells in the 1800-800 cm^{-1} Region

The 1800-800 cm^{-1} contains several bands that originate from the protein, carbohydrates, nucleic acid vibrational modes and from the interfacial and head group vibrational modes of the membrane lipids (Mendelsohn and Mantsch, 1986). Therefore, this region is called as fingerprint region.

The band located at about 1740 cm^{-1} is assigned to the >C=O ester stretching vibration in phospholipids (Melin *et al.*, 2000; Cakmak *et al.*, 2003; Severcan *et al.*, 2003). The area of this band was significantly higher in pre-transplant group BM-MSCs (0.48±0.01) ($p<0.05$) than the healthy controls (0.40±0.01). Following BMT therapy, significant decline was observed in the post-transplant group BM-MSCs (0.41±0.02) ($p<0.05$) with respect to the pre-transplant group.

The bands located at around 1639 cm^{-1} and 1545 cm^{-1} are attributed to the amide I and amide II vibrational modes of structural proteins, respectively. The band at 1639 cm^{-1} (amide I) correspons to the C=O and C-N stretching (60%) modes of vibrations weakly coupled with the N-H bending (40%) of the polypeptide and protein backbone (Manoharan *et al.,* 1993; Haris and Severcan, 1999). However; the band at 1545 cm^{-1} (amide II) correspons to the N-H bending (60%) and the C-N stretching (40%) modes of proteins (Melin *et al*., 2000; Takahashi *et al*., 1991; Wong *et al*., 1991; Haris and Severcan, 1999; Cakmak *et al*., 2003). The band area of amide I was significantly increased in pre-tranplant MSCs (19.22±0.366) ($p<0.05$) when compared with the healthy control values (17.37±0.456). The area of amide II band was significantly higher in both the pre-tranplant group MSCs (11.78±0.759) ($p<0.001$) and post-transplant group MSCs (10.07±0.484) ($p<0.01$) with respect to the healthy control group (7.158±0.339).

The CH_2 bending vibrations of lipids are located at around 1453 cm^{-1} (Cakmak *et al.,* 2003; Di Giambattista *et al.,* 2011) and COO^- symmetric stretching vibrations of fatty acid and amino acid side chains, at around 1400 cm^{-1} (Peuchant *et al.,* 2008; Cakmak *et al.,* 2006; Melchiori *et al.,* 2010). As can be seen from Table 3.3, there were significant ($p<0.001$) increase in the areas of these two bands both in the pre- and post-transplant group BM-MSCs. The band area values of post-transplant group BM-MSCs diminished with respect to the pre-transplant group as a result of transplantation therapy.

The band located at around 1310 cm^{-1} is attributed to amide II band components and peptide side chains of protein structures (Yang *et al.,* 2005; Fujioka *et al.,* 2004; Richter *et al.,* 2002). The area of this band showed significant increase in the pre-transplant (2.294±0.227) ($p<0.01$) and post-transplant group BM-MSCs (1.898±0.178) ($p<0.05$) with respect to the healthy control BM-MSCs (1.234±0.042).

The bands, which are located in the region between 1300-1000 cm^{-1}, provide insigth about several important macromolecules such as polysaccharides and phosphate carrying compounds like phospholipids and nucleic acids (Melin *et al.,*2000; Cakmak *et al.,* 2003). The relatively strong bands at 1234 cm^{-1} and 1080 cm^{-1} are mainly due to the antisymmetric and symmetric phosphate stretching modes, respectively. They are originated from phosphodiester groups in cellular nucleic acids in addition to phospholipids, respectively (Rigas *et al.,* 1990, Wong *et al*, 1991; Wang *et al*, 1997; Cakmak *et al*., 2003). There were significant increases in the area values of phosphate antisymmetric stretching band (1234cm^{-1}) of pre-transplant (3.704±0.286) ($p<0.01$) and post-transplant BM-MSCs (3.29±0.359) ($p<0.05$) according to the healthy controls (1.904±0.173). Phosphate symmetric stretching band (1080 cm^{-1}) area also showed significant increases in similar direction in the pre-transplant (3.107±0.046) ($p<0.001$) and post-transplant

BM-MSCs (2.852±0.092) ($p<0.001$). BMT therapy caused significant decrease in the area of this band in post-transplant group (2.852±0.092) ($p<0.05$) with respect to the control group (1.452±0.066). It has been reported that the three strong peaks at 1025, 1045, 1152 cm^{-1} as a spectral contribution of glycogen might mask the PO_2^- symmetric stretching band (Chiriboga *et al*, 2000; Cakmak *et al*, 2006). The band at 1152 cm^{-1} is assigned to stretching mode of the CO-O-C groups in glycogen and nucleic acids (Rigas *et al*, 1990; Cakmak *et al*, 2003). As can be seen in Table 3.3, significant increases ($p<0.001$) were observed in the band area for pre- and post-transplant group BM-MSCs. The bands at 1025 cm^{-1} and 1045 cm^{-1} are attributed to the vibrational frequencies of $-CH_2OH$ groups and the C-O stretching frequencies coupled with C-O bending frequencies of the C-OH groups of carbohydrates (including glucose, fructose, glycogen, etc. (Parker, 1971). We observed significant increases ($p<0.001$) in the area of the bands located at 1025 cm^{-1} and 1045 cm^{-1} for pre- and post-transplant group BM-MSCs with respect to the healthy control BM-MSCs (Figure 3.12 and Table 3.3).

The 1000-800 cm^{-1} wavenumber region is composed of spectral bands that are originated from the CO stretching vibrations of protein structures and the symmetric stretching mode of dianionic phosphate (PO_3^{-2}) monoester of nucleic acids especially for DNA (Taillandier *et al*., 1992; Sahu *et al*., 2004; Lee *et al*., 2009). Relatively weak spectral bands were observed at about 925 cm^{-1} and 855 cm^{-1} which were assigned as sugar vibrations in backbone of DNA-Z form and vibrations in N-type sugars in nucleic acid backbone, respectively (Banyay and Gräslund, 2003). The area of the band located at 925 cm^{-1} was significantly higher in the pre-transplant BM-MSCs (0.276±0.03) ($p<0.01$) and post-transplant (0.242±0.027) ($p<0.05$) when compared to the healthy control BM-MSCs (0.142±0.016). As seen in Table 3.3, there were non- significant increases in the area of 855 cm^{-1} band in pre and post-transplant groups with respect to the control group.

The ratio of peak area values of the CH_2 antisymmetric strectching band (2924 cm^{-1}) to the amide I (1639 cm^{-1}) band was significantly higher ($p<0.05$) in the pre-transplant group with respect to the control group MSCs (Table 3.4). The area ratio of the bands located at 1045 cm^{-1} and 1545 cm^{-1} provide an information about the carbohydrates such as glucose, fructose and glycogen etc. in the cells (Steiner *et al*., 2003).

Table 3.4 Numerical summary of the detailed differences in the lipid-to-protein and carbohydrate-to-protein ratios of control and thalassemic BM-MSCs spectra. The values are the "mean ± standart error" for each sample. The degree of significance was denoted as *p<0.05 according to the healthy control group.

Ratio of band areas			
	Healthy Control (n=5)	**Pre-Transplant (n=5)**	**Post-Transplant (n=5)**
(CH2 antisymmetric/ amide I)	0.142 ± 0.005	0.17 ± 0.007 *↑	0.154 ± 0.007
(1045 cm-1/ amide II)	0.224 ± 0.022	0.316± 0.032 *↑	0.294 ± 0.012

3.4.2.3. Cluster Analysis

The spectra of healthy, pre- and post-transplant group BM-MSCs showed considerable differences as it was observed from general representative spectra of thalassemic and healthy BM-MSCs in Figure 3.10. In this context, on the basis of spectral differences in ATR-FTIR data, hierarchical cluster analysis was employed to differentiate and characterize healthy, pre and post-transplant group BM-MSCs. The analysis was applied to first-derivative and vector normalized spectra belonging to the samples in three different regions namely 3050-800 cm^{-1}, 3050-2800 cm^{-1} and 1800-800 cm^{-1}. The results of cluster analysis are demonstrated in Figure 3.13, 3.14 and 3.15. As seen from the dendograms, all samples were

successfully distinguished for three different spectral regions. Higher heterogeneity in cluster analysis demonstrates higher differences between sampling groups. The heterogeneity value obtained from the cluster analysis in the 3050-800 cm^{-1} region was 1.2, in the 3050-2800 cm^{-1} region was 2 and in the 1800-800 cm^{-1} region was 1.6. Macromolecular alterations that were observed from the spectral changes among control, pre- and post-transplant group BM-MSCs were clarified and supported by cluster analysis. As seen from Figure 3.13, there was only one misclassification in the cluster analysis belonging to the 3050-800 cm^{-1} region. One of the sample from pre-transplant group that was marked with ‡ mixed into post-transplant group. There were two misclassification in the cluster analysis of the 1800-800 cm^{-1} region that is presented in Figure 3.15. One sample from the control group and one sample from the post-transplant that were marked with # mixed into pre-transplant group. These results revealed that different groups can be successfully differentiated based on the spectral changes obtained from ATR-FTIR spectroscopy by cluster analysis.

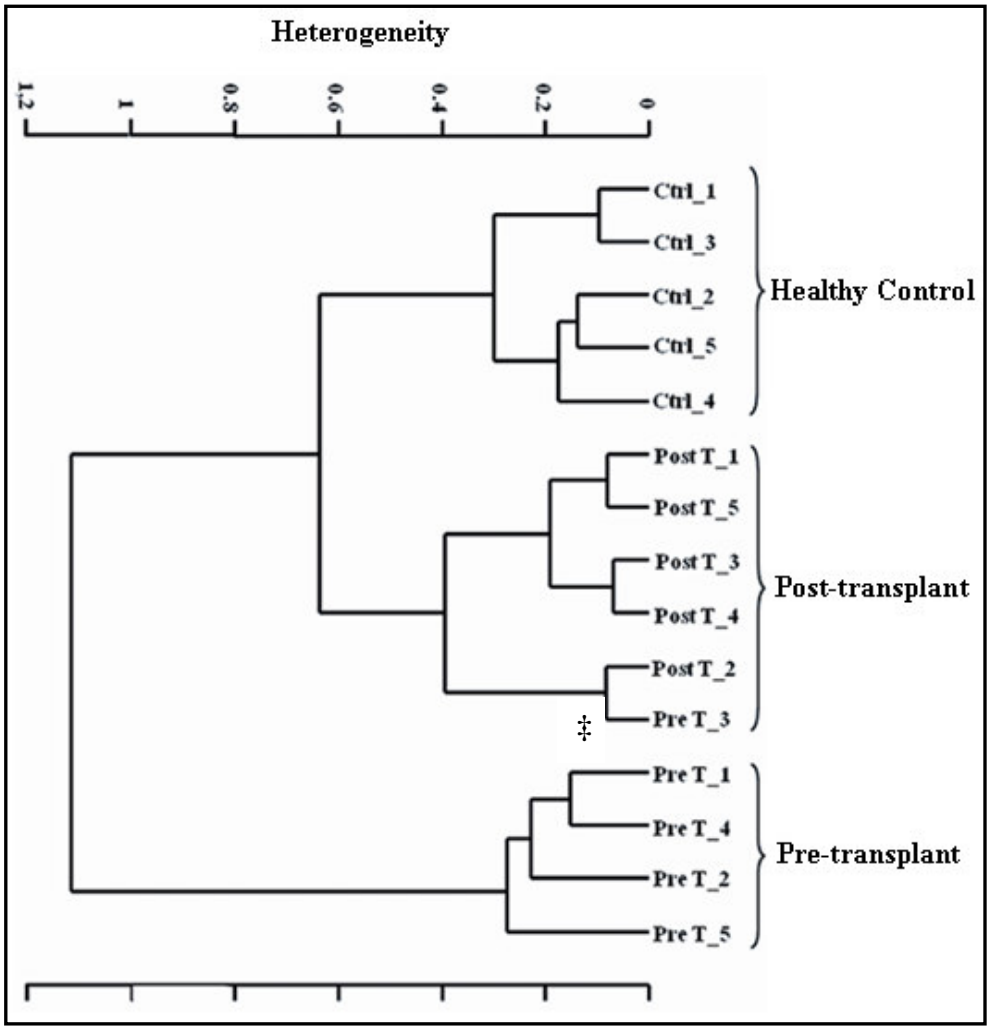

Figure 3.13 Hierarchical cluster analysis performed on the first-derivative and vector normalized spectra of control, pre- and post-transplant group BM-MSCs and resulting from Ward's algorithm. The analysis was applied in the 3050-800 cm^{-1} spectral region. The mixed sample was marked with ‡.

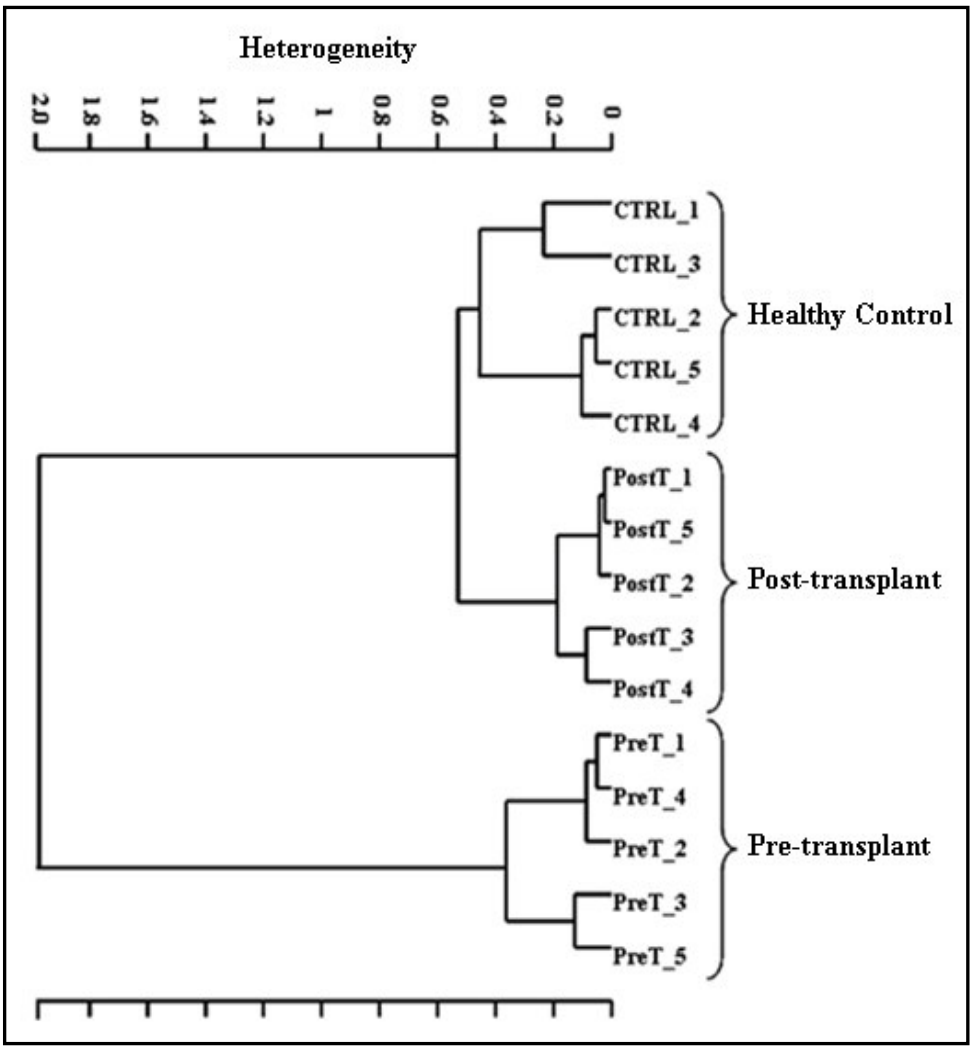

Figure 3.14 Hierarchical cluster analysis performed on the first-derivative and vector normalized spectra of control, pre- and post-transplant group BM-MSCs and resulting from Ward's algorithm. The study was applied in the 3050-2800 cm^{-1} spectral region.

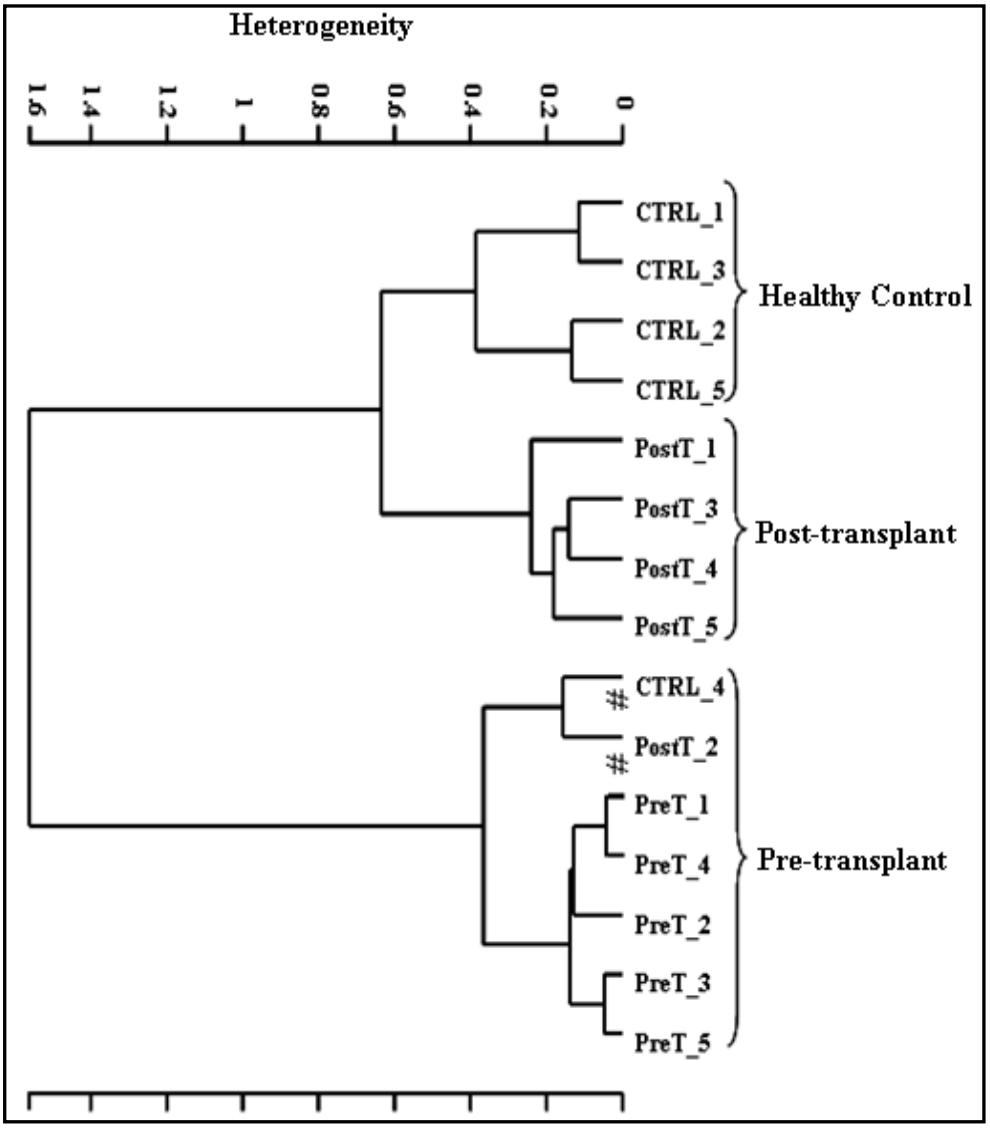

Figure 3.15 Hierarchical cluster analysis performed on the first-derivative and vector normalized spectra of control, pre and post-transplant group BM-MSCs and resulting from Ward's algorithm. The study was applied in the 1800-800 cm^{-1} spectral region. The mixed samples were marked with #.

3.4.2.4. FTIR Microspectroscopic Analysis and Comparison of Thalassemic and Healthy Control Bone Marrow Mesenchymal Stem Cells

FTIR microspectroscopy provides spatially resolved information on unstained thin tissue samples or cell monolayers by allowing the generation of IR images with high image contrast. Unlike staining techniques, IR spectroscopy with its label-free, non-invasive and non-destructive properties generates information about relative concentrations and structure of macromolecules by considering alterations in the infrared spectra and the specific heterogeneties (Krafft *et al*., 2006, Diem *et al*., 2008). In this context, "FTIR imaging contains a multiplicity of contrast yielding mechanisms that are derived from variations in the chemical composition, without the addition of extrinsic markers or stains" (Lester *et al.*, 1998).

In the first part of the study, the chemical maps of thalassemic and healthy control BM-MSCs were obtained by FTIR microspectroscopy to get functional group images of the main biological molecules of interest. Figures 3.16, 3.17, 3.18 and 3.19 show the chemical maps of pre-transplant, post-transplant thalassemic and healthy MSCs. These figures were obtained using high resolution aperture size (6.25µm x 6.25µm pixel size). Chemical maps that are obtained from IR microspectroscopy allow us to track the distribution of chemical entities in accordance with their relative absorbance intensity level for a chosen wavenumber in a pixel-by-pixel fashion. In the chemical maps, the absorbance intensity is proportional with the color changes that are represented by color scales from blue (lowest intensity) to red (highest intensity).

The average colored chemical maps of lipids which was derived from the peak integrated areas of the CH_2 antisymmetric stretching and CH_2 symmetric stretching bands are seen in Figure 3.16 and 3.17, respectively. Each chemical map is composed of thousands of spectra. The mean area values of mentioned bands from

the highest (red color) to lowest (blue color) concentrations are demonstrated by absorbance values in color bars. As seen from the figures and the mean absorbance values stated under the figures, lipid concentration of thalassemic BM-MSCs were higher than healthy MSCs. Lipid contents in post-transplant group decreased after BMT therapy. The changes in the lipid content that were obtained by IR microspectroscopy similar with the ATR-FTIR spectroscopy results.

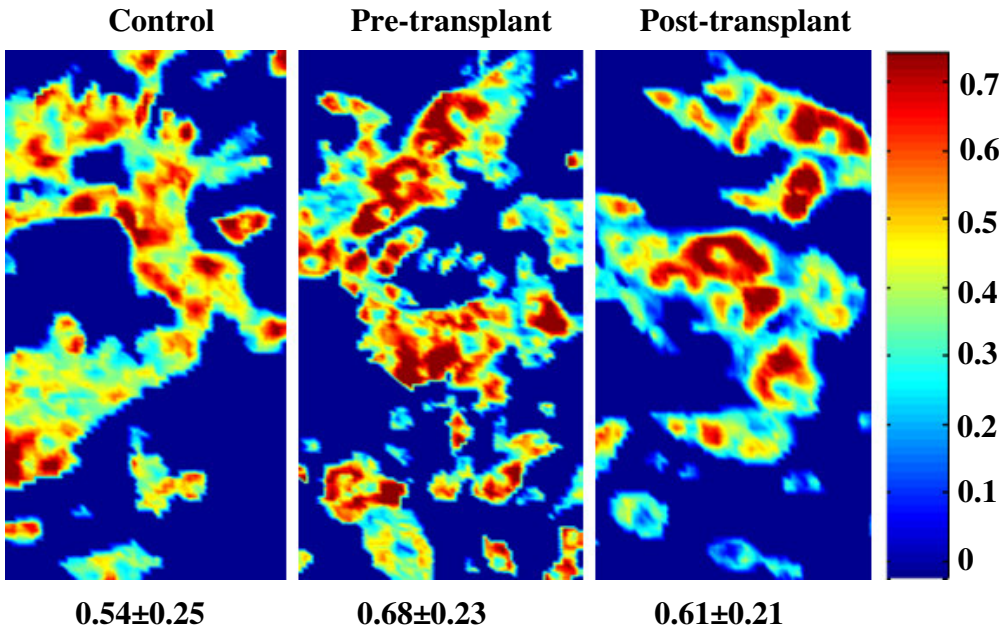

Figure 3.16 Spectral image maps of control, pre- and post-transplant BM-MSCs, which were derived from the peak integrated areas of CH_2 antisymmetric stretching band, reflect lipid distribution in cells. Mean absorbance values of each map was given under the maps.

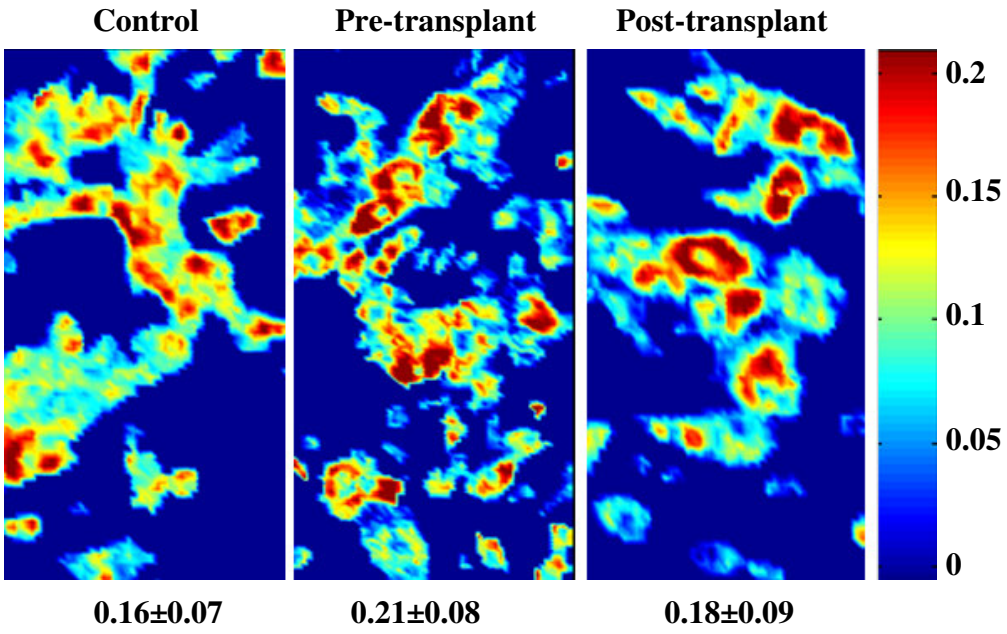

Figure 3.17 Spectral image maps of control, pre and post transplant BM-MSCs, which were derived from the peak integrated areas of CH_2 symmetric stretching band, reflect lipid distribution in cells. Mean absorbance values of each map was given under the maps.

The protein distributions in control, pre- and post-transplant group BM-MSCs are seen in Figure 3.18A and 3.18B. Chemical maps were derived by calculating integrated area values of the amide I and amide II vibrational modes of structural proteins, respectively. The absorbance values reflected that the protein content in the BM-MSCs was higher in pre-transplant group BM-MSCs and decreased following BMT therapy. The results of FTIR imaging supported the results of ATR-FTIR spectroscopy.

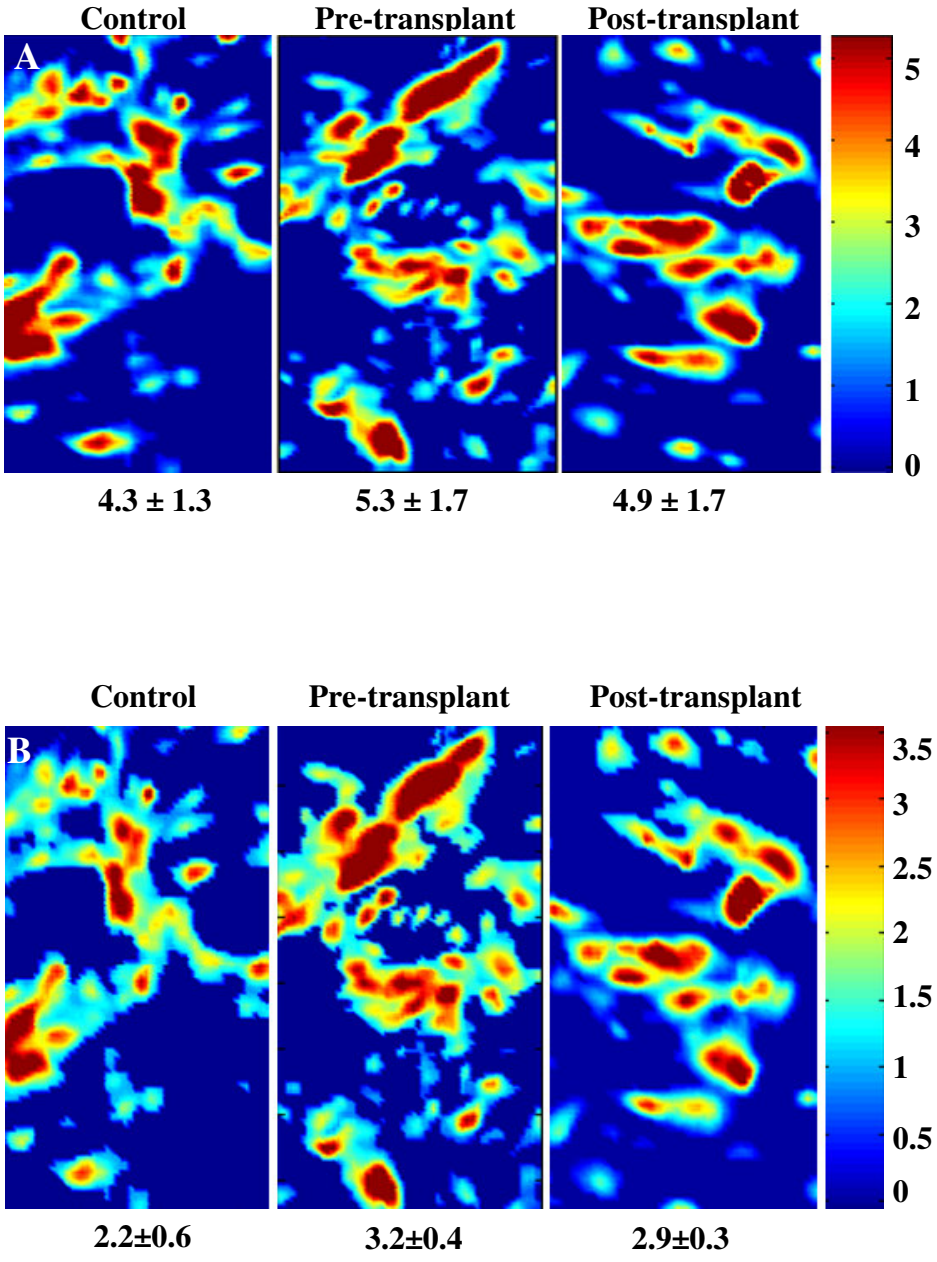

Figure 3.18 Spectral image maps of control, pre and post transplant BM-MSCs. **A)** Chemical maps were derived from the peak integrated areas of amide I and **B)** chemical maps were derived from the peak integrated areas of amide II band, reflect protein distribution in cells. Mean absorbance values of each map was given under the maps.

The distribution of nucleic acids in BM-MSCs is given in Figure 3.19. Chemical maps of thalassemic and healthy control BM-MSCs were derived by calculating integrated band area value of PO_2^- antisymmetric band. As it can be seen from the figure**,** the nucleic acid content in the BM-MSCs was the highest in pre-transplant group BM-MSCs and decreased after BMT therapy. These results are in agreement with the results of ATR- FTIR imaging data

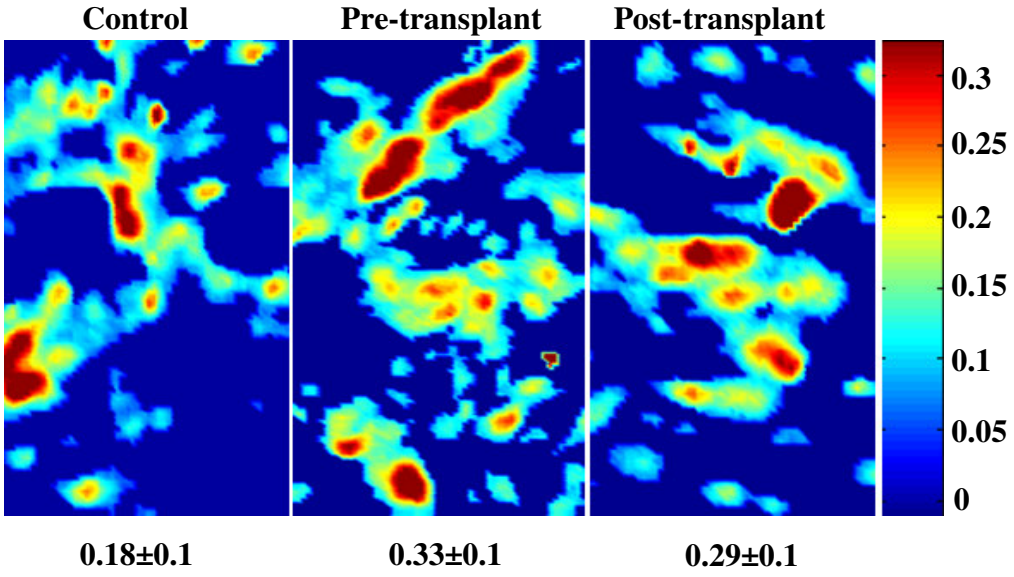

Figure 3.19 Spectral image maps of control, pre and post transplant BM-MSCs, which were derived from the peak integrated areas of PO_2^- antisymmetric stretching band, reflects nucleic acid distribution in cells. Mean absorbance values of each map was given under the maps.

3.4.3. Comparison of Spectra of Bone Marrow Mesenchymal Stem Cells from Different Age Groups

In the second part of the thesis study, molecular level differences or similarities between healthy BM-MSCs from different age groups were investigated by FTIR spectroscopy and microspectroscopy.

3.4.3.1. General Information about Numerical Comparisons of the Bands of Bone Marrow Mesenchymal Stem Cells from Different Age Groups

The spectrum of each sample was analyzed by Spectrum 100 Software by considering different spectral parameters like band frequencies, band widths and band areas that were expressed in terms of "means and the standard errors". Then the data were evaluated by normality test in order to decide whether the parametric or non-parametric statistical test to be used. Since the data showed normal distribution, spectral measurements were compared to each other by using One Way Anova and Tukey Multiple Comparison Test. Statistical significances were conveyed in terms of $p<0.05$, $p<0.01$, $p<0.001$. The changes in band area values are given in Table 3.5

3.4.3.2. Detailed Spectral Analysis of Bone Marrow Mesenchymal Stem Cells from Different Age Groups

Figure 3.20 shows the general representative FTIR spectrum of the healthy human BM-MSCs from different age donors in 3800-800cm^{-1} spectral region. As can be seen from the quite complex spectrum that contains several bands representing many different functional groups of lipids, proteins, carbohydrates and nucleic acids. The positions of these bands are assigned in Table 3.1. The spectra of BM-MSCs from all age groups were analyzed in two major regions; 3050-2800 cm^{-1}

and 1800-900 cm^{-1}. The baseline-corrected average spectra were used to perform accurate measurements of the spectral parameters like band frequencies, band widths and band areas. All spectra presented in the figures were normalized with respect to the amide A band centered at around 3330 cm^{-1} for illustrative purposes.

3.4.3.2.1. Comparison of Bone Marrow Mesenchymal Stem Cells from Different Age Groups in the 3050-2800 cm^{-1} region

Figure 3.21 represents the deconvolved and normalized FTIR spectra of BM-MSCs from five different age groups in the 3000-2800 cm^{-1} region. This region contains five main bands belonging to stretching modes of the olefinic =CH, CH_2 and CH_3 groups of unsaturated and saturated lipids. The bands at 2957 cm^{-1} and 2873 cm^{-1} are assigned to the CH_3 antisymmetric and symmetric stretching vibrations. The CH_3 antisymmetric streching band originates mainly from lipids, whereas CH_3 symmetric stretching bands originates with th contribution of proteins (Cakmak et al., 2011; Gorgulü *et al*., 2007; Takahashi *et al*., 2001). The CH_2 antisymmetric and symmetric stretching vibrations of methylene ($-CH_2$) groups of fatty acids are located at around 2924 and 2852 cm^{-1}, respectively (Kneipp *et al*., 2002; Melin *et al*., 2000; Cakmak *et al*., 2003).

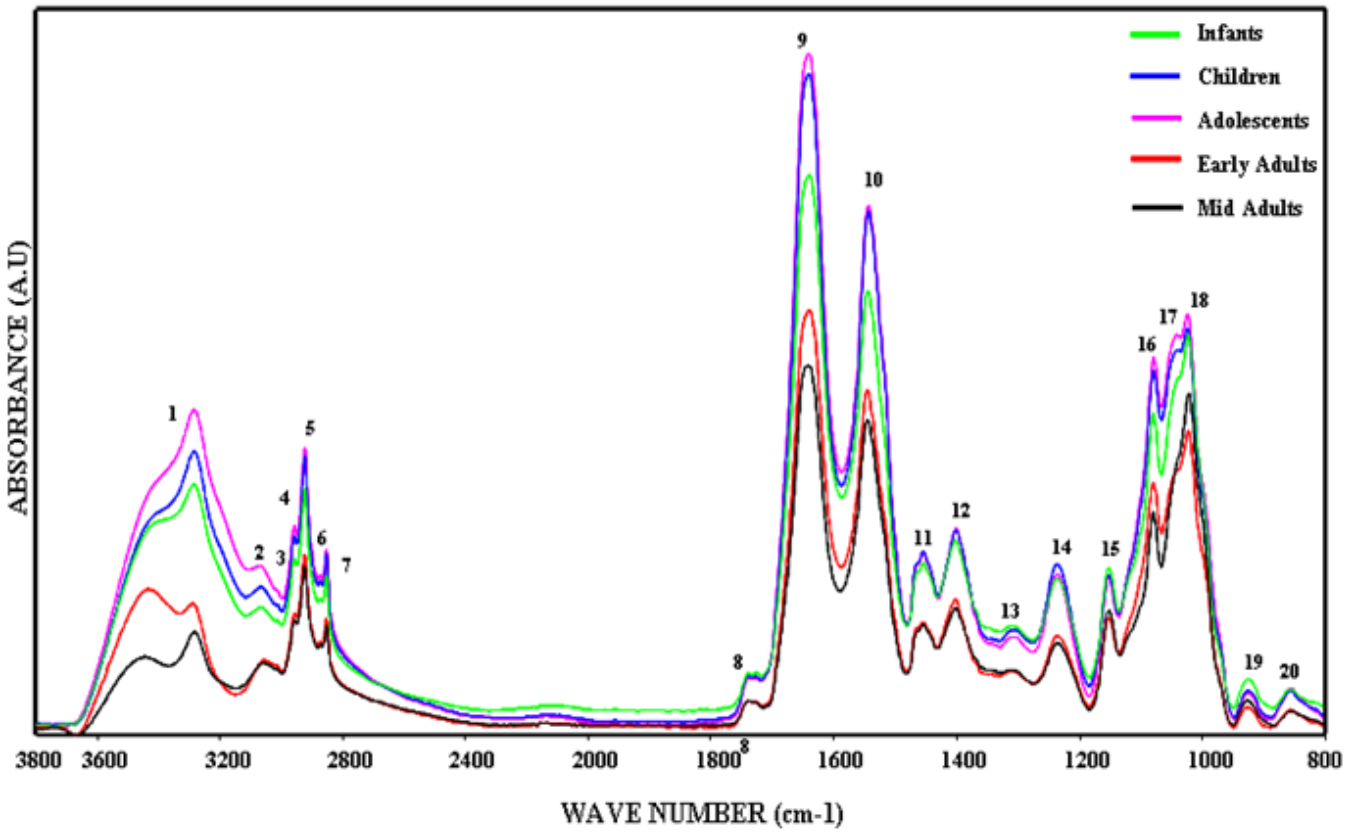

Figure 3.20 The represantative infrared spectra of healthy BM-MSCs from five different age groups. Green line represents infants's MSCs, blue line represents children's MSCs, pink line represents adolescents's MSCs, red line represents early adults's MSCs and black line represents mid-adults MSCs in the 1800-800 cm^{-1} region. (The spectra were normalized with respect to the amide A band).

Table 3.5 The band area values of healthy MSCs from five different age groups. The values were shown as 'mean ± standard error' for each group. The degree of significance was denoted as: *p<0.05, **p<0.01, ***p<0.001 with respect to the infants, †p<0.05, ††p<0.01, †††p<0.001 with respect to the children, #p<0.05, ##p<0.01, ###p<0.001 with respect to the adolescents.

	Band Area					
Band No	**Wavenumber (cm-1)**	**Infants**	**Children**	**Adolescents**	**Early Adults**	**Mid Adults**
3	**3015**	0.046±0.01	0.046±0.002	0.066±0.01	0.04±0.004	0.04±0.004
4	**2954**	0.85±0.022	1.08±0.047 **↑	1.18±0.059 ***↑	0.89±0.042 ††,###↓	0.84±0.015 ††,###↓
5	**2924**	2.09±0.064	2.57±0.048 ***↑	2.82±0.029 ***↑	1.99±0.119 †††,###↓	1.93±0.026 †††,###↓
6	**2873**	0.26±0.011	0.33±0.016 *↑	0.35±0.023 **↑	0.25±0,009 †,##↓	0.25±0.012 †,###↓
7	**2852**	0.61±0.013	0.68±0.021	0.71±0.02 **↑	0.61±0.022 ††↓	0.60±0.009 †,###↓
8	**1740**	0.35±0.019	0.38±0.014	0.39±0.008	0,34±0.017	0.34±0.01
9	**1639**	12.92 ±0.408	16.13±0.249 ***↑	17.87±0.646 ***,†↑	12.01±0.285 †††↓	11.41±0.193 †††,###↓
10	**1545**	10.60±0.945	12.52±0.163	13.44±0.552 **↑	9.02±0.181 †††,### ↓	8.49±0.228 †††,###↓
11	**1453**	2.77±0.184	3.02±0.271	3.15±0.11	2.17±0.063 †,##↓	2.13±0.113 ††,###↓
12	**1402**	3.77±0.308	4.38±0.135	4.41±0.143	3.61±0.221	3.50±0.161 †,#↓
13	**1310**	2.42±0.19	2.70±0.178	2.73±0.109	2.27±0.05	2.20±0.059 †,#↓
14	**1234**	3.89±0.23	4.84±0.117 **↑	4.87±0.101 **↑	3.54±0.33 †††,### ↓	3.44±0.182 †††,###↓
15	**1152**	2.63±0.119	2.69±0.112	2.75±0.087 †↑	2.17±0.101 *,††,## ↓	2.12±0.084 *,††, ## ↓
16	**1080**	3.12±0.054	3.76±0.146	3.85±0.171	3.07±0.242 #↓	2.90±0.194 †,#↓
17	**1045**	3.72±0.096	4.50±0.139 ** ↑	4.74±0.149 *** ↑	2.94±0.111 **, †††, ### ↓	3.09±0.075 *,†††, ### ↓
18	**1025**	3.62±0.32	4.74±0.292 **↑	5.52±0.119 *** ↑	3.47±0.227 ††, ### ↓	4.14±0.151 ## ↓
19	**925**	0.20±0.009	0.24±0.014	0.29±0.01 ** ↑	0.23±0.011 #↓	0.22±0.02 ## ↓
20	**855**	0.10±0.009	0.15±0.021	0.20±0.033 *↑	0.15±0.012	0.10±0.022 #↓

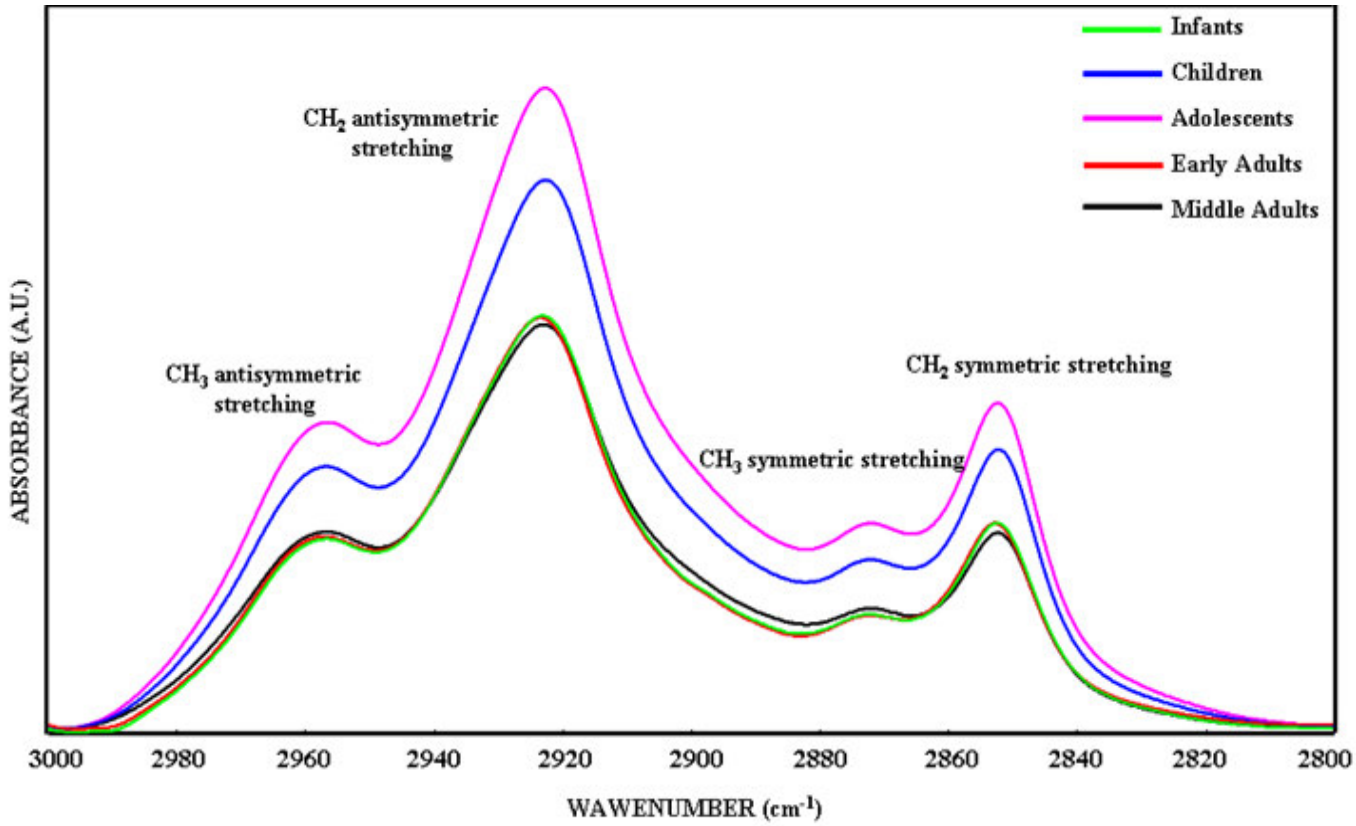

Figure 3.21 The representative infrared spectra of healthy MSCs from five different age groups in the 3000-2800 cm^{-1} region. (The deconvolved spectra were normalized with respect to the amide A band).

The band area values under the spectral bands gives us an information about the concentration of the corresponding functional groups (Kneipp *et al*., 2002; Bruno *et al*., 1999; Krafft *et al*., 2007; Manoharan *et al*., 1993). As can ben seen in Table 3.5, the band area values of the CH_3 antisymmetric stretching band at 2957 cm^{-1} was significantly higher in the children group ($p<0.01$) and adolescents group ($p<0.001$) with respect to the infants group. The area of this band decreased significantly in early adults ($p<0.01$) and mid adults BM-MSCs ($p<0.01$) in comparison to the area of children group BM-MSCs. The area of this band decreased significantly in early adults ($p<0.001$) and mid adults BM-MSCs ($p<0.001$) according to the area of adolescents groups MSCs.

As seen from Figure 3.21 and Table 3.5, the area of the CH_2 antisymmetric stretching band of BM-MSCs increased significantly in the children group ($p<0.001$) and the adolescents group ($p<0.001$) with respect to the infants group. Meanwhile, the area of this band decreased significantly in early adults ($p<0.001$) and mid adults ($p<0.001$) when they were compared with the area of children and adolescents groups BM-MSCs.

As it is given in Table 3.5, the area values of the CH_3 symmetric stretching band were higher in children ($p<0.05$) and adolescents ($p<0.01$) groups with respect to the infants group BM-MSCs. The area of this band decreased in early adults BM-MSCs ($p<0.05$) and mid adults BM-MSCs ($p<0.05$) according to the value of children groups BM-MSCs. Similarly, the area of this band decreased in early adults BM-MSCs ($p<0.01$) and mid adults BM-MSCs ($p<0.001$) according to the value of adolescents groups BM-MSCs.

The CH_2 symmetric stretching band area was higher in adolescents group BM-MSCs ($p<0.01$) with respect to infants groups BM-MSCs. The band area degrees decreased

in early adults BM-MSCs ($p<0.01$) and mid adults BM-MSCs ($p<0.05$) with respect to children group BM-MSCs. The band area value of mid adults BM-MSCs decreased significantly ($p<0.05$) when compared with the area value of adolescents group (Table 3.5).

3.4.3.2.2. Comparison of Bone Marrow Mesenchymal Stem Cells from Different Age Groups in the 1800-800 cm^{-1} region

In Figure 3.22, the 1800-900 cm^{-1} spectral region is shown. This region contains vibrational modes of several distinct functional groups belonging to lipids, proteins, carbohydrates and nucleic acids. The band centered at 1740 cm^{-1} is associated with C=O stretching vibrations of esters bonds of tryglycerides (Mantsch, 1984; Steiner *et al*., 2003; Cakmak *et al*., 2006). As it is given Table 3.5, the band area values of this band were higher for children and adolescent group BM-MSCs than the infants, early and mid adults BM-MSCs non-significantly. However, such an unsignificant increase is in the same direction with the band area changes of other lipid bands located at 3000-2800 cm^{-1} spectral region.

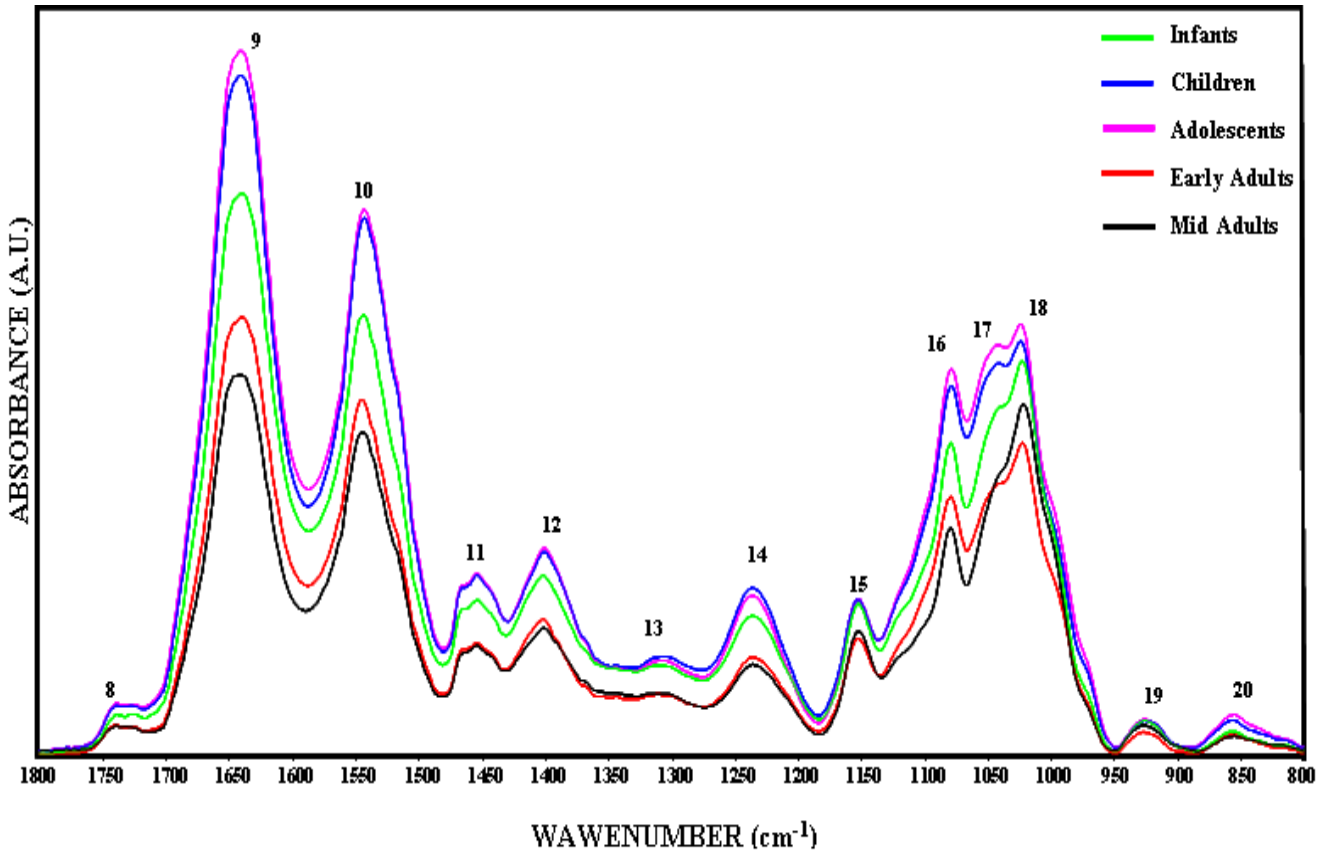

Figure 3.22 The represantative infrared spectra of of healthy MSCs from five different age groups in the 1800-800 cm^{-1} region. (The spectra were normalized with respect to the amide A band).

The amide I band is located in the same region at around 1639 cm^{-1} which arises from the C=O hydrogen bonded stretching and C=N bending vibrations (60%) weakly coupled with the N-H bending (% 40) of polypeptides and protein backbone. The another protein band, which is called as amide II at 1545 cm^{-1}, is assigned to the C-N stretching (40%) and NH bending vibrations (60%) (Manoharan *et al.*, 1993; Haris and Severcan, 1999). As it is shown in the Figure 3.22 and Table 3.5, amide I band and amide II band area values of BM-MSCs were higher in children and adolescents groups than infants, early and mid adults groups. The increases in the area of amide I band were significant in children ($p<0.001$) and adolescents ($p<0.001$). However, significant decreases were observed in the amide I band area of early adults MSCs ($p<0.001$) and mid adults BM-MSCs ($p<0.001$) with respect to the area of children BM-MSCs. The amide I band area also decreased significantly in mid adults BM-MSCs ($p<0.001$) according to the adolescents BM-MSCs. Amide II band area value of adolescents BM-MSCs were higher significantly ($p<0.001$) when compared with the value of infants BM-MSCs. The area of amide II band, significanty decreased in early adults ($p<0.001$) and mid adults ($p<0.001$) according to the children and adolescents BM-MSCs.

From the FTIR spectrum, a precise lipid-to-protein ratio can be derived by calculating the ratio of the areas of the bands arising from lipids and proteins. The ratio was calculated as the ratio of the sum of the areas of the CH_2 antisymmetric and CH_2 symmetric stretching bands to the area of the amide I band, which was non-significantly lower in adolescents's BM-MSCs (0.198±0.007) when it was compared with infants's BM-MSCs (0.211±0.011), children's BM-MSCs (0.202±0.005), early adults's BM-MSCs (0.216±0.006) and mid adults's BM-MSCs (0.222±0.004). The decrease in the lipid to protein ratio reflected that there was a more pronounced increase in protein content than an increase in the lipid content. Elevated levels of lipid and protein contents in the adolescents BM-MSCs

with respect to the other groups were supported by the results of lipid to protein ratio.

There were non-significant increases in the area of CH_2 bending vibration of lipids at 1453 cm^{-1} for children and adolescents BM-MSCs (Table 3.5) (Cakmak et al., 2003; Manoharan et al., 2003). However, the area value of the band decreased significantly in early adults BM-MSCs ($p<0.05$) and mid adults BM-MSCs ($p<0.01$) with respect children BM-MSCs. Significant decreases in the area of this band of early adults BM-MSCs ($p<0.01$) and mid adults BM-MSCs ($p<0.001$) were also observed according to adolescents BM-MSCs (Table 3.5).

The band at 1401 cm^{-1} corresponds to the stretching vibration mode of C=O in the COO^- group of amino acid side chains and fatty acids (Krafft *et al.*, 2007; Parker, 1971). The area of this band was higher in children and adolescent BM-MSCs than the infants, early and mid adults BM-MSCs. Area of this band decreased significantly in mid adults BM-MSCs ($p<0.05$) with respect to children and adolescent BM-MSCs.

The band at 1310 cm^{-1} is assigned to amide III band components and peptide side chain vibrations of protein structures (Yang *et.al*., 2005; Fujioka *et al*., 2004; Richter *et al*., 2002). BM-MSCs of children and adolescents demonstrated higher band area values, while significant decreases were observed in the area of mid adults BM-MSCs ($p<0.05$) with respect of children and adolescent BM-MSCs.

The strong bands at 1234 cm^{-1} and 1080 cm^{-1} arise from antisymmetric and symmetric stretching vibrations of phosphodiester groups that are present in the phosphate moieties (PO_2^-) of nucleic acid backbone structures and phospholipids (Melin *et al*., 2000, Rigas *et al*., 1990). Children and adolescents BM-MSCs had significantly ($p<0.01$) higher PO_2^- antisymmetric stretching band area values with

respect to the infants BM-MSCs. As it is illustrated in Table 3.5, the lower band area values for PO_2^- antisymmetric stretching band in early and mid adults BM-MSCs were significant ($p<0.001$) according to the children and adolescents BM-MSCs. Similar band area alterations were observed in the PO_2^- symmetric stretching band is located at around 1080 cm^{-1}. There was a significant decrease in the band area degree of early adults and mid adults BM-MSCs ($p<0.05$) with respect to children and adolescents BM-MSCs.

The area of the band at 1152 cm^{-1}, which is due to stretching mode of the C-O-O-C groups existing in glycogen and nucleic acids (Rigas et al., 1990; Cakmak et al., 2003), was higher in children and adolescents BM-MSCs. The band area of early adults ($p<0.01$) and mid adults ($p<0.01$) BM-MSCs tended to decrease significantly when compared with the band area values of infants, children and adolescents BM-MSCs. The other two bands located at about 1025 cm^{-1} and 1045 cm^{-1} are attributed from the vibrational frequency of $-CH_2OH$ groups and the C-O stretching frequencies coupled with C-O bending frequencies of the C-OH groups of carbohydrates (including glucose, fructose, glycogen, etc.) (Parker, 1971). As it is given in Table 3.5, while increases in the area values of 1045 cm^{-1} band of children ($p<0.01$) and adolescents ($p<0.001$) were significant with respect to infants BM-MSCs, early adults ($p<0.01$) and mid adults ($p<0.05$) BM-MSCs showed significant decreases with respect to the infants BM-MSCs. We also observed significant decreases in the area of this band in early adults ($p<0.001$) and mid adults ($p<0.001$) BM-MSCs according to the band area values of children and adolescents BM-MSCs. Children ($p<0.05$) and adolescents ($p<0.001$) BM-MSCs had also significantly higher intensity values for 1025 cm^{-1} band than infants. On the contrary, early adults ($p<0.01$ and $p<0.001$) and mid adults ($p<0.01$) BM-MSCs had lower band areas according to the children and adolescents BM-MSCs, respectively.

The two bands at about 925 cm^{-1} and 855 cm^{-1} are assigned to sugar vibrations in left handed Z type DNA (Dovbeshko *et al*., 2002). The area of these bands increased in adolescent BM-MSCs significantly ($p<0.05$), ($p<0.01$) according to the infants BM-MSCs. However, in early adult ($p<0.05$) and mid adults BM-MSCs ($p<0.05$) band area values decreased significantly with respect to the adolescent BM-MSCs.

3.4.3.3. Cluster Analysis

The spectra of BM-MSCs of infants, children, adolescents, early and mid adults shows considerable differences as can be seen from Figure 3.20. Therefore, hierarchical cluster analysis was employed to discriminate and characterize BM-MSCs belonging to the different age groups healthy donors by evaluating the spectral differences in ATR-FTIR data. The analysis was applied to first-derivative and vector normalized spectra of twenty-five independent spectra of five sampling groups in three different regions 3000-800 cm^{-1}, 3000-2800 cm^{-1} and 1800-800 cm^{-1}. The results of cluster analysis are demonstrated in Figures 3.23, 3.24 and 3.25. As seen from the dendograms, all samples were successfully distinguished for five different spectral regions. Higher heterogeneity value in cluster analysis demonstrates higher differences among analyzed groups. The heterogeneity value obtained from the cluster analysis in the 3000-800 cm^{-1} region was 1.4 and one sample from children group that was marked with # mixed into the adolescents (Figure 3.23). The heterogeneity value of cluster analysis was 1 for 3000-2800 cm^{-1} region and was 1.4 for 1800-800 cm^{-1} region. As seen from these two dendograms, all samples were successfully distinguished for five sampling groups as in distinct clusters. Cluster analysis verified and strengthened the spectral differences that reflected significant macromolecular alterations among MSCs of infants, children, adolescents, early and mid adults.

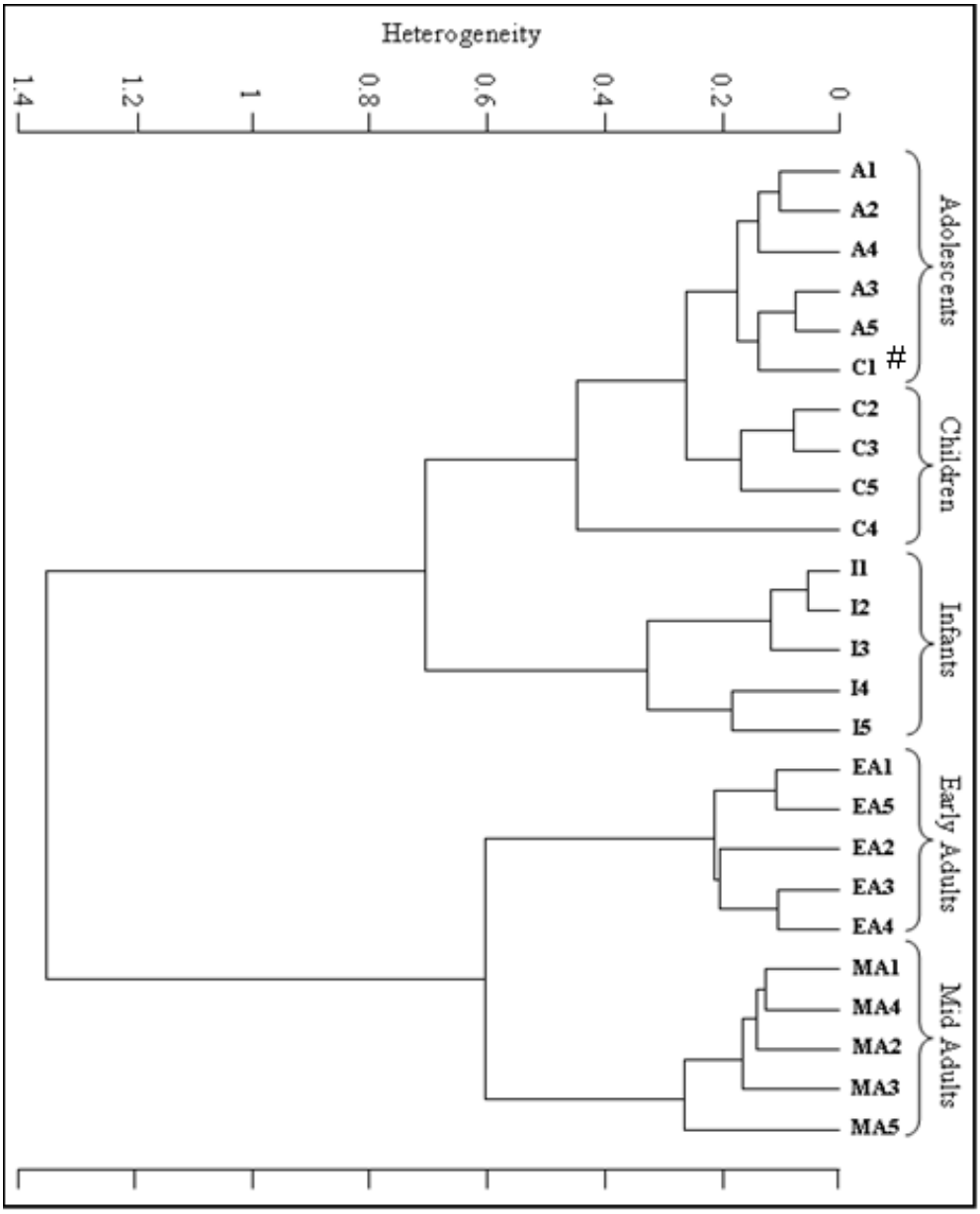

Figure 3.23 Hierarchical cluster analysis performed on the first-derivative and vector normalized spectra of BM-MSCs of infants, children, adolescents, early and mid adults, and resulting from Ward's algorithm. The study was conducted in the 3000-800 cm^{-1} spectral region.

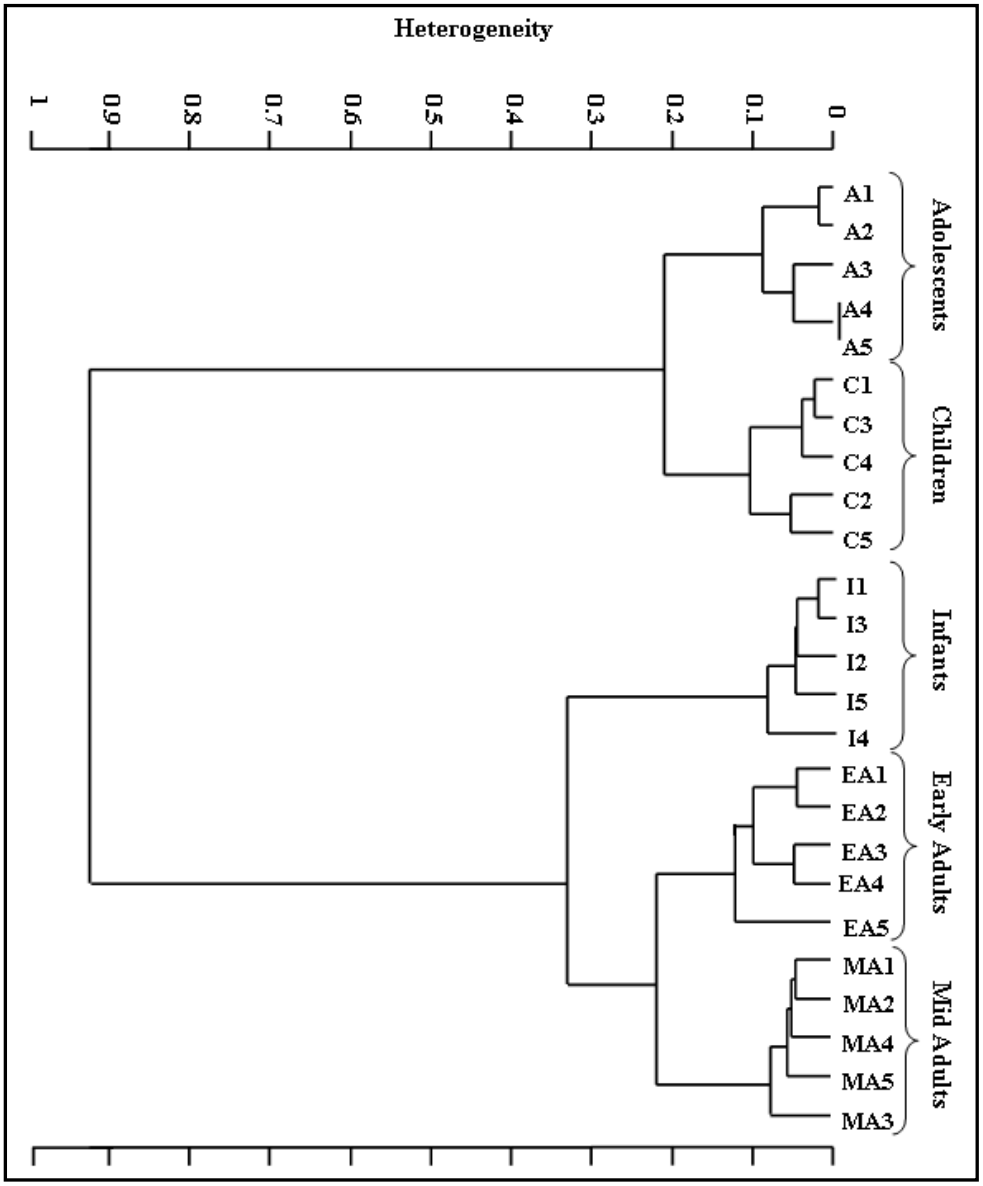

Figure 3.24 Hierarchical cluster analysis performed on the first-derivative and vector normalized spectra of BM-MSCs of infants, children, adolescents, early and mid adults, and resulting from Ward's algorithm. The study was conducted in the 3000-2800 cm^{-1} spectral region.

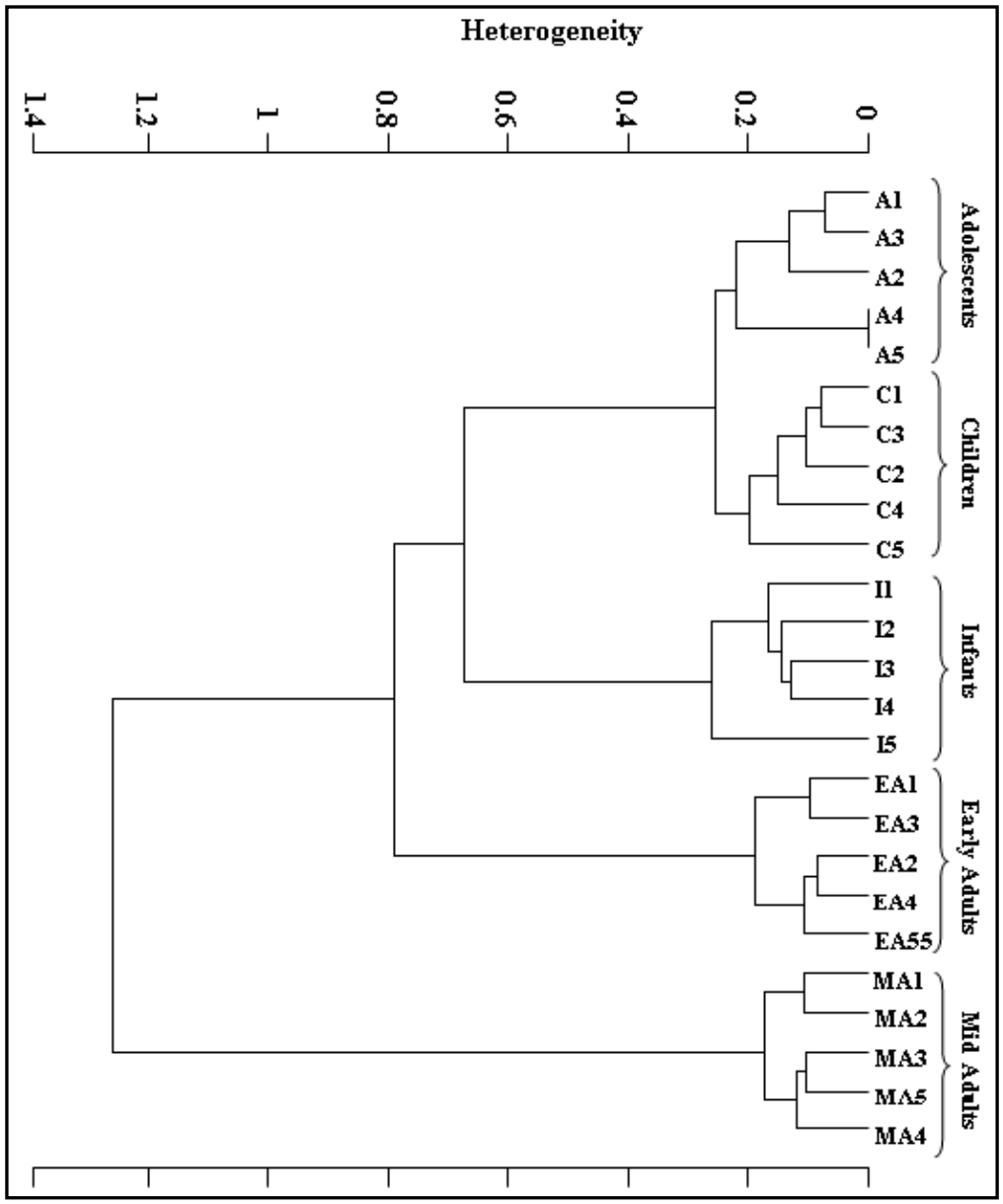

Figure 3.25 Hierarchical cluster analysis performed on the first-derivative and vector normalized spectra of BM-MSCs of infants, children, adolescents, early and mid adults, and resulting from Ward's algorithm. The study was conducted in the 1800-800 cm^{-1} spectral region.

3.4.3.4. FTIR Microspectroscopic Analysis and Comparison of Bone Marrow Mesenchymal Stem Cells from Different Age Groups

The C-H region was used to evaluate the total lipid content in the cells. The another band in this region is CH_3 symmetric stretching band located at 2873 cm^{-1} that is mainly resulted from proteins. Since this band is very weak, the CH region is concidered in terms of contribution of lipid bands. The average maps were colored according to the peak integrated areas of CH_2 antisymmetric and CH_2 symmetric stretching bands that are two main lipid bands located in C-H region. While red color corresponds to the highest ratio and blue color corresponds to the lowest ratio in the color bar. The mean absorbance values of each map stated under the figures. As it can be seen from the Figures 3.26 and 3.27, lipid concentration of adolescent BM-MSCs was the highest value supporting to the ATR-FTIR spectroscopy results.

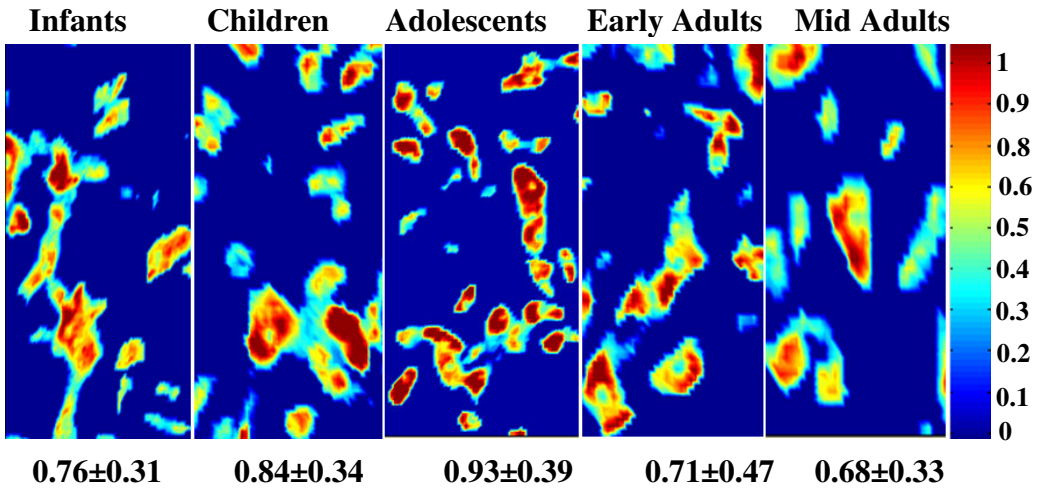

Figure 3.26 Spectral image maps of BM-MSCs from five different age groups, which were derived from the peak integrated areas of CH_2 antisymmetric stretching band, reflect lipid distribution in cells. Mean absorbance values of each map was given under the maps.

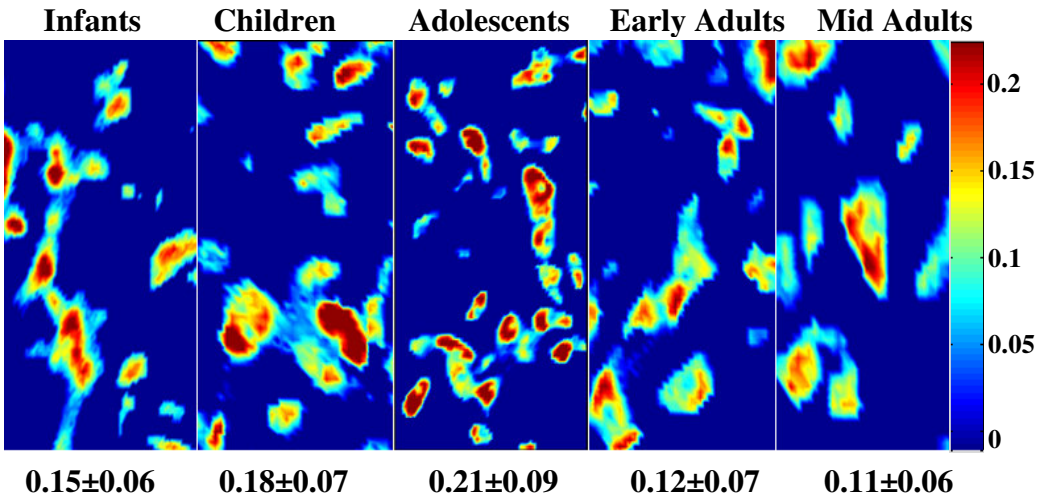

Figure 3.27 Spectral image maps of BM-MSCs from five different age groups, which were derived from the peak integrated areas of CH_2 symmetric stretching band, reflect lipid distribution in cells. Mean absorbance values of each map was given under the maps.

In order to examine protein distribution in BM-MSCs, chemical maps of cells were constituted according to the integrated band area of amide I and amide II bands from IR images. Figure 3.28 and Figure 3.29 show amide I and amide II band area images, respectively. The difference in the protein contents can be understand from the values of band areas that were stated under the chemical maps of each group, in addition to the representative differences among chemical maps. The absorbance values reflected that the protein content in the adolescents was higher then the other sampling groups. The results of FTIR imaging are in agreement with the results of ATR-FTIR spectroscopy.

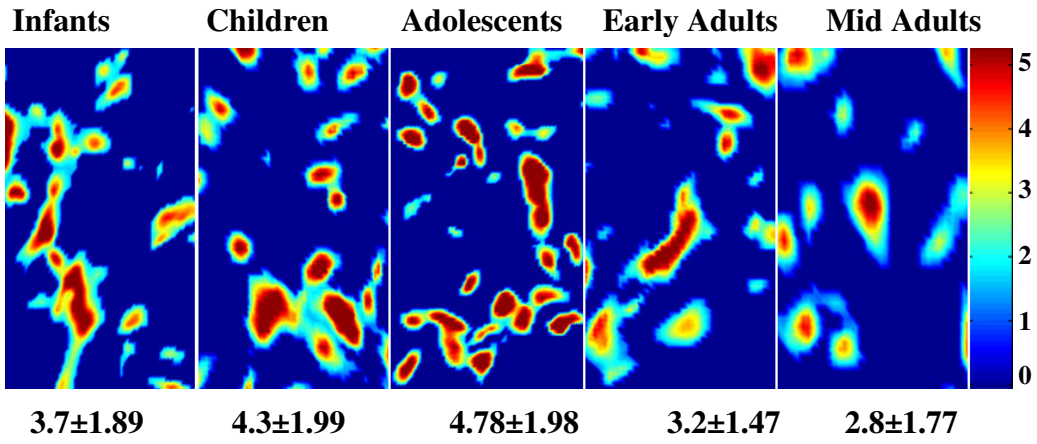

Figure 3.28 Spectral image maps of from five different age groups BM-MSCs, which were derived from the peak integrated areas of amide I band, reflect lipid distribution in cells. Mean absorbance values of each map was given under the maps.

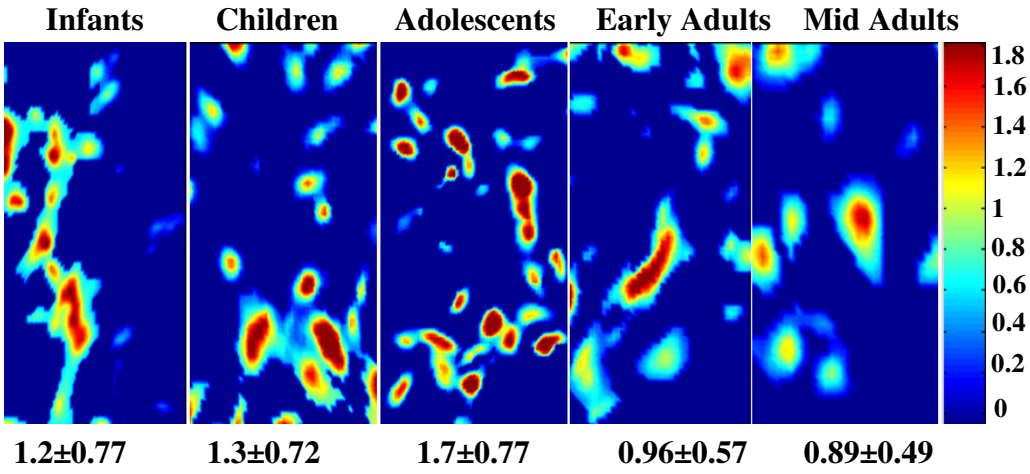

Figure 3.29 Spectral image maps of from five different age groups BM-MSCs, which were derived from the peak integrated areas of amide II, reflect lipid distribution in cells. Mean absorbance values of each map was given under the maps.

The alterations in nucleic acid distribution in BM-MSCs from different age groups were determined by considering the changes in PO_2^- integrated band area. As it is given in the mean absorbance values (Figure 3.30), the nucleic acid concentration of adolescents BM-MSCs was the highest degree according to the other groups. The alterations in the concentration of nucleic acid in BM-MSCs from different age groups were similar with the results of ATR-FTIR spectroscopy data.

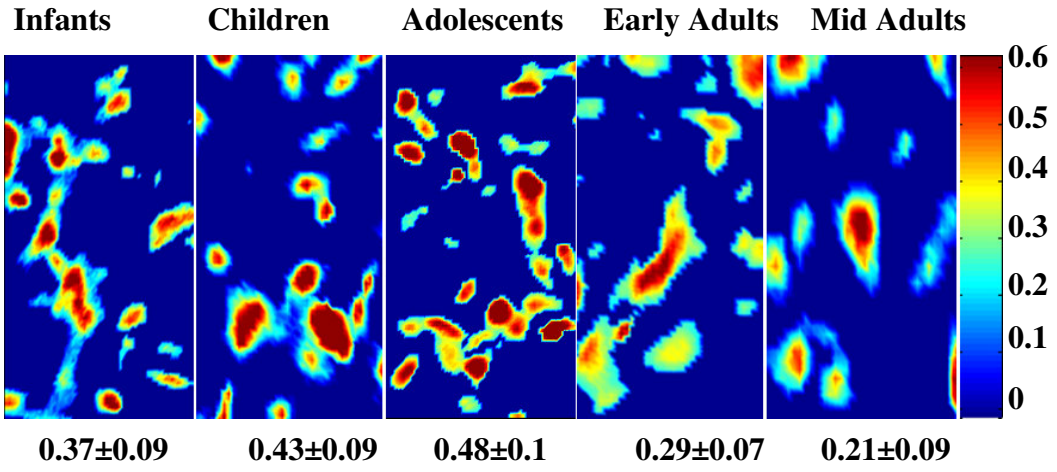

Figure 3.30 Spectral image maps of from five different age groups MSCs, which were derived from the peak integrated areas of PO_2^- antisymmetric stretching band, reflect lipid distribution in cells. Mean absorbance values of each map was given under the maps.

3.5. MTT *(Thiazolyl Blue Tetrazolium Bromide)* Proliferation Assay

MTT proliferation assay was used to support FTIR spectroscopy results which reflects global alterations in the concentrations of different macromolecules of P3 MSCs. These concentrational changes were interpreted as in the differences in

metabolic and cellular activity of BM-MSCs. MTT proliferation assay is based on the cleavage of the yellow MTT (3-(4.5-Dimethylthiazol-2-yl)-2.5-diphenyltetrazolium bromide, a tetrazole) salt to purple formazan crystals in the mitochondria of metabolically active and highly proliferative viable cells (Van de Loosdrecht *et al.,* 1994).

MTT proliferation assay was used into both topics of the thesis study that were mentioned above. In the first part, thalassemic BM-MSCs before and after BMT therapy and healthy control BM-MSCs were compared in terms of their cellular activity by MTT assay during 11 days. Metabolic and cell proliferation activities of healthy control and thalassemic BM-MSCs were measured at day 1, 3, 5, 7, 9 and 11 by measuring the purple solution of formazan crystals in SDS (sodium dodesyl sulphate) by spectrophotometry at 620 nm wavelength. As it can be seen in Table 3.6, the proliferation activity in thalassemic BM-MSCs was higher when compared to the healthy controls. The cellular activity in post-transplant samples decreased after BMT therapy. These results suggested that increase in the content of macromolecules can be attributed to the increase in the cell proliferation activity in thalassemic bone marrow microenvironment.

In the second part, the MTT assay was also applied to different aged BM-MSCs during 11 days. Table 3.7 represents the results of MTT assay of healthy BM-MSCs from different age groups. As can be seen from the table, adolescent group had the highest cellular activity with respect to the other four age groups. Also the cellular activity BM-MSCs of infans and children groups were higher. The results showed that proliferative activity of BM-MSCs decreased by aging and we observed that there were lower cellular activity in early and mid adults groups with respect to the the younger infants, children and adolescent group BM-MSCs.

Table 3.6 MTT proliferation assay results of thalassemic and healthy control BM-MSCs at P3 during 11 days. The values were shown as 'mean ± standard error' for each group. The degree of significance was denoted as: *p<0.05 with respect to healthy control group.

	Absorbance		
	Healthy Control Group	**Pre-Transplant Group**	**Post-Transplant Group**
Day 1	0.184±0.003	0.232±0.021	0.203±0.025
Day 3	0.225±0.013	0.299±0.019 $^{*}\uparrow$	0.276±0.017
Day 5	0.262±0.024	0.331±0.009	0.312±0.021
Day 7	0.277±0.023	0.366±0.01 $^{*}\uparrow$	0.329±0.025
Day 9	0.325±0.024	0.388±0.015	0.364±0.012
Day 11	0.338±0.029	0.400±0.013	0.374±0.016

Table 3.7 MTT proliferation assay results of P3 BM-MSCs obtained from healthy donors of different age groups. The values were shown as 'mean ± standard error' for each group. The degree of significance was denoted as: *p<0.05, **p<0.01, ***p<0.01 with respect to infants, †p<0.05, ††p<0.01, †††p<0.01 with respect to children, $^{\#}$p<0.05, $^{\#\#}$p<0.01, $^{\#\#\#}$p<0.01 with respect to adolescents.

	Absorbance				
	Infants	**Children**	**Adolescents**	**Early Adults**	**Mid Adults**
Day 1	0.148±0,002	0.157±0.014	0.167 ± 0.002	0.141± 0.011	0.132 ± 0.005
Day 3	0.165±0.004	0.171±0,005	0.179 ± 0.002	0.156 ± 0.007	0.150 ±0.002$^{\dagger,\#\#\#}\downarrow$
Day 5	0.173±0.005	0.177±0.002	0.188± 0.001$^{*}\uparrow$	0.163 ± 0.006$^{\#\#}\downarrow$	0.158±0.004$^{\dagger\dagger,\#\#\#}\downarrow$
Day 7	0,179±0.032	0.183±0.006	0.195±0.003	0.169 ± 0.001$^{\#\#\#}\downarrow$	0.165 ± 0.003
Day 9	0.185±0.003	0.191±0.003	0.21±0.003$^{**,\dagger\dagger}\uparrow$	0.176±0.003$^{***,\dagger,\#\#}\downarrow$	0.170±0.003 $^{*,\dagger\dagger\dagger,\#\#\#}\downarrow$
Day11	0.180±0.006	0.196±0.015	0.214±0.004$^{*}\uparrow$	0.179±0.008 $^{\#}\downarrow$	0.173 ± 0.003 $^{\#}\downarrow$

3.6. Erythropoietin (EPO) and Growth Differentiation Factor 15 (GDF 15) Levels in Bone Marrow Plasma Samples

The levels of erythropoietin (EPO) and growth differentiation factor 15 (GDF 15) in the bone marrow plasma samples is used to determine the level of massive erythropoiesis and apoptotic pathways in hematological diseases such as thalassemia. Spectral results in the first part of the study indicated that there was an increase in cell proliferation activity in thalassemic bone marrow. The higher cellular activity was supported by EPO and GDF 15 levels in bone marrow plasma samples of thalassemic and healthy control BM-MSCs. EPO and GDF 15 levels in bone marrow plasma samples of pre- and post-transplant thalassemia patients were measured by Duo-Set Enzyme-Linked Immunosorbent Assay (ELISA). The results of thalassemic BM-MSCs were compared with the results of healthy controls. EPO levels were significantly higher in thalassemic patients before tranplantation (44.91±12.30) ($p<0.01$) than the healthy control group (0.706±0.70). However, EPO levels decreased significantly (10.71±2.13) ($p<0.05$) following BMT therapy with respect to the pre-transplant group (44.9±12.30). ELISA results of GDF 15 in bone marrow plasma samples showed similar alterations with EPO results. GDF 15 levels of pre-transplant group BM-MSCs were significantly higher (1466±407) ($p<0.01$) compared with the healthy controls (104.2±18.51). On the other hand, significant decrease was measured in GDF 15 levels of post-transplant group BM-MSCs (777.5±275.9) ($p<0.05$) after BMT therapy with respect to pre-transplant group MSCs (1466±407).

CHAPTER 4

DISCUSSIONS

4.1. The Effects of Beta Thalassemia Major on Bone Marrow Mesenchymal Stem Cells

In the first part of thesis study, the global molecular changes in the structure and the composition of bone marrow mesenchymal stem cells (BM-MSCs) during beta thalassemica major (β-TM) disease conditions were investigated by infrared spectroscopy and microspectroscopy. The whole experimental results of pre- and post-transplant thalassemic MSCs were compared with the healthy control BM-MSCs. Meanwhile, the experimental results of post-transplant group BM-MSCs were also compared with respect to the pre-transplant group in order to be able to demonstrate the effects of bone marrow transplantation (BMT) therapy on thalassemic BM-MSCs. Thalassemic and healthy BM-MSCs were characterized in terms of according to their adherence to plastic surfaces of culture flask and their fibroblast like morphology by considering the rules of ISCT (International Society for Cellular Therapy) (Horwitz *et al.,* 1999; Dominici *et al.,* 2006). There was no difference in morphological properties of thalassemic and healthy BM-MSCs. In addition to that they were assessed for their expression of BM-MSCs CD105, CD73 and CD90 surface antigens. Both thalassemic and healthy MSCs showed ≥95% expression for CD105, CD73 and CD90 antigens while they were lack of expression for heamatopoietic markers CD45 and CD34. In accordance with the ISCT criteria, differentiation capacities of thalassemic and healthy BM-MSCs into

osteoblasts and adipocytes were evaluated by using standart differentiation inducing mediums. Thalassemic and healthy BM-MSCs differentiated into adipogenic and osteogenic lineages and they stained by Oil red O and Alizarin Red similarly (Figures 3.6 and 3.7).

Infrared spectra of biological samples contains some characteristic absorbtion bands that belong to infrared-active vibrational modes of the different molecules. These absorbtion bands represent different kinds of molecules in the sample like carbohydrates, lipids, proteins and nucleic acids. Therefore, an infrared spectrum of the biological sample provides valuable information about biochemical structure of it. The typical wavenumbers, bandwidths and area values of these bands give fingerprint-like information about functional groups in biomolecules. The determination of mentioned spectral parameters enables us to characterize detailed biochemical make-up of biological sample in non-destructively label-free manner (Kneipp *et al.,* 2000; Kretlow *et al.,* 2006). The area of infrared bands of particular functional groups is directly proportional to the concentration of them (Ozek *et al.,* 2009).

The level of unsaturation in the lipid acyl chains were examined by determining the changes in the band area of olefinic band at 3010 cm^{-1} (Leskovjan *et al.,* 2010; Severcan *et al.,* 2005; Krishnakumar *et al.,* 2009). As it can be seen from Table 3.3, there was a significant increase in the area of this band in pre-transplant group BM-MSCs when compared with the value of healthy control BM-MSCs. This increase represents the increase in the amount of unsaturation in the acyl chains of lipid molecules. The olefinic band area of the pre-transplant MSCs significantly higher with respect to the post-transplant BM-MSCs (Leskovjan *et al.,* 2010; Severcan *et al.,* 2005; Krishnakumar *et al.,* 2009). This result demonstrated an increase in the synthesis of unsaturated fatty acids that are known to have an important role in cell proliferation by exerting growth supporting ability

(Kasayama *et al.,* 1994). We also found an increase in the concentration of saturated lipids that was determined by the analysis of the band area of CH_2 antisymmetric and CH_2 symmetric stretching bands originating from lipid acyl chains. As shown in Table 3.3, the area degrees of these bands were significantly ($p<0.05$) higher in the pre-transplant group BM-MSCs with respect to the healthy control BM-MSCs. After BMT therapy, there was a tendecy to decline in the area values of these bands towards the control group BM-MSCs. The increase in saturated lipid content was further supported by the increase in the area of CH_2 bending vibrations of lipids, at 1453 cm^{-1} (Cakmak *et al.,* 2003, Di Giambattista *et al.,* 2011) and COO^- symmetric stretching vibrations of fatty acid side chains, at around 1400 cm^{-1} (Table 3.3) (Cakmak *et al.,* 2006; Jackson *et al.,* 1998; Peuchant *et al.,* 2008). The increase in saturated and unsaturated lipid contents may indicate an increase in lipid synthesis in cells as a result of increased cellular activity.

Spectral alterations in the wavenumber (frequency) values of the absorption bands give an information about the structure/conformation and intermolecular interactions of that species (Jackson *et al.,* 1997; 1999; Toyran *et al.,* 2003). The shifts in the band frequencies CH_3 and CH_2 antisymmetric, CH_2 symmetric stretching bands can be used as a marker for the detection of order/disorder states of membrane lipids (Liu *et al.,* 2002; Mantsch, 1984; Severcan *et al.,* 1997). In our study, the frequency of the CH_3 antisymmetric stretching band shifted to lower values both in pre- and post-transplant BM-MSCs compared to the control BM-MSCs. These results reflected to increase in the order of the deep interior part of the fatty acyl chains (Bruno, 1999) of thalassemic BM-MSCs. The changes in the wavenumber of CH_2 antisymmetric and symmetric stretching bands give information about the chain fleixibility of fatty acids, which also reflects the order/diorder status of the membrane lipids (Toyran *et al.,* 2004; Melin *et al.,* 2000). As can be seen from Table 3.3, there was a significant decrease in the wavenumber values of CH_2 antisymmetric stretching band of pre- and post-

transplant BM-MSCs that reflected decrease in acyl chain flexibility. Such a decrease in flexibility of fatty acids indicated an increase in the number of trans-conformers of lipid molecules that was resulted in higher lipid order in membranes (Severcan *et al.,* 1997). The cells membranes have vital role in numerous functions of cells such as adhesion, cell proliferation, differentiation, motility and interactions with their microenvironment via signaling and metabolite traffic. Therefore, the mechanical properties of cell membranes have been investigated in many studies to get information about details of mentioned biological processes (Emoto and Umeda 2001; Lundbaek *et al.,* 2004; Titushkin *et al.,* 2006). Active and dynamic structure of cell plasma membrane provides specific cell shape (Titushkin *et al.,* 2006) which is affected from alterations in the lipid order (Moore *et al.,* 1997). According to the results of present study, the increase in the order of membrane lipids in thalassemic BM-MSCs may effect membrane thickness and cell shape which are important characteristics of the stem cell membrane in mediating dynamic interactions with cellular microenvironment and external stimuli particularly during bone marrow remodeling in disease conditions (Titushkin *et al.,* 2006; Spector *et al.,* 1985).

As it can be seen from Figure 3.22 and Table 3.3, the area of amide I (1639 cm^{-1}) was significantly higher in pre-tranplant group ($p<0.05$) when compared with the control group. The area of amide II mode (1545 cm^{-1}) was increased significantly both in the pre-tranplant ($p<0.001$) and post-transplant BM-MSCs ($p<0.01$) with respect to the control BM-MSCs. These bands are mainly resulted from proteins and alterations in their area and frequency values are used to monitor changes in total protein content and structure of the cells (Manoharan *et al.,* 1993; Haris and Severcan, 1999). The significant increase in the area of the band located at aroun 1310 cm^{-1} which is assigned to peptide side chain vibrations (Steiner *et al.,* 2003), was used to support the data that were obtained from amide I and II. As noted in ATR-FTIR data, there were significant increases in protein synthesis in

thalassemic BM-MSCs according to healthy control BM-MSCs and the increase in the area of amide I and amide II bands was prominent in the pre-transplant BM-MSCs than the post-transplant group. This finding was attributed to reduction in total protein content and protein biosynthesis after BMT therapy. Existing studies in the literature in accordance with the accumulation of protein in β-TM are mainly about destruction of erythroid cells due to aggregation of free α-globin and deficient hemoglobin production (Lithanatudom *et al.,* 2010, Trombetta *et al.,* 2006, Khandros *et al.,* 2010). However, there has been no specific investigation about protein alterations in BM-MSCs in β-TM. The increase in protein content in thalassemic BM-MSCs may also imply increased cellular activity in bone marrow (BM) due to ineffective erytropoiesis. Khandros *et al.,* 2010 suggested that β-TM resembles protein aggregation disorders of the nervous system, liver and other tissues.

As it is given in Table 3.4, the alteration in lipid to protein ratio was significantly higher ($p<0.05$) in pre-transplant BM-MSCs with respect to the control BM-MSCs. Such an increase in the lipid to protein ratio reflected that there was a profound increase in the concentrations of lipids according to the increase in protein concentrations of thalassemic BM-MSCs (Gorgulu, 2009). We can concluded from that results, BM activity considerable affects lipid metobolism in thalassemic BM-MSCs than protein metabolism.

The spectral region between 1300-1000 cm^{-1} contains infrared bands of the stretching modes of phosphate moieties (PO_2^-) in phospholipids and nucleic acids (Diem *et al.,* 1999; Liquier and Taillandier, 1996). These phosphate-stretching vibrations give an information about head-groups of the phospholipids in the polar-nonpolar interface of cell membranes (Mendelsohn and Mantsch, 1986). In addition to that they can be used to monitor variations in the quantity, conformational state, degree and the position of phosphorylation of the nucleic

acids in DNA and RNA (Dovbeshko *et al.,* 2000; Kneipp *et al.,* 2000). Antisymmetric phosphate stretching vibrations at 1234 cm^{-1} are mainly resulted from nucleic acids, while symmetric-phosphate stretches at 1080 cm^{-1} assign C-O skeletal stretching vibrations from nucleic acid sugars and C-O-P stretching vibrations of phosphorylated lipids (Wood *et al.,* 2000). As it is given in Table 3.3, there were significant increases in the band area values of the antisymmetric and symmetric phosphate stretching bands in pre-transplant and post-transplant group with respect to the control group BM-MSCs. These results reflected an increases in the concentrations of phospholipids and nucleic acids in thalassemic BM-MSCs. Higher phosholipid concentration can be correlated with higher saturated and unsaturated lipid contents in cells as a result of increased lipid biosynthesis in abnormally active thallasemic bone marrow. The area of the band at 925 cm^{-1} which is assigned to Z type DNA (Banyay and Gräslund, 2003) was used to to support nucleic acid related changes that were obtained from phosphate stretching vibrations. The band area of this band (925 cm^{-1}) was found significantly higher in pre-transplant ($p<0.01$) and post-transplant group ($p<0.05$) thalassemic BM-MSCs than the control MSCs. These findings, related with an increase in the nucleic acid content, were suggested as a result of increased proliferation activity of thalassemic BM-MSCs that was induced by ineffective erythropoiesis in thalassemic BM microenvironment.

In the current study, significant increases in the area of the bands located at 1152 cm^{-1}, 1045 cm^{-1} and 1025 cm^{-1}, which are mainly resulted from carbohydrates including glucose, fructose, glycogen and nucleic acids, were obtained in thalassemic BM-MSCs (Parker, 1971; Cakmak *et al.,* 2006). These significant increases in the area of pre-transplant BM-MSCs ($p<0.001$) and also post-transplant group BM-MSCs ($p<0.001$) revealed an enhanced glycogen and carbohydrate concentrations in thalassemic BM-MSCs with respect to the control BM-MSCs (Table 3.3). The area ratio of the bands located at 1045 cm^{-1} and 1545

cm^{-1} provides an information about carbohydrate levels such as glucose, fructose and glycogen etc. in the cells (Parker, 1971) which was supported by higher glycogen concentration in thalassemic MSCs with an increase in the ratio 1045 cm^{-1}/1545 cm^{-1} (Table 3.4). These results were explained with increased synthesis of glycogen in abnormally active thallasemic bone marrow because of ineffective eythropoiesis. Previous studies in the literature reported that glycogen is used as an alternative energy source in metabolic stress conditions of diseases like cancers to enable cellular growth (Steiner *et al.,* 2003, Emerman *et al.,* 1980, Tsavachidou *et al.,*2010). Significant increases in glycogen content of thalassemic cells with respect to the healthy controls may support the increase in the content of other macromolecules as a result of an enhanced cell proliferation in thalassemic bone marrow microenvironment.

On the basis of the spectral variations, cluster analysis was also performed to differentiate the control, pre- and post-transplant group thalassemic BM-MSCs. The analysis was applied to the first-derivative and vector normalized spectra of fifteen independent samples in three different regions, namely 3050-800 cm^{-1}, 3050-2800 cm^{-1} and 1800-800 cm^{-1}. As can be seen from the Figure 3.14, all samples were successfully distinguished in 3050-2800 cm^{-1} region, while there was only one misclassification for the cluster of 3050-800 cm^{-1} region (Figure 3.13) and there were two misclassification for the cluster of 1800-800 cm^{-1} (Figure 3.15). The higher heterogenity values for three different clusters implied that there were important macromolecular alterations among control, pre- and post-transplant group BM-MSCs. These results revealed that the spectral changes obtained from ATR-FTIR spectroscopy can be successfully determined by cluster analysis.

Thalassemic bone marrow dramatically expands during β-TM disease conditions to get rid of deep anemic symptoms and iron accumulation (Melchiori *et al.,* 2010). This uncontrolable expansion of bone marrow is called as ineffective erythropoiesis and it can be defined by increased level of erythropoietin (EPO) and growth differentiation factor 15 (GDF15) in bone marrow plasma samples. Higher level of EPO drive huge expansion of additional erythroid precursor with an enhanced proliferative and survival capacity, while over expression of GDF15 controls differentiation and proliferation of erythroid precursors during ineffective erythropoiesis (Melchiori *et al.,* 2010; Lithanatudom *et al.,* 2010; Ramirez *et al.,* 2009; Tanno *et al.,* 2010). According to spectral results of the present study, we made a suggestion that the global increases in the concentrations of different macromolecules in thalassemic BM-MSCs with respect to the healthy controls can be resulted from increased cell proliferation activity in abnormally active thalassemic bone marrow. In this context, EPO and GDF15 levels were measured in thalassemic and healthy bone marrow samples by ELISA assay, in order to prove the existence of ineffective erythropoiesis in thalassemic bone marrows. The EPO and GDF15 levels were found significantly higher in pre-transplant BM-MSCs when compared with the healthy controls. However, following BMT therapy the EPO and GDF15 levels of thalassemic patients showed tendency to a significant decrease with respect to the pre-transplant patients. The higher EPO and GDF15 levels in thalassemic bone marrow plasma samples before BMT therapy were the robust indicators of abnormal erythropoietic activity of thalassemic bone marrow as a response of bone marrow microenvironment to IE that can be induced by secretory functions of BM-MSCs which are the main cellular components of bone marrow microenvironment (Melchiori *et al.,*2010, Lithanatudom *et al.,* 2010). The significant decreases in the EPO and GDF15 levels after BMT therapy can indicate rapid adaptation of transplanted HSCs into thalassemic bone marrow microenvironment and recovery effect of healthy HSCs

on thalassemic BM-MSCs as a result of cellular interactions in bone marrow microenvironment. Therefore, the EPO and GDF15 levels were used to support the results of ATR-FTIR spectroscopy which showed increased biosynthesis of lipids, proteins, carbohydrates and nucleic acids because of increased cellular activity in pre-transplant group thalassemic BM-MSCs. Additionally, the spectral results showed that there were significant decreases in the concentrations of mentioned macromolecules in post-transplant group BM-MSCs as a result of diminished ineffective erythropoiesis and recovered abnormal cellular activity after BMT therapy. MTT proliferation assay in Table 3.6 reflected that the proliferation activity in thalassemic BM-MSCs was significantly higher than the control MSCs. The cellular activity was still higher than the controls in the post-transplant samples with the closer values to the healthy control group. These findings were in the same direction with the results of ELISA assays. Such an increased proliferation activity clarified higher concentration of macromolecules in thalassemic BM-MSCs than the healthy control BM-MSCs.

Since post-transplant marrow samples were obtained shortly after engraftment (between days +25 and day +35), the significant changes in BM-MSCs towards normal values suggested that the interaction between hematopoetic and mesenchymal cells is very dynamic, leading to a change in the abnormal patients bone marrow microenvironment towards normal by achievement of healthy donor eythropoesis following BMT. Therefore, the spectroscopic changes observed in post-transplant group BM-MSCs can be used to interprete cellular interactions between healthy HSCs and thalassemic BM-MSCs with an other supportive experimantal data of ELISA and MTT proliferation assays. The significant reductions in the concentrations of cellular macromolecules in post-transplant BM-MSCs with respect to the pre-transplant BM-MSCs may reflects an adaptation of patients's BM-MSCs to the recovered bone marrow microenvironment by decreasing cell proliferation rate and secretory activities after BMT therapy.

All these experimental results discussed above were performed according to the suggestion that post-transplant group BM-MSCs were patients's origin after BMT therapy. Therefore; chimerism analysis was performed to determine whether the origin of BM-MSCs belongs to the recipient or the donor after allogenic bone marrow transplantation. Chimerism status of post-transplant samples can be analyzed by fluorescence in situ hybridization (FISH) using X/Y gene probes in sex-mismatched patients or short tandem repeat polymorphism analysis by polimerase chain reaction (STR-PCR). In our study STR-PCR chimerism test was used to analyze the polymorphic DNA loci of the donor and recipient cells. In addition to that engraftment status was also determined by analyzing STRs of donor, pre- and post-transplant recipient that are interspersed throughout the genome. The unique but not the shared STR loci of the donor and recipient were usually used to evaluate chimerism. As a result of chimerism test we found that in all our 5 patients, MSCs were shown to be 100% recipient origin and BM-MSCs of donor origin could not be detected. That is; BM-MSCs isolated from recipients after allogenic BMT therapy, were not of donor genotype, despite the presence of 95%-99% donor type hematopoietic engraftment in a short engfraftment time. The earlier chimerism studies in literature showed that MSCs remained of host origin (patient origin) even a long time after allogenic BMT therapy while donor chimerism was achieved in HSCs (Rieger *et al.,* 2005; Villaron *et al.,* 2004; Koc *et al.,* 1999). In summary, our chimerism analysis showed that even in short engraftment time (between +25 and +35 days) after BMT therapy, adequate cellular interections between HSCs-MSCs can be achieved to observe the healing of disease related alterations in patient's bone marrow.

In addition to the β-TM disease related molecular alterations in BM-MSCs which were indicated by using ATR-FTIR spectroscopy, FTIR imaging was also

performed by FTIR microspectroscopy for visual demontrations of the changes in biochemical structure and composition in small sample regions on microscopic scales (Szczerbowska-Boruchowska *et al.,* 2007). Tens of thousands of individual spectra can be collected rapidly and in parallel, each referring to a distinct and identifiable spatial location on the sample. Besides the information about chemical composition and molecular structure, which can also be obtained from conventional IR spectra, the integration of spatial and spectral information in vibrational imaging data sets provides representative demonstration of spectral results (Lester *et al.,* 1998). The band area of spectral vibrations originating from a particular functional groups are directly proportional to the concentrations of that species (Ozek *et al.,* 2009). In this study, using FTIR imaging, the differences in the distribution of concentrations of lipids, proteins and nucleic acids in MSCs of control, pre- and post-transplant groups were demostrated representatively which can also be used as a supportive data to the results ATR-FTIR spectroscopy.

The intensity/area changes of CH_2 antisymmetric stretching and CH_2 symmetric stretching bands give an information about saturated lipid concentration in the system (Severcan *et al.,* 2000; Severcan *et al.,* 2003; Cakmak *et al.,* 2006). We constituted the chemical maps of saturated lipids by taking the peak integrating maps of the CH_2 antisymmetric stretching and CH_2 symmetric stretching bands. In order to observe changes in concentrations of proteins, we constitute the chemical maps by taking the area distrubition of bands arising from the C=O stretching vibration of the amide I and N-H bending vibration of amide II (Manoharan *et al.,* 1993, Haris and Severcan 1999). In addition to these bands, the integrated band area distrubition PO_2^- antisymmetric stretching of nucleic acids was used to make a chemical maps of nucleic acid changes in the cells (Rigas *et al.,* 1990, Wong *et al.,* 1991). For each sample belonging to the groups mentioned in the results, the mean absorbance values of FTIR images were also calculated. It is aimed to show that these mean absorbance values are in agreement with the results

based on the concentrational changes obtained by using ATR-FTIR. As it is given in the mean absorbance in the Figures 3.16, 3.17, 3.18 and 3.19, there were an increase in the concentrations of saturated lipids, proteins and nucleic acids in thalassemic BM-MSCs according to healthy controls. Following BMT therapy, the mean absorbance values of mentioned spectral bands decreased with respect to pre-transplant group BM-MSC. The average chemical maps were colored according to the intesity/area values of mentioned bands, where red color corresponds to the highest ratio and blue color corresponds to the lowest ratio as shown on the color bar in the figures. As it was observed from the color changes in these chemical maps, pre-transplant groups BM-MSCs had the highest lipid, protein and nucleic acid concentrations with respect to the post-transplant and healthy control BM-MSCs. All these results belonging to the FTIR imaging study were in agreement with the results of ATR-FTIR spectroscopy.

4.2. The Effects of Donor Age on Healthy Bone Marrow Mesenchymal Stem Cells

In the second part of this study, effects of donor age on healthy BM-MSCs were investigated by ATR-FTIR spectroscopy and FTIR microspectroscopy. Spectral investigations were performed by using BM-MSCs from healthy donors which were classified according to their ages in five different age groups labeled as infant, children, adolescents, early and mid adults. Each group was statistically compared with the remaining four groups in order to reveal the differences between them.

Healthy BM-MSCs from different aged donors at passage 3 were characterized with their adherence to plastic surfaces of culture flask and their fibroblast like morphology. There were no difference in morphological properties and CD73, CD90, CD105 expression profiles at passage 3. These results were supported by

the study of Mareschi *et.al.,* 2006 where it was reported that there were no differences in morphology and antigenic expression profiles of BM-MSCs of young adult donors (range of age: 20-50) and pediatric donors (range of age: 6-11) until passage 10. On the other hand, in the study of Huang *et al.,* 2005, it was demonstrated that BM-MSCs of fouetuses, 0-20 years old donors, 20-40 years old donors, and donors older than 40 years old had similar morphology and antigenic phenotype. In the scope of second part of the study, the cells from five different age groups were characterized according to their adipogenic and osteogenic differentiation capacities. Adipogenic and osteogenic differention was assessed by using Oil red O and Alizerin Red staining, respectively. As seen in representative (Figure 3.7 and 3.8) results, there were decreases in the adipogenic and osteogenic differentiation potentials in early and mid adults (range of ages: 20-50) when compared with the younger donors (range of ages: 0-19). The study of Kretlow *et al.,* 2008 showed that chondrogenic, osteogenic and adipogenic differentiation potentials of cells from oldest donor decreased. In the study of Roura *et al.,* 2006, the effects of donor age on $CD105^{+}$ mesenchymal stem cells in young (n=10, 24±6.4 years) and elderly (n=9, 77±8.4 years) donors were investigated. They reported non-significant decrease in adipogenic differentiation potential by Oil Red O staining and significant decrease in osteogenic differentiation potentials by von Kossa staining in elderly donors. Although most of the existing studies support our results, there are many conflicting data available in the literature about the effects of aging on the differentiation potentials of MSCs since the donors and the sample models used in these studies were different.

There is limited information about how donor age affects the fate of stem cells and whether the changes caused by aging alter the stem cell niche (Campisi and Sedivy, 2009). Stem cells are required for homeostasis and tissue regenaration. It is thought that impaired tissue homeostasis and regenaration capacity can be assumed to be arising from alterations in the number and/or function of stem cells

(Beltrami *et al.,* 2011; Rando*,* 2006). In this context, the question arises whether age related changes are due to the intrinsic aging of stem cells or due to the aged stem cell microenvironment (niche) (Wagner *et al.,* 2008). Age-related alterations in stem cells and their external environment should be investigated in order to standardize quality products and cellular therapies. Up to now, the numbers of passages and population doublings, and senescence-associated molecular changes have not been clarified whether they are tolarable to optimize therapeutic effects of clinical applications. These findings make it inevitable to define a reliable and easy method to track cellular aging of MSCs (Wagner *et al.,* 2010; Stolzing and Scutt, 2006). Studies in the literature have reflected that cellular senescence does not significantly effect the viability, morphology, function, proliferation and differentiation capacity of cells, while it causes decline in cellular metabolism (Wagner *et al.,* 2008; 2010; Stolzing and Scutt, 2006). Until now senescence associated β-galactosidase (SA-β-gal) has been used to determine senescence. Although SA-β-gal is overexpressed and accumulates specifically in senescent cells, it is not the only marker of senescence. The enlarged and apoptotic cells in higher passages also become SA-β-gal positive. This means that β-galactosidase activity is associated with mainly replicative senescence in-vitro (Wagner *et al.,* 2010; Stolzing, A., and Scutt, A., 2006). The study of Stolzing and Scutt, 2006 showed that there was no correlation between the age of organism and the level of SA-β-gal staining in fresh ex-vivo or in-vivo tissue. In summary, no specific molecular marker is available to determine the degree of cellular aging in MSCs. In this context, we hyphothesized that IR spectroscopy as a novel, non-destructive research method with its real-time chemical monitoring and high-quality data collection properties, can be used to identify molecular marker(s) reflecting the stem cell aging.

Spectral region between 3000-2800 cm^{-1} was used to determine the level of saturation in the lipid acyl chains by examining the changes in the CH_3, CH_2 antisymmetric and CH_2 symmetric stretching bands (Severcan *et al.,* 2005; Krishnakumar *et al.,* 2009; Leskovjan *et al.,* 2010). As it is shown in Table 3.5, there were significant increases in these bands for children and adolescents groups when compared with the other groups. These increases indicate an increase in the amount of saturation in the acyl chains of lipid molecules as a result of increase in synthesis of saturated fatty acids that are known to have an important role in cell proliferation by exerting growth supporting ability (Kasayama *et al.,* 1994). The increase in saturated lipid content was further supported by the increase in the area of CH_2 bending vibrations of lipids, at 1453 cm^{-1} (Cakmak *et al.,* 2003; Di Giambattista *et al.,* 2011) and COO^- symmetric stretching vibrations of fatty acid side chains, at around 1400 cm^{-1} (Table 3.5) (Peuchant *et al.,* 2008; Cakmak *et al.,* 2006; Jackson *et al.,* 1998). These two bands were slightly higher for children and adolescents MSCs. These increases in saturated lipid concentrations in children and adolescents may indicate an increase in lipid synthesis in cells as a result of increased metabolic activity.

Changes in the band areas of amide I, amide II and amide III reflected the alterations in the protein concentrations in cells. As it is shown in Table 3.5, for children and adolescents groups, the band area values of amide I and amide II were significantly higher while was non-significantly higher for the amide III. As noted in ATR-FTIR data, there were significant increases in protein synthesis in children and adolescents MSCs when compared with the infants, early and mid adults MSCs. Significant decreases in the area values of amide I, amide II and amide III bands for early and mid adults leaded to the decrease in protein synthesis in these groups.

The changes in lipid to protein ratio were non-significant. This ratio slightly decreased in children and adolescents group MSCs with respect to infants, early and mid adults MSCs. Such a decrease in the lipid to protein ratio meaned that there may be a profound increase in the protein concentration compared to the increase in lipid concentration in MSCs (Gorgulu, 2009). By using these findings, we concluded that the increase in cellular activity considerably affected protein metobolism in healthy MSCs than the lipid metabolism.

The area changes in the infrared bands of PO_2^- antisymmetric vibrations at 1234 cm^{-1} and symmetric stretching vibrations at 1080 cm^{-1} were used to investigate the variations in the quantity, conformational state, degree and the position of phosphorylation of the nucleic acids in DNA and RNA (Dovbeshk *et al.,* 2000; Kneipp *et al.,* 2000). As it can be seen in Table 3.5, there were significant increases in the band area values of the antisymmetric phosphate stretching bands for children and adolescents groups MSCs when compared with the infant group MSCs. However, non-significant increases were observed in the PO_2^- symmetric stretching band areas for the same groups. The bands at 925 cm^{-1} and 855 cm^{-1} were used to support nucleic acid related changes. The area values in these bands were significantly higher for adolescent MSCs and non-significantly higher for children MSCs. There were significant decreases in the area of these four bands for early and mid adults MSCs with respect to the adolescents and children MSCs. The findings about an increase in the nucleic acid content were suggested to be resulting from increased proliferative activity of adolescents and children MSCs.

There were significant increases in the areas of the bands at 1152 cm^{-1}, 1045 cm^{-1} and 1025 cm^{-1}, for children and adolescent MSCs. These increases mainly resulted from carbohydrates including glucose, fructose, glycogen and nucleic acids (Parker, 1971; Cakmak *et al.,* 2006). These findings indicated enhanced glycogen

and carbohydrate concentrations in children and adolescent MSCs, whereas significant declines were observed in early and mid adult MSCs (Table 3.5).

MTT proliferation assay was carried out in order to prove increased cellular activity. The results of MTT proliferation assay was used to support the data obtained from ATR-FTIR spectroscopy. As it is given in Table 3.7, MTT proliferation assay results showed that the proliferation activity in adolescents MSCs were significantly higher than the activities in other sample groups MSCs. It was shown that the children and infant MSCs also had an higher level of proliferative activity than early and mid adults MSCs. We observed significant decreases in proliferation capacity in cells of early and mid adults. Mareschi *et al.,* 2006 found that cell growth was related to the age of donors. Their study reflected that MSCs of pediatric donors (range of age: 6-11) were proliferate twice as high as MSCs of adult donors (range of age: 20-50). Scutt *et al.,* 1996 investigated the age effect on rats whose ages were 3, 7, 12 and 56 weeks. They found that apoptosis and reduced proliferation capacity levels were higher in the cells of older rats.

On the basis of the spectral variations, cluster analysis was also performed to discriminate MSCs of infants, children, adolescents, early and mid adults. The analysis was applied to the first-derivative and vector normalized spectra of twenty five samples in three different regions of 3000-800 cm^{-1}, 3000-2800 cm^{-1} and 1800-800 cm^{-1}. As seen in Figures 3.23, 3.24 and 3.25, there was only one misclassification for the cluster of 3000-800 cm^{-1} region while all samples were successfully distinguished in clusters of 3000-2800 cm^{-1} and 1800-800 cm^{-1} regions. The higher heterogenity values for three different clusters implied that there were important macromolecular alterations among the MSCs of different age groups. These results revealed that the spectral changes obtained from ATR-FTIR spectroscopy can be successfully determined by cluster analysis.

In this part of the study, we used FTIR spectroscopy as a novel method to determine unique molecular marker(s) in order to identify the effects of donor age on bone marrow MSCs. We observed some differences in the concentrations of cellular macromolecules. These findings were interpreted as the differences in the proliferative activity of cells in accordance with the age differences of donors. These interpretations were supported by MTT assay results that were in accordance with the ATR-FTIR data.

As an other supportive method, FTIR microspectroscopy was used. This method is known to be providing information about biochemical structure and composition of cells in a small sample region with microscopic scales (Szczerbowska-Boruchowska *et al.,* 2007). The differences in the distribution of concentration of lipids, proteins and nucleic acids in MSCs of five different age groups were demonstrated representetively. The intensity/area changes of the CH_2 antisymmetric stretching and CH_2 symmetric stretching bands give an information about saturated lipid concentration in the system (Severcan *et al.,* 2000; Severcan *et al.,* 2003, Cakmak *et al.,* 2006). We constituted the chemical maps of saturated lipids by using the peak integrating maps of the CH_2 antisymmetric stretching and CH_2 symmetric stretching bands. In order to observe the changes in concentrations of proteins, we constitute the chemical maps by using the area distribution of bands which arises mainly from the C=O stretching vibration of the amide I and N-H bending vibration of amide II (Manoharan *et al.,* 1993, Haris and Severcan 1999). In addition to these bands, the integrated band area distribution of PO_2^- antisymmetric stretching of nucleic acids was used to make a chemical map of nucleic acid changes in the cells (Rigas *et al.,* 1990; Wong *et al.,* 1991). As it is given in the mean absorbance values in Figures 3.26, 3.27, 3.28, 3.29 and 3.30, the concentrations of saturated lipids, proteins and nucleic acids for children and adolescents groups were higher when compared with the infants, early and mid adults. The mean absorbance values in these spectral bands were lower for older

donors. The average chemical maps were colored according to the intensity/area values of mentioned bands where red color corresponds to the highest ratio and blue color corresponds to the lowest ratio as shown on the color bar in the figures. As it was understood from the color changes in these chemical maps, concentrational changes can be ordered from higher to lower values as adolescents, children, infants, early and mid adults. All the results obtained from FTIR imaging study were in agreement with our ATR-FTIR data and allowed the generation of IR maps with high image contrast as a supportive data.

CHAPTER 5

CONCLUSION

In the first part of the study, it was aimed to investigate the molecular level changes in human bone marrow mesenchymal stem cells (BM-MSCs) in pathological bone marrow microenvironment during disease beta thalassemica major (β-TM). The results of the study showed that β-TM had significant influence on the structure and the concentration of biological macromolecules and secretory functions of BM-MSCs. However, β-TM did not cause any changes on the main characteristics of cells that were used to define BM-MSCs. Thalassemic and healthy BM-MSCs had similar cellular morphology under inverted light microscope. Their expression profile for CD105, CD90, CD73, CD45 and CD34 surface antigens were also similar. Both thalassemic and healthy BM-MSCs were differentiated into adipocytes and osteocytes. The spectral results showed that there were significant increases in the contents of saturated and unsaturated lipids, protein, glycogen and nucleic acids in thalassemic BM-MSCs. Lipid order in cell membrane also increased in thalassemic BM-MSCs. These results suggested that increase in the concentration of macromolecules can be attributed to the increase in the proliferation activity of cells during ineffective erythropoiesis in thalassemic bone marrow. Erythropoietin (EPO) and growth differentiation factor 15 (GDF 15) levels and MTT proliferation assay results were used in order to support ATR-FTIR results and determine the degree of ineffective erythropoiesis. The concentration of macromolecules in post-transplant BM-MSCs was shown to be decreased when compared to the pre-transplant BM-MSCs. On the other hand,

EPO and GDF15 levels, and proliferation activity in the MTT assay results following bone marrow transplantation (BMT) therapy were shown to decrease for the case of post-transplant BM-MSCs as well. All of these results could be interpreted as a decrease in cellular activity as a result of restoring effect of BMT therapy on abnormal erythropoiesis by leading the normalization of abnormal host microenvironment.

The chimerism test, which was performed +25 and +35 days after transplantation, showed that there were complete donor type hematopoietic engraftment in the patients's bone marrows while BM-MSCs remained 100% recipient (patient) origin. The restoring effect of BMT therapy observed during attenuated total reflection Fourier transform infrared (ATR-FTIR) spectroscopy study can be used to identify hematopoietic stem cells (HSCs) and BM-MSCs dynamic interactions in bone marrow microenvironment. The results of the ATR-FTIR spectroscopy study were also supported by FTIR imaging which was used to demonstrate distribution of macromolecules in the cells as in chemical maps. Thalassemic and healthy control BM-MSCs were successfully separated by using the hierarchical cluster analysis where alterations in structure and composition of macromolecules obtained from FTIR data were considered. These results showed the differences between thalassemic and healthy control BM-MSCs. Moreover, they provided better understanding of the in-vivo cell-to-cell interactions between HSCs and MSCs. Therefore, this study became to be the first model study which may contribute to future studies for investigating cellular interactions in the bone marrow microenvironment.

In the second part of the study, we aimed to identify new molecular marker(s) in order to determine the effects of donor age on healthy BM-MSCs. The results showed that donor age had significant influence on the concentrations of important macromolecules existing in the cells. The BM-MSCs from healthy donors in

different ages had similar cellular morphology under inverted light microscope at passage 3. Also, their expression profiles for CD105, CD90, CD73, CD45 and CD34 surface antigens were same. In addition to this, adipogenic and osteogenic differentiation potentials of older MSCs were lower when compared to the younger cells representatively. The spectral results reflected that there were significant increases in the concentration of saturated lipids, proteins, glycogen and nucleic acids in children and adolescent group BM-MSCs when compared to the infants, early and mid adults. The concentrations of mentioned macromolecules in early and mid adults BM-MSCs were significantly lower than the concentrations in the children and adolescents BM-MSCs. These increases in the concentrations of macromolecules were decided to be a result of the increase in the proliferation activity in younger BM-MSCs. The cellular activity degree was determined through the MTT proliferation assay results and this was used to support ATR-FTIR spectroscopy results. The MTT assay results showed that BM-MSCs obtained from younger donors, such as infants, children and adolescents, had higher cellular activity than the BM-MSCs obtained from early and mid adults. FTIR microspectroscopy revealed the distribution of macromolecules in the cells as chemical maps whose results also are in agreement with the ATR-FTIR results. BM-MSCs of five different age groups were discriminated by making the hierarchical cluster analysis where the ATR-FTIR spectroscopy data according to alterations in structure and composition of macromolecules were considered.

REFERENCES

Aerts, F.S.F., and Wagemaker, G., (2004). *Mesenchymal stem cell engineering and transplantation*, Springer, Dordrecht, The Netherlands , 1-44.

Aggarwal, S., (2003). Stem cell tranplantation in thalassemia. Int. J. Hum. Genet., **3:** 205-208.

Aggarwal, S., and Pittenger, M.F., (2005). Human mesenchymal stem cells modulate allogeneic immune cell responses. Blood, **15:** 1815-1822.

Akkas, S.B., Severcan, M., Yilmaz, O., and Severcan, F., (2007). Effects of lipoic acid supplementation on rat brain tissue: An FTIR spectroscopic and neural network study. Food Chem., **105:** 1281-1288.

Akkas, S.B., Inci, S., Zorlu, F., and Severcan, F., (2007). Melatonin affects the order, dynamics and hydration of brain membrane lipids. J. Mol. Struct., **834:** 207-215.

Ami, D., Neri, T., Natalello, A., Mereghetti, P., Doglia, S.M., Zanoni, M., Zuccotti, M., Garagna, S., and Redi, C.A., (2008). Embryonic stem cell differentiation studied by FT-IR spectroscopy, Biochimica et Biophysica Acta., **1783:** 98–106.

Angelucci, E. and Baronciani, D., (2008). Allogeneic stem cell transplantation for thalassemia major. Heamatologica, **93:** 1780-1784.

Argov, S., Ramesh, J. Salman, A., Sinelnikov, I., Goldstein, J., Guterman, H., and Mordechai, S., (2002). Diagnostic potential of Fourier-transform infrared microspectroscopy and advanced computational methods in colon cancer patients. J. Biomed. Opt., **7:** 248-254.

Asanuma, H., Meldrum, D.R., and Meldrum, K.K., (2010). Therapeutic applications of mesenchymal stem cells to repair kidney injury. J. Urol., **184:** 26-33

Askmyr, M., Quach, J., Purton, E.L., (2011). Effects of the bone marrow microenvironment on hematopoietic malignancy. Bone, **48**: 115-120.

Babrah, J., McCarthy, K., Lush, R.J., Rye, A.D., Bessant C., and Stone, N., (2009). Fourier transform infrared spectroscopic studies of T-cell lymphoma, B-cell lymphoid and myeloid leukaemia cell lines. Analyst, **134:** 763-768.

Baksh, D., Song, L., and Tuan, R.S., (2004). Adult mesenchymal stem cells: Characterization, differentiation, and application in cell and gene therapy. J. Cell. Mol. Med., 8(3): 301-316.

Banyay, M., and Gräslund, A., (2003). A library of IR bands of nucleic acids in solution. Biophys. Chem., **104:** 477-488.

Barry, F.P., (2003). Biology and clinical applications of mesenchymal stem cells. Birth Defects Res. C. Embryo Today, **69:** 250-256.

Bartsch, K., Al-Ali, H., Reinhardt, A., Franke, C., Hudecek, M., Kamprad, M., Tschiedel, S., Cross, M., Niederwieser, D., and Gentilini, C., (2009). Mesenchymal stem cells remain host-derived independent of the source of the stem-cell graft and conditioning regimen used. Transplantation, **87:** 217-221.

Baxter, M.A., Wynn, R.F., Jowitt, S.N., Wraith J.E., Fairbairn, L.J., and Bellantuono, I., (2004). Study of telomere length reveals rapid aging of human marrow stromal cells following in vitro expansion. Stem Cells, **22:** 675-682.

Becerra, J., Santos-Ruiz, L., Andrades, J.A., Marí-Beffa, M., (2011). The stem cell niche should be a key issue for cell therapy in regenerative medicine. Stem Cell Rev., **7:** 248-255.

Bechtel, H.A., Martin, M.C., May, T.E., and Lerch, P., (2009). Improved spatial resolution for reflection mode infrared microscopy. Rev. Sci. Instrum., **80:** 126106.

Beier, J.P., Bitto, F.F., Lange, C., Klumpp, D., Arkudas, A., Bleiziffer, O., Boos, A., Horch, R.E., and Kneser, U., (2010). Myogenic differentiation of mesenchymal stem cells co-cultured with primary myoblasts. Cell Biol. Int., **35:** 397-406.

Beltrami, A.P., Cesselli, D., and Beltrami, C.A., (2011). At the stem of youth and health. Pharmacol Ther., **129**: 3-20.

Birgens, H., and Ljung, R., (2007). The thalassaemia syndromes. Scand. J. Clin. Lab. Invest., **67:** 11-25.

Bizeau, M.E., Salano, J.M., and Jeffrey, R., (2000). Menhaden oil feeding increases lypolysis without changing plasma membrane order in isolated rat adipocytes. Nutrition Research, **20:** 1633-1644.

Bozkurt, O., Bilgin, M.D., and Severcan, F., (2007). The effect of diabetes mellitus on rat skeletal Extensor digitorum longus muscle tissue: An FTIR study, Spectroscopy - Int. J., 21: 151-160.

Bozkurt, O., Severcan, M., Severcan, F., (2010). Diabetes induces compositional, structural and functional alterations on rat skeletal soleus muscle revealed by FTIR spectroscopy: a comparative study with EDL muscle. Analyst, **135**: 3110-3119.

Bruno, T.J., (1999). Sampling accessories for infrared spectrometry. Appl. Spectr. Rev., 34: 91–120.

Bullen, H.A., Oehrle, S.A., Bennett, A.F., Taylor, N.M., and Barton, H.A., (2008). Use of attenuated total reflectance Fourier transform infrared spectroscopy to identify microbial metabolic products on carbonate mineral surfaces. Appl. Environ. Microbiol., **74:** 4553-4559.

Cakmak, G., Zorlu, F., Severcan, M., Severcan, F., (2011). Screening of protective effect of amifostine on radiation-induced structural and functional variations in rat liver microsomal membranes by FT-IR spectroscopy. Anal Chem., **83**: 2438-2444.

Cakmak, G., Togan, I., and Severcan, F., (2006). 17β-Estradiol induced compositional, structural and functional changes in rainbow trout liver, revealed by FT-IR spectroscopy: A comparative study with nonylphenol. Aquatic. Tox., **77:** 53–63.

Cakmak, G., Togan I., Uğuz, C., and Severcan, F. (2003). FT-IR spectroscopic analysis of rainbow trout liver exposed to nonylphenol. Appl. Spectr., **57:** 835-841.

Campbell, J.D., and Dwek, R.A., (1984). *Biological Spectroscopy*. The Benjamin/ Cummings Publishing Company, Inc.

Campisi, J., Sedivy, J., (2009). How does proliferative homeostasis change with age? What causes it and how does it contribute to aging? J. Gerontol. Biol. Sci. Med. Sci., **64**: 164-166.

Caplan, A.I., (2000). Mesenchymal stem cells and gene therapy. Clin. Orthop. Relat. Res., **379:** 67-70.

Caplan, A.I., (2009). Why are MSCs therapeutic? New data: new insight. J. Pathol., **217:** 318–324.

Chan, J.W., and Lieu, D.K., (2009). Label-free biochemical characterization of stem cells using vibrational spectroscopy. J. Biophotonics, **2:** 656–668.

Chan, J.W., Lieu, D.K., Huser, T., and Li, R.A., (2009). Label-free separation of human embryonic stem cells (hESCs) and their cardiac derivatives using Raman spectroscopy. Anal. Chem., **81:** 1324–1331.

Chang, M.C., Tanaka, J., (2002). FT-IR study for hydroxyapatite/collagen nanocomposite cross-linked by glutaraldehyde. Biomaterials, **23:** 4811–4818.

Chen, D.P., Tseng, C.P., Tsai, S.H., Wu, T.L., Chang, P.Y., Sun, C.F., (2008). Systematic analysis of stutters to enhance the accuracy of chimerism testing. Ann Clin Lab Sci., **38**: 264-272.

Ci, X.Y., Gao, T.Y., Feng, J., and Guo, Z.Q., (1999). Fourier transform infrared characterization of human breast tissue: Implications for breast cancer diagnosis. Appl. Spectr., 53: 312-315.

Cole, K.C., (2009). The use of attenuated total reflection infrared spectroscopy to study the intercalation of molten polymer into layered silicates in real time. Appl. Spectr., 63: 1343-1350.

Coleman, P.B., (1993). Practical Sampling Techniques for: Infrared Analysis. CRC Press.

Colthup, N.B., Daly, L.H., and Wiberley, S.E., (1975). *Introduction to infrared and raman spectroscopy.* New York: Academic Press.

Dennis, J.E., and Caplan. A.I., (2004). Advances in mesenchymal stem cell biology. Current Opinion in Orthopaedics, **15:** 341-346.

Di Giambattista, L., Pozzi, D., Grimaldi, P., Gaudenzi, S., Morrone, S., and Castellano A.C., (2011). New marker of tumor cell death revealed by ATR-FTIR spectroscopy. Anal. Bioanal. Chem., **399:** 2771-2778.

Dicko, A., Morissette, M., Ameur, S.B., Pezolet, M., and Di Paolo, T., (1999). Effect of estradiol and tamoxifen on brain membranes: investigation by infrared and fluorescence spectroscopy. Brain Res. Bull., **49:** 401-405.

Diem, M., Boydston-White, S., and Chiriboga, L., (1999). Infrared spectroscopy of cells and tissues: shining light onto a novel subject. Appl. Spectr., **53:** 148-161.

Diem, M., Romeo, M.J., Mattheaus C., Miljkovic, M., Miller, L., and Lasch, P., (2004). Comparison of Fourier transform infrared (FTIR) spectra of individual cells acquired using synchrotron and conventional sources. Infrared Physics & Tech., 45, 331–338.

Diem, M., Chalmers, J.M., and Griffiths, P.R., (2008). *Vibrational spectroscopy for medical diagnosis.* John Wiley & Sons, Chichester, England; Hoboken, NJ.

Dogan, A., Ergen, K., Budak, F., and Severcan, F., (2007). Evaluation of disseminated candidiasis on an experimental animal model: a Fourier Transform Infrared study. Appl. Spectr., **61:** 199-203.

Dominici, M., Le Blanc, K., Mueller, I., Slaper-Cortenbach, I., Marini, F.C., Krause, D.S., Deans, R.J., Keating, A., Prockop, D.J., and Horwitz, E.M., (2006). Minimal criteria for defining multipotent mesenchymal stromal cells. The International Society for Cellular Therapy position statement. Cytotherapy, **8:** 315-317.

Dormady, S.P., Bashayan, O., Dougherty, R., Zhang, X.M., and Basch, R.S., (2001). Immortalized multipotential mesenchymal cells and the hematopoietic microenvironment. J. Hematother Stem Cell Res., **10:** 125-140.

Dovbeshko, G.I., Gridina, N.Y., Kruglova, E.B., and Pashchuk, O.P., (2000). FTIR spectroscopy studies of nucleic acid damage. Talanta, **53:** 233-246.

Dovbeshko, G.I., Chegel, V.I., Gridina, N.Y., Repnytska, O.P., Shirshov, Y.M., Tryndiak, V.P., Todor, I.M., and Solyanik, G.I., (2002). Surface enhanced IR absorption of nucleic acids from tumor cells: FTIR reflectance study. Biopolymer (Biospectroscopy), **67:** 470-486.

Downes, A., Mouras, R., and Elfick, A., (2010). Optical Spectroscopy for NoninvasiveMonitoring of Stem Cell Differentiation. Journal of Biomedicine and Biotechnology. J. Biomed. Biotechnol., 101864.

Drummond-Barbosa, D., (2008). Stem cells, their niches and the systemic environment: an aging network. Genetics, **180:** 1787-1797.

Dukor, R., (2002). In Handbook of Vibrational Spectroscopy, Chalmers, J., Griffiths, P., Eds., Wiley: New York, 3335–3361.

Emerman, J.T., Bartley J.C., and Bissell, M.J., (1980). Interrelationship of glycogen metabolism and lactose synthesis in mammary epithelial cells of mice. Biochem. J., **192:** 695-702.

Emoto, K., and Umeda, M., (2001). Membrane lipid control of cytokinesis. Cell Struct. Funct. **26:** 659-665.

Erukhimovitch, V., Talyshinsky, M., Souprun, Y., Huleihel, M., (2005). FTIR microscopy detection of cells infected with viruses. Methods Mol. Biol., **292:** 161-172.

Fang, J., Menon, M., and Kapelle, W., (2007). EPO modulation of cell-cycle regulatory genes, and cell division, in primary bone marrow erythroblasts. Blood, **110:** 2361-2370.

Freifelder, D., (1982). *Physical chemistry applications to biochemistry and molecular biology.* New York.

Friedenstein, A.J., Piatetzky, S., and Petrakova, K.V., (1966). *Osteogenesis transplants of bone marrow cells.* J. Embryol. Exp. Morphol., **16:** 381-390.

Fujioka, N., Morimoto, Y., Arai, T., and Kikuchi, M., (2004). Discrimination between normal and malignant human gastric tissues by Fourier transform infrared spectroscopy. Cancer Detection & Prevention, **28:** 32-36

Gazi, E., Dwyer, J., Lockyer, N. P., Miyan, J., Gardner, P., Hart, C., Brown, M., and Clarke, N. W., (2005). Fixation protocols for subcellular imaging by synchrotron-based Fourier transform infrared microspectroscopy. Biopolymers, **77**:18-30.

Gaigneaux, A., Ruysschaert, J.M., and Goormaghtigh, E., (2006). Cell Discrimination by Attenuated Total Reflection–Fourier Transform Infrared Spectroscopy: The Impact of Preprocessing of Spectra. Appl. Spect., **60:** 1022-1028.

Garip, S., Bozoğlu, F., and Severcan, F., (2007). Differentiation of Mesophilic and Thermophilic Bacteria with Fourier Transform Infrared Spectroscopy. Appl. Spectr., **61:** 186-192.

Goldberg, M.E., and Chaffotte, A.F., (2005). Undistorted structural analysis of soluble proteins by attenuated total reflectance infrared spectroscopy. Protein Sci., **14:** 2781-2792.

Gordon, M., (2010). *Postgraduate Haematology*. Wiley-Blackwell, 6th edition, Chapter 1, 1-12.

Gorgulu, S.T., Doğan M., and Severcan, F., (2007). The Characterization and Differentiation of Higher Plants by Fourier Transform Infrared Spectroscopy. Appl. Spect., **61:** 300-308.

Gorgulu, S.T., (2009). Molecular investigation of PTZ-induced epileptic activites in rat brain cell membranes and the effects of vigabantin. PhD Thesis, Middle East Technical University.

Greco, SJ., and Rameshwar, P., (2008). Microenvironmental considerations in the application of human mesenchymal stem cells in regenerative therapies. Biologics., **2:** 699-705.

Haris, P.I., and Severcan, F., (1999). FTIR spectroscopic characterization of protein structure in aqueous and non-aqueous media. J. Mol. Catal. B: Enzymatic, **7:** 207-221.

Hastings, G., Wang, R., Krug, P., Katz, D., and Hilliard, J., (2008). Infrared Microscopy for the Study of Biological Cell Monolayers. Spectral Effects of Acetone and Formalin Fixation. Biopolymers, **89:** 921-930.

Haynesworth, S.E., Baber, M.A., and Caplan, A.I., (1996). Cytokine expression by human marrow-derived mesenchymal progenitor cells in vitro: effects of dexamethasone and IL-1 alpha. J. Cell. Physiol., **166:** 585-592.

Horwitz, E.M., Le Blanc, K., Dominici, M., Mueller, I., Slaper-Cortenbach, I., Marini, F.C., Deans, R.J., Krause, D.S., Keating, A., (2005). Clarification of the nomenclature for MSC: The International Society for Cellular Therapy position Statement. Cytotherapy **7:** 393-395.

Hsu S.C.P., (1997). *Handbook of Instrumental Techniques for Analytical Chemistry*. Mallinckrodt, Inc. Mallinckrodt Baker Division, pp. 247-283.

Huang, K., Zhou, D.H., Huang, S.L., and Liang S.H., (2005). Age-related biological characteristics of human mesenchymal stem cells from different age donors. J. Exp. Hematol., **13**: 1049-1053.

Ishii, K., Kimura, A., Kushibiki T., and Awazu K., (2007). Fourier transform infrared spectroscopic analysis of cell differentiation. Opt. in Tissue Eng. and Reg. Med. 6439.

Jackson, L., Jones, D.R., Scotting, P., and Sottile, V., (2007). Adult mesenchymal stem cells: differentiation potential and therapeutic applications. J. Postgrad. Med., **53:** 121-127.

Jackson. M., Ramjiawan, B., Hewko, M., and Mantsch, H.H., (1998). Infrared microscopic functional group mapping and spectral clustering analysis of hypercholesterolemic rabbit liver. Cell Mol. Biol., **44:** 89-98.

Jing, D., Fonseca, A.V., Alakel, N., Fierro, F.A., Muller, K., Bornhauser, M., Ehninger, G., Corbeil, D., and Ordemann, R., (2010). Hematopoietic stem cells in co-culture with mesenchymal stromal cells - modeling the niche compartments in vitro. Haematologica, **95:** 542-550.

Kaplan, R.N., Psaila B., and Lyden, D., (2006). Niche-to-niche migration of bone marrow-derived cells. Trends Mol. Med. **13:** 72-81.

Kasayama S, M Koga, H Kouhara. (1994). Unsaturated fatty acids are required for continuous proliferation of transformed androgen-dependent cells by fibroblast growth factor family proteins. Cancer Res 54:6441-6445.

Kazarian, S.G., and Chan, K.L.A., (2006). Applications of ATR-FTIR spectroscopic imaging to biomedical samples. Biochimica et Biophysica Acta, **1758:** 858-867.

Kelly, E.B., (2007). *Stem Cells*, Green Wood Press, Wesport, Connecticut, London.

Kemp, K.C, Hows, J, and Donaldson, C., (2005). Bone marrow-derived mesenchymal stem cells. Leuk Lymphoma. **46:** 1531-44.

Khandros**,** E., and Weiss, M.J., (2010). Protein quality control during erythropoiesis and hemoglobin synthesis. Hemat. Onco. Clinic. North Amer., **24:** 1071-1088.

Khanmohammadi, M., Ansari, M.A., Garmarudi, A.B., Hassanzadeh, G., and Garoosi, G., (2007). Cancer diagnosis by discrimination between normal and malignant human blood samples using attenuated total reflectance-Fourier transform infrared spectroscopy. Cancer Invest., **25:** 397-404.

Kneipp, J., Lasch, P., Baldauf, E., Beekes, M., and Naumann, D., (2000). Detection of pathological molecular alterations in scrapie-infected hamster brain

by fourier transform infrared (FT-IR) spectroscopy. Biochim. Biophys. Acta, **1501:** 189-199.

Kneipp, J., Beekes, M., Lasch P., and Naumann, D., (2002). Molecular changes of preclinical scrapie can be detected by infrared spectroscopy. J. Neurosci., **22:** 2989-2997.

Krebsbach, P.H., Mankani, M.H., Satomura, K., Kuznetsov, S.A., and Robey, P.G., (1998). Repair of craniotomy defects using bone marrow stromal cells. Transplantation, **66:** 1272-1278.

Kretlow, A., Wang, Q., Kneipp, J., Lasch, P., Beekes, M., Miller, L., and Naumann, D., (2006). FTIR-microspectroscopy of prion-infected nervous tissue. Biochim. Biophys. Acta, **1758:** 948-959.

Kretlow, J.D., Jin, Y.Q., Liu, W., Zhang, W.J., Hong, T.H., Zhou, G., Baggett, L.S., Mikos, A.G., Cao, Y., (2008). Donor age and cell passage affects differentiation potential of murine bone marrow-derived stem cells. BMC Cell Biol., **9**: 60.

Kiel, M.J., and Morrison, S.J., (2006). Maintaining hematopoietic stem cells in the vascular niche. Immunity., **25:** 977-988.

Kirschstein, R., (2001). *Stem Cells: Scientific Progress and Future Research Directions*. National Institutes of Health, Department of Health and Human Services.

Kneipp, J., Lasch, P., Baldauf, E., Beekes, M., and Naumann, D., (2000). Detection of pathological molecular alterations in scrapie-infected hamster brain by Fourier transform infrared (FT-IR) spectroscopy. Biochim. Biophys. Acta, **1501:** 189-199.

Koc, O.N., Peters, C., Aubourg, P., Raghavan, S., Dyhouse, S., De Gasperi, R., Kolodny, E.H., Yoseph, Y.B., Gerson, S.L., Lazarus, H.M., Caplan, A.I., Watkins, P.A. and Krivit, W., (1999). Bone marrow-derived mesenchymal stem cells remain host-derived despite successful hematopoietic engraftment after allogeneic transplantation in patients with lysosomal and peroxisomal storage diseases. Exp. Hematol., **27**: 1675-1681.

Koch, T.G., Heerkens, T., Thomsen, P.D., Betts, D.H., (2007). Isolation of mesenchymal stem cells from equine umbilical cord blood. BMC Biotechnol., **30**: 7:26.

Konorov, S.O., Schulze, H.G., Piret, J.M., Aparicio, S.A., Turner, R.F., and Blades, M.W., (2011). Raman microscopy-based cytochemical investigations of potential niche-forming inhomogeneities present in human embryonic stem cell colonies. Appl. Spectr., **65:** 1009-1116.

Krishnakumar, N., Manoharan, S., Palaniappan, P.L., Venkatachalam P., and Manohar, M.G., (2009). Chemopreventive efficacy of piperine in 7,12-dimethyl benzanthracene (DMBA)-induced hamster buccal pouch carcinogenesis: an FT-IR study. Food Chem. Toxicol., **47:** 2813-2820.

Krafft, C., Knetschke, T., Funk, R.H., and Salzer, R., (2006). Studies on stress-induced changes at the subcellular level by Raman microspectroscopic mapping. Anal. Chem., **78:** 4424-4429.

Krafft, C., Salzer, R., Seitz, S., Ern, C., and Schieker, M., (2007). Differentiation of individual human mesenchymal stem cells probed by FTIR microscopic imaging. Analyst, **132:** 647–653.

Lanzkowsky, P., (2000). *Manual of Pediatric Hematology and Oncology*. Third ed., San Diego, Academic Pres, 97-152.

Lazarus, H.M., Koc, O.N., Devine, S.M., Curtin, P., Maziarz, R.T., Holland, H.K., Shpall, E.J., McCarthy, P., Atkinson, K., and Cooper, B.W., (2005). Cotransplantation of HLA-identical sibling culture-expanded mesenchymal stem cells and hematopoietic stem cells in hematologic malignancy patients. Biol. Blood Marrow Transplant., **11:** 389-398.

Lee, S.Y., Yoon, K.A., Jang, S.H., Ganbold, E.O., Uuriintuya, D., Shin, S.M., Ryu, P.D., and Joo, S.W., (2009). Infrared spectroscopy characterization of normal and lung cancer cells originated from epithelium. J. Vet. Sci., **10:** 299-304.

Leitermann, F., Syldatk, C., and Hausmann, R., (2008). Fast quantitative determination of microbial rhamnolipids from cultivation broths by ATR-FTIR Spectroscopy. J. Biol. Eng., **7:** 2-13.

Leskovjan, A.C., Kretlow, A., and Miller, L.M., (2010). Fourier transform infrared imaging showing reduced unsaturated lipid content in the hippocampus of a mouse model of Alzheimer's disease. Anal. Chem., **82:** 2711-2716.

Lester, D.S., Kidder, L.H., Levin, I.W., and Lewis, E.N., (1998). Infrared microspectroscopic imaging of the cerebellum of normal and cytarabine treated rats. Cell Mol. Biol., **44:** 29-38.

Libani, I.V., Guy, E.C., and Melchiori, L., (2008). Decreased differentiation of erythroid cells exacerbates ineffective erythropoiesis in β-thalassemia. Blood, **112:** 875-885.

Li, L., Xie, T., (2005). Stem Cell Niche: Structure and Function, Annu. Rev. Cell Dev. Biol.. **21:** 605-631.

Liquier, J., and Taillandier, E., (1996). *Infrared spectroscopy of nucleic acids, Infrared Spectroscopy of Biomolecules*, Wiley-Liss, Inc., USA, 131-158.

Lithanatudom, P., Leecharoenkiat, A., Wannatung, T., Svasti, S., Fucharoen, S., and Smith, D.R., (2010). A mechanism of ineffective erythropoiesis in Beta-thalassemia/Hb E disease. Haematologica, **95:** 716-723.

Liu, K., Jackson, M., Sowa, M.G., Ju, H., Dixon, I.M.C., and Mantsch, H.H., (1996). Modification of the extracellular matrix following myocardial infarction monitored by FTIR spectroscopy, Biochim. Biophys. Acta, **1315:** 73–77.

Liu, Z.J., Zhuge, Y., and Velazquez, O.C., (2009). Trafficking and differentiation of mesenchymal stem cells. J. Cell Biochem., **106:** 984-991.

Liu, K.Z., Bose, R., and Mantsch, H.H., (2002). Infrared spectroscopic study of diabetic platelets. Vibrational Spectroscopy, **28:** 131-136.

Loukopoulos, D., (1991). Thalassemia: Genotypes and phenotypes. Ann. Hematol., **62:** 85-94.

Lundbaek, J.A., Birn, P., Hansen, A.J., Sogaard, R., Nielsen, C., Girshman, J., Bruno, M.J., Tape, S.E., Egebjerg, J., Greathouse, D.V., Mattice, G.L., Koeppe R.E., and Andersen O.S., (2004). Regulation of sodium channel function by bilayer elasticity: the importance of hydrophobic coupling. Effects of micelle-forming amphiphiles and cholesterol. J. Gen. Physiol., **123:** 599-621.

Mader, S.S., *Inquiry into Life*, (1997). The McGraw-Hill Companies, Inc.

Majumdar, M.K., Thiede, M.A., Mosca, J.D., Moorman, M., and Gerson, S.L., (1998). Phenotypic and functional comparison of cultures of marrow-derived mesenchymal stem cells (MSCs) and stromal cells. J. Cell Physiol., **176:** 57-66.

Majumdar, M.K., Thiede, M.A,. Haynesworth, S.E., Bruder, S.P., and Gerson, S.L., (2000). Human marrow-derived mesenchymal stem cells (MSCs) express hematopoietic cytokines and support long-term hematopoiesis when differentiated toward stromal and osteogenic lineages. J. Hematother. Stem Cell Res., **9:** 841-848.

Mareschi, K., Ferrero, I., Rustichelli, D., Aschero, S., Gammaitoni, L., Aglietta, M., Madon, E., and Fagioli, F., (2006). Expansion of mesenchymal stem cells isolated from pediatric and adult donor bone marrow. J. Cell Biochem., **97:** 744-754.

Manoharan, R., Baraga, J.J., Rava, P.R., Dasari, R.R., Fitzmaurice, M., Feld, M.S., (1993). Biochemical analysis and mapping of atherosclerotic human artery using FT-IR microspectroscopy. Atherosclerosis **103:** 181-193.

Mantsch, H.H., (1984). Biological application of Fourier Transform Infrared Spectroscopy: A study of phase transitions in biomembranes. J. Mol. Struc., **113:** 201-212.

Matthaus, C., Boydston-White, S., Miljkovic, M., Romeo, M.J., and Diem, M., (2006). Raman and infrared microspectral imaging of mitotic cells. Appl Spectr., **60:** 1–8.

Melchiori, L., Gardenghi S., and Rivella, S., (2010). β-Thalassemia: HiJAKing ineffective erythropoiesis and iron overload. Adv. Hemat., Article ID 938640.

Melin, A., Perromat, A., and Deleris, G., (2000). Pharmacologic application of Fourier transform IR spectroscopy: In vivo toxicity of carbon tetrachloride on rat liver. Biopolymers (Biospectroscopy), **57:** 160-168.

Mendelsohn, R., and Mantsch, H.H., (1986). Fourier transform infrared studies of lipid protein interaction. In: Progress in Protein-Lipid Interactions. **2:** 103-147.

Minguell, J.J., Erices, A., and Conget, P., (2001). Mesenchymal stem cells. Exp. Biol. Med., (Maywood) **226:** 507-520.

Mitsiadis, T.A., Barran, O., Rochat, A., Barrandon, Y., and De Bari, C., (2007). Stem cell niches in mammals. Exp. Cell Res., **313:** 3377-3385.

Moerman, E.J., Teng., K, and Lipschitz, D.A., (2004). Aging activates adipogenic and suppresses osteogenic programs in mesenchymal marrow stroma/stem cells:

the role of PPAR-γ2 transcription factor and TGF-β/BMP signaling pathways. Aging Cell, **3:** 379-389.

Mohsin, S., Shams, S., Khan, M., Javaid, A.S., Khan, S.N., and Riazuddin, S., (2011). Enhanced hepatic differentiation of mesenchymal stem cells after pretreatment with injured liver tissue. Differentiation, **81:** 42-48

Moody, B., Haslauer, C.M., Kirk, E., Kannan, A., Loboa, E.G., and McCarty, G.S., (2010). In situ monitoring of adipogenesis with human-adipose-derived stem cells using surface-enhanced Raman spectroscopy. Appl Spectr. **64:** 1227-1233.

Moore, D.J., Sills, R.H., and Mendelsohn R., (1997). Conformational order of specific phospholipids in human erythrocytes: correlations with changes in cell shape. Biochemistry, **36:** 660-664.

Olivieri, N.F., (1999). The β thalassemias. N. Engl. J. Med.**341:**99-109.

Ozek, N.S., Sara, Y., Onur, R., and Severcan, F., (2009). Low dose simvastatin induces compositional structural and dynamical changes in rat skeletal extensor digitorum longus muscle tissue. Biosci. Rep., **30:** 41-50.

Ozek, N.S., Tuna, S., Erson-Bensan, A.E., Severcan, F., (2010). Characterization of microRNA-125b expression in MCF7 breast cancer cells by ATR-FTIR spectroscopy. Analyst, **135**: 3094-3102.

Panno J., (2005). *Stem Cell Research: Medical Applications and Ethical Controversy*.

Parker F.S., (1971). Application of Infrared Spectroscopy in Biochemistry, Biology and Medicine. Plenum Press, New York.

Peak D., (2004), *Fourier transform tnfrared spectroscopy.* Elsevier.

Perkin Elmer Life and Analytical Sciences, (2005). FT-IR Spectroscopy-Attenuated Total Reflectance (ATR).

Perkins A.C., (1998). Enrichment of blood from embryonic stem cells in vitro. Reprod. Fertil. Dev., **10:** 563-572.

Peuchant, E., Richard-Harston, S., Bourdel-Marchasson, I., Dartigues, J.F., Letenneur, L., Barberger-Gateau P., Arnaud-Dabernat, S., and Danie, J.Y.,

(2008). Infrared spectroscopy: a reagent-free method to distinguish Alzheimer's disease patients from normal-aging subjects. Transl. Res., **152:** 103-112.

Pijanka, J.K., Kumar, D., Dale, T., Yousef, I., Parkes, G., Untereiner, V., Yang, Y., Dumas, P., Collins, D., Manfait, M., Sockalingum, G.D., Forsyth N.R., and Suso, J.S., (2010). Vibrational spectroscopy differentiates between multipotent and pluripotent stem cells, Analyst, **135:** 3126-3132.

Pittenger, M.F., Mackay, A.M., Beck, S.C., Jaiswal, R.K., Douglas, R., Mosca, J.D., Moorman M.A., Simonetti, D.W., Craig, S, and Marshak, D.R., (1999). Multilineage potential of adult human mesenchymal stem cells. Science **284:** 143-147.

Ponticiello, M.S., Schinagl, R.M., Kadiyala, S., and Barry, F.P., (2000). Gelatin-based resorbable sponge as a carrier matrix for human mesenchymal stem cells in cartilage regeneration therapy. J. Biomed.l Mat. Res., **52:** 246–255.

Purton L.E., and Scadden, D.T., (2011). *The hematopoietic stem cell niche, Stem Book*, Harward Stem Cell Institute.

Ramirez, J.M., Schaad, O., Durual, S., Cossali, D., Docquier, M., Beris, P., Descombes P., and Matthes, T., (2009). Growth differentiation factor 15 production is necessary for normal erythroid differentiation and is increased in refractory anaemia with ring-sideroblasts. Br J Haematol 144: 251-262.

Rando, T.A., (2006). Stem cells, ageing and the quest for immortality. Nature, **441:** 1080-1086.

Richter, T., Steiner, G., Abu-Id, M.H., Salzer, R., Gergmann, R., Rodig, H., and Johannsen, B., (2002). Identification of tumor tissue by FTIR spectroscopy in com-bination with positron emission tomography. Vib. Spectr., **28:** 103-110.

Rigas, B., Morgello, S., Goldman, I.S., and Wong, P.T.T., (1990). Human colorectal cancers display abnormal Fourier transform infrared spectra. Proc Natl Aca Sci USA, **87:** 8140-8144.

Rieger, K., Marinets, O., Fietz, T., Körper, S., Sommer, D., Mücke, C., Reufi, B., Blau, W.I., Thiel, E., and Knauf, W.U., (2005). Mesenchymal stem cells remain of host origin even a long time after allogeneic peripheral blood stem cell or bone marrow transplantation. Exp. Hematol. **33:** 605-611.

Romeo, M.J., B. Mohlenhoff, and M. Diem, (2006). Infrared micro-spectroscopy of human cells: Causes for the spectral variance of oral mucosa (buccal) cells, Vib. Spectr., **42:** 9-14.

Romeo M.J., Boydston-White S., Matthaues C., Milkovic M., Bird B., Chernenko T., Lash P., nd Diem M., (2008). *Infrared and Raman Microscopic Studies of Individual Human Cells.*

Roura S, Farré J, Soler-Botija C, Llach A, Hove-Madsen L, Cairó JJ, Gòdia F, Cinca J, Bayes-Genis A., (2006). Effect of aging on the pluripotential capacity of human CD105+ mesenchymal stem cells., Eur. J. Heart Fail., **8**: 555-563.

Orlic D., Bock, T.A., and Kanz, L., (1999). Hematopoietic stem cells biology and transplantation. Annals of The New York Academy of Sciences (New York, NY).

Quarto, R., Mastrogiacomo, M., Cancedda, R., Kutepov, S.M., Mukhachev, V., Lavroukov, A., Kon, E., and Marcacci, M., (2001). Repair of large bone defects with the use of autologous bone marrow stromal cells. The New England Journal of Medicine, **344:** 385–386.

Sahu, R.K., Argov, S., Salman, A., Huleihel, M., Grossman, N., and Hammody, Z., (2004). Characteristic absorbance of nucleic acids in the Mid-IR region as possible common biomarkers for diagnosis of malignancy. Tech. Cancer Res. Treat., **3:** 629-638.

Sahu, R.K, Zelig U., Huleihel, M., Brosh, N., Talyshinsky, M., Ben-Harosh, M., Mordechai S., and Kapelushnik, J., (2006). Continuous monitoring of WBC (biochemistry) in an adult leukemia patient using advanced FTIR-spectroscopy. Leuk. Res., **30:** 687-693.

Schrier, S.L., (2002). Pathophysiology of thalassemia. Curr. Opin. Hematol., **9:** 123-126.

Schultz, C.P., Liu, K.Z., Kerr, P.D., and Mantsch, H.H., (1998). In situ infrared histopathology of keratinization in human oral/oropharyngeal squamous cell carcinoma, Oncol. Res., **10:** 277-286.

Scutt, A., Kollenkirchen, U., and Bertram, P., (1996). Effect of age and overiectomy on fibroblastic colony-forming unit numbers in rat bone marrow. Calcif. Tissue Int., **59**: 309-310.

Severcan, F., (1997). Vitamin E decreases the order of the phospholipid model membranes in the gel phase: An FTIR study. Biosci. Reports, **17:** 231-235.

Severcan, F., and Haris, P.I., (1999). FTIR spectroscopic characterization of protein structure in aqueous and non-aqueous media. J. Mol. Cat. B. Enzy., **7:** 207-221.

Severcan, F., Toyran, N., Kaptan, N., and Turan, B., (2000). Foruier transform infrared study of the effect of diabetes on rat liver and heart tissues in the C-H region, Talanta, **53:** 55-59.

Severcan, F., Kaptan, N., and Turan, B., (2003). Fourier transform infrared spectroscopic studies of diabetic rat heart crude membranes, Spectroscopy, **17:** 569–577.

Severcan, M., Severcan, F., and Haris, I.P., (2004). Using artificially generated spectral data to improve protein secondary structure prediction from FTIR spectra of proteins, Anal. Biochem. **332:** 238-244.

Severcan, F., Gorgulu, G., Gorgulu, S.T., and Guray, T., (2005). Rapid monitoring of diabetes induced lipid peroxidation by Fourier transform infrared spectroscopy: Evidence from rat liver microsomal membranes, Anal. Biochem., **339**: 36–40.

Severcan F, O Bozkurt, R Gurbanov and G Gorgulu. (2010). FT-IR spectroscopy in diagnosis of diabetes in rat animal model. J Biophotonics **3**: 621–631.

Shamblott, M.J., Axelman, J., Wang, S., Bugg, E.M., Littlefield, J.W., Donovan, P.J., Blumenthal P.D., Huggins, G.R., Gearhart, J.D., Proc. Natl. Acad. Sci., **95**: 13726-13731.

Spector A.A., and Yorek, M.A., (1985). Membrane lipid composition and cellular function. J. Lipid Res., **26**: 1015-1035.

Steele, D., (1971). *The Interpretation of Vibrational Spectra*, William Clowes and Sons Lim., Great Britain.

Steiner, G., Shaw, A., Choo-Smith, L.P., Abuid, M.H., Schackert, G., Sobottka, S., Steller, W., Salzer R., and Mantsch H.H., (2003). Distinguishing and grading human gliomas by IR spectroscopy. Biopolymers, **72**: 464-471.

Stenderup, K., Justesen, J., Claudsen, C., (2003). Aging is associated with decreased maximal life span and accelerated senescence of bone marrow stromal cells. Bone, **33**: 919-926.

Stolzing, A., Scutt, A., (2006). Age-related impairment of mesenchymal progenitor cell function. Aging Cell, **5**: 213-224.

Stuart, B., (1997). *Biological Applications of Infrared Spectroscopy*. John Wiley and Sons, Ltd., England.

Szczerbowska-Boruchowska, M., Dumas, P., Kastyak, M.Z., Chwiej, J., Lankosz, M., Adamek, D., Krygowska-Wajs, A., (2007). Biomolecular investigation of human substantia nigra in Parkinson's disease by synchrotron radiation Fourier transform infrared microspectroscopy, Archives of Biochemistry and Biophysics, **459**: 241-248.

Tabbara, I. A., Zimmerman, K., Morgan, C., and Nahleh, Z., (2002). Allogeneic hematopoietic stem cell transplantation: complications and results. Archives of Internal Medicine, **162**: 1558-1566.

Taillandier, E., and Liquier, J., (1999). Infrared spectroscopy of DNA. Methods Enzymol., **211**: 307-335.

Takahashi, H., French, S.M., and Wong, P.T.T., (1991). Alterations in hepatic lipids and proteins by Chronic ethanol Intake: A highpressure fourier transform Infrared spectroscopic study on alcoholic liver disease in the rat alcohol. Clin. Exp. Res., **15**: 219-223.

Tanno, T., Noel, P., and Miller, J.L., (2010). Growth differentiation factor 15 in erythroid health and disease. Curr Opin Hematol **17**: 184-90.

Tanthanuch, W., Thumanu, K., Lorthongpanich, C., Parnphi R., and Heraud P., (2010). Neural differentiation of mouse embryonic stem cells studied by FTIR spectroscopy. J. Mol. Structr., **967**: 189-195.

Thalmeier., K, Meissner., P, Reisbach, G, Hültner, L., Mortensen, B.T., Brechtel, A., Oostendorp, R.A., and Dörmer, P., (1996). Constitutive and modulated cytokine expression in two permanent human bone marrow stromal cell lines. Exp. Hematol., **24**: 1-10.

Thumanu, K., Tanthanuch, W., Ye, D., Sangmalee, A., Lorthongpanich, C., Parnpai, R., and Heraud, P., (2011). Spectroscopic signature of mouse embryonic

stem cell-derived hepatocytes using synchrotron Fourier transform infrared microspectroscopy, J.Biomed.Opt., **16**: 057005.

Timlin, J.A., Laura, E.M., Lyons, C.R., Hjelle, B., and Alam, M.K., (2009). Dynamics of cellular activation as revealed by attenuated total reflectance infrared spectroscopy. Vibr. Spect., **50:** 78–85.

Titushkin, I., and Cho, M., (2006). Distinct membrane mechanical properties of human mesenchymal stem cells determined using laser optical tweezers. Biophys. J., **90:** 2582–2591.

Tokalov, S.V., Grüner, S., and Schindler, S., (2007). Age-related changes in the frequency of mesenchymal stem cells in the bone marrow of rats. Stem Cells Dev., **16:** 439-446.

Toyran, N., and Severcan, F., (2003). Competitive effect of vitamin D2 and Ca_2^+ on phospholipids model membranes: An FTIR study, Chem. Phys. Lipids, **123:** 165-176.

Toyran, N., Zorlu, F., Donmez, G., Oge, K., Severcan, F., (2004). Chronic hypoperfusion alters the content and structure of proteins and lipids of rat brain homogenates: a Fourier Transform Infrared Spectroscopic study, Eur. Biophy. J. , **33:** 549-554.

Trombetta, D., Gangemi, S., Saija A., Minciullo, P.L., Cimino, F., Cristani, M., Briuglia, S., Piraino, B., Isola, S., and Salpietro, C.D., (2006). Increased protein carbonyl groups in the serum of patients affected by thalassemia major. Ann. Hematol. **85:** 520–522.

Tsavachidou, D., Li, Y., Guo, H., Liu, W., Jonasch, E., Tamboli, P., and Mills, G.B., (2010). Glycogen metabolism provides nutritional support to renal cancer cells under conditions of stress and may serve as a marker of response to antiangiogenic therapy with bevacizumab. Fourth AACR International Conference on Molecular Diagnostics in Cancer Therapeutic. Denver, CO. Oral Prensentation.

Umemura, J., Cameron, G., and Mantsch, H.H., (2000). A Fourier transform infrared spectroscopic study of the molecular interaction of cholesterol with 1,2-dipalmitoyl-sn-glycero-3-phosphocholine. Biochim. Biophys. Acta, **602:** 32-44.

Vacek, A., (2000). Proliferation activity and number of stromal (CFU-f) and haemopoietic (CFUs) stem cells in bone marrow and spleen of rats of different ages. Acta Vet., **69:** 25-31.

Van de Loosdrecht, A.A., Beelen, R.H., Ossenkoppele, G.J., Broekhoven, M.G., Langenhuijsen, M.M., (1994). A tetrazolium-based colorimetric MTT assay to quantitate human monocyte mediated cytotoxicity against leukemic cells from cell lines and patients with acute myeloid leukemia. J. Immunol. Methods, **174:** 311-320.

Villaron, E.M., Almeida, J., López-Holgado, N., Alcoceba, M., Sánchez-Abarca, L.I., Sanchez-Guijo, F.M., Alberca, M., Pérez-Simon, J.A., San Miguel, J.F., Del Cañizo M.C., (2004). Mesenchymal stem cells are present in peripheral blood and can engraft after allogeneic hematopoietic stem cell transplantation. Haematologica, **89**:1421-1427.

Wagner, W., Roderburg, C., Wein, F., Diehlmann, A., Frankhauser, M., Schubert, R., (2007). Molecular and secretory profiles of human mesenchymal stromal cells and their abilities to maintain primitive hematopoietic progenitors. Stem Cells, **25:** 2638-2647.

Wagner, W., Horn, P., Bork, S., Ho, A.D., (2008). Aging of hematopoietic stem cells is regulated by the stem cell niche. Exp. Gerontol., **43**: 974-980.

Wagner, W., Bork, S., Lepperdinger, G., Joussen, S., Ma, N., Strunk, D., Koch, C., (2010). How to track cellular aging of mesenchymal stromal cells? Aging (Albany NY), **2:** 224-230.

Walkley, C.R., (2011). Erythropoiesis, anemia and the bone marrow microenvironment. Int. J. Hematol., **93**:10-13.

Wang, J., Chi, C., Lin, S., and Chern, Y., (1997). Conformational changes in gastric carcinoma cell membrane protein correlated to cell viability after treatment with adamantyl maleimide, Anticancer Research, **17:** 3473-3478.

Whitman, M., (1998). Smads and early developmental signaling by the TGF beta superfamily. Genes Dev., **12:** 2445-2462.

Wilson, A., Shehadeh, L.A., Yu, H., Webster, K.A., (2010). Age-related molecular genetic changes of murine bone marrow mesenchymal stem cells. BMC Genomics, **7:** 11:229.

Winder, C.L., Goodacre, R., (2004). Comparison of diffuse-reflectance absorbance and attenuated total reflectance FT-IR for the discrimination of bacteria. Analyst, **129:** 1118-11122.

Wong, P.T.T., Wong, R.K., Caputo, T.A., Godwin, T.A., Rigas, B., (1991). Infrared spectroscopy of exfoliated human cervical cells: Evidence of extensive structural changes during carcinogenesis. Proc. Nati. Acad. Sci., **88:** 10988-10992.

Wood, B.R., Tait, B., and McNaughton, D., (2000). Fourier transform infrared spectroscopy as a tool for detecting early lymphocyte activation: A new approach to histocompatibility matching. Human Immuno, **61:** 1307–1315.

Yan, X., Anlin, L., Xing, Y., Wang, L., Zhao, W., (2010). Recent progress in the differentiation of bone marrow derived mesenchymal stem cells (BMMSCs) to cardiomyocyte- like cells and their clinical application. African J. of Biotech., **9:** 5042-5047.

Yang, Y., Sule-Suso, J., Sockalingum, G.D., Kegelaer, G., Manfait, M., and El Haj, A.J., (2005) Study of tumor cell invasion by Fourier transform infrared micro-spectroscopy. Biopolymers, **78:** 311-317.

Yano, K., Ohoshima, S., Shimmizu, Y., Moriguchi, T., Katayama, H., (1996). Evaluation of glycogen level in human lung carcinoma tissues by an infrared spectroscopic method, Cancer Lett., **110:** 29-34.

Young, R.G., Butler, D.L., Weber, W., Caplan, A.I., Gordon, S.L., and Fink, D.J., (1998). Use of mesenchymal stem cells in a collagen matrix for Achilles tendon repair. J. Orth. Res., **16:** 404-413.

Yu, J., He, H., Tang, C., Zhang, G., Li, Y., Wang, R., Shi, J., and Jin, Y. (2010). Differentiation potential of STRO-1+ dental pulp stem cells changes during cell passaging. BMC Cell Biol., **8:** 11- 32.

Zeng, R., Wang, L.W., Hu Z.B., Guo, W.T., Wei J.S., Lin H., Sun, X., Chen, L.X., Yang L.J., (2011). Differentiation of Human Bone Marrow Mesenchymal Stem Cells into Neuron-like Cells in-vitro. Spine (Phila Pa 1976), **36**: 997-1005.

Zheng , H., Martin, J.A., and Duwayri, Y., (2007). Impact of aging on rat bone marrow-derived stem cell chondrogenesis. J. Gerontol. A Biol. Sci. Med. Sci., **62:** 136-148.

Zhukareva, V., Obrocka, M., Houle, J.D., Fischer, I., and Neuhuber, B., (2010). Secretion profile of human bone marrow stromal cells: Donor variability and response to inflammatory stimuli. Cytokine, **50:** 317-321.

APPENDIX A

CHEMICALS

AlizerinRed Stain	Sigma
Ascorbic acid	Sigma
Beta glycerophosphate	Sigma
Dexamethasone	Sigma
DiMethylSulfoxide	Applichem
Dulbeco's Modified Eagle Medium-Low Glucose	BiochromAG
EPO	R&D Systems
Fetal Bovine Serum	Biochrom AG
Ficoll	Biochrom AG
Formol	Sigma
GDF 15	R&D Systems
IBMX	Sigma
Igepal/isopropanol	Sigma
Indomethacine	Sigma
Insulin	Sigma
L-glutamine	Biochrom AG
Oil Red O	Sigma
Penicillin/Streptomycin	Biochrom AG
Phosphate Buffer Saline	Sigma
Quantichrom Calcium Assay Kit	Bioassay Systems
Thiazolyl Blue Tetrazolium Bromide	Sigma

CURRICULUM VITAE

PERSONEL INFORMATION

Surname, Name: Aksoy, Ceren
Nationality: Turkish (TC)
Date and Place of Birth: 05 November 1979, Ankara
Marital Status: Single
Phone: +90 312 210 51 57
E-mail: cerenaksoyyy@yahoo.com
Foreign Languages: English

EDUCATION

Degree	Institution	Graduation	C.GPA
Ph.D.	METU Biology Dept.	2012	3.21/4
M.Sc.	METU Biology Dept.	2004	3.1/4
B.Sc.	Ankara Univ. Biology Dept.	2000	89/100

WORK EXPERIENCE

Year	Place	Enrollment
2004-2011	Technopark-METU	Project Developer&Manager

AWARDS and SCHOLARSHIPS

The Best Scientific Poster Award "1st International Conference on Stem Cell Research and Applications" to be held between October 7-9, 2011 in Kayseri, Turkey".

Scholarship from Turkish Scientific and Research Council of Turkey during my MSc.

PUBLICATIONS

A) Book Chapters

"Characterization of Stem Cells by Vibrational Spectroscopy" in Application of Vibrational Spectroscopy in Diagnosis and Screening" by Feride Severcan and Parvez I. Haris, IOS Press in 2012.

B) Articles in refereed Journals (SCI)

1. **Aksoy C.,** Guliyev A., Kilic E., Uckan D., Severcan F.; "Bone Marrow Mesenchymal Stem Cells in Patients with Beta Thalassemia Major: Molecular Analyses with Attenuated Total Reflection-Fourier Transform Infrared (ATR-FTIR) Spectroscopy Study As A Novel Method". In press, *Stem Cells and Development*, DOI number: 10.1089/scd.2011.0444.

2. **Aksoy C.,** Severcan F. "Role of Vibrational Spectroscopy in Stem Cell Research". Invited Review Article, submitted for publication. Paper has been accepted for publication by *Spectroscopy–Biomedical Applications*.

3. Gurakan G. C., **Aksoy C.**, Ogel Z. B., Oren N. G.; "Differentiation of Salmonella Typhimurium from Salmonella Enteritidis and other Salmonella serotypes using Random Amplified Polymorphic DNA Analysis". *Poultry Science,* **2008**; 87: 1068-1074.

C) Articles in preperation:

1. **Aksoy C.,** Uckan D., Severcan F. "Characterization of Donor Age Effect in Mesenchymal Stem Cell by ATR-FTIR spectroscopy. (Research Article)

2. **Aksoy C**., Uckan D., Severcan F. "FTIR microspecroscopy as a novel method in characterization of Mesenchymal Stem Cells at healthy and disease states. (Research Article)

D) Poster Presentations in International Meetings:

Aksoy C., Uckan D., Severcan F.; "Investigation of Bone Marrow Mesenchymal Stem Cell Properties in Patients with Beta Thalassemia Major: FTIR Spectroscopy and Imaging Study." "FT-IR Spectroscopy in Microbiological and Medical Diagnostics", Robert Koch-Institute, October 20-21, 2011 in Berlin, Germany.

Aksoy C., Guliyev A., Kilic E., Uckan D., Severcan F.; "Investigation of Bone Marrow Mesenchymal Stem Cell Properties in Patients with Beta Thalassemia

Major: Attenuated Total Reflection-Fourier Transform Infrared (ATR-FTIR) Spectroscopy Study".

Presented at;

"1st Annual Congress on Stem Cell Research", September 28-October 2 in Kocaeli, Turkey.

and

"1st International Conference on Stem Cell Research and Applications" October 7-9, 2011 in Kayseri, Turkey" (Best Scientific Poster Award).

Aksoy C., Uckan D., Severcan F.; "Investigation of Donor Age Effect on Healthy Human Bone Marrow Mesenchymal Stem Cells".
"1st International Conference on Stem Cell Research and Applications" October 7-9, 2011 in Kayseri, Turkey.

E) Poster Presentations in National Meetings:

Aksoy C., Guliyev A., Kilic E., Uckan D., Severcan F.; "Beta Talasemi Major Hastalığında Kemik İliği Mezenkimal Kök Hücrelerinin ATR-FTIR (Attenuated Total Reflectance- Fourier Dönüşüm Kızıl Ötesi) Spektroskopisi Yöntemi ile Moleküler Seviyede İncelenmesi. 23. Ulusal Biyofizik Kongresi, 13-16 Eylül 2011, Edirne, Türkiye.

Aksoy C., Severcan F., Uckan D. "Investigation of Donor Age Effect on Healthy Human Bone Marrow Mesenchymal Stem Cells". ODTÜ Biyolojik Bilimler Bölümü Araştırma Günü, 2011, ODTÜ-Ankara, Türkiye.

Aksoy C., Severcan F., Uckan D.; "Biomedical Applications of FTIR Spectroscopy on Human Mesenchymal Stem Cells", The 5th Nanoscience and Nanotechnology Conference (NanoTR5) , June 08-12 2009, Eskişehir, Turkiye.

Aksoy C., Severcan F., Çetinkaya Uçkan D., "Insan Mezenkimal Kök Hücrelerinde Donor Yaşının Etkilerinin Moleküler Düzeyde FTIR-Spektroskopisi Yöntemi ile Saptanması", 20. Ulusal Biyofizik Kongresi, 2008, Mersin, Türkiye.

Aksoy C., Ögel Z.B., Gürakan G.C., "Salmonella typhimurium için Serotip Spesifik DNA İşaretleyicisinin RAPD-PCR Metodu ile Tanısı". "XIV. Biyoteknoloji Kongresi, 2005 Eskişehir, Türkiye.

PROJECTS

- "Investigation of Donor Age Effect on Healthy Human Bone Marrow Mesenchymal Stem Cells at Molecular Level by FTIR Spectroscopy" (ODTU-BAP Project Funds).

- *Project Preparation and Management:*: "Interactive Educational Material for Pediatric Bone Marrow Transplantation Nurses" (EC-Leonardo da Vinci Project Programme, 503223-LLP-1-2009-1-TR-Leonardo-LMP).
- *Project Preparation and Management:* "A Guardian Angel for Extended Home Environment" (2008 ITEA2 Project Programme, ITEA2 08018).

- *Project Preparation:* "Improvement of the Scientific and Technological Research Capacity of "Pediatric Stem Cell Research, Development, Cellular therapy and Continuous Training Centre (PEDI-STEM)"" (FP7-REGPOT-2008-1 Project Programme)

- *Project Preparation and Management:* "E-Training of Medical Staff to Reach Adolescents of Different Cultures" (EC-Leonardo da Vinci Project Programme, 2006-TR/06/B/F/PP/178010).

- *Project Preparation:* "Early Identification of Alzhemier Disease by Multi-Mode Optical Imaging Systems"2534 programme code, 2+2 Turkey-Germany International Cooperation Project Programme. Project was accepted in first evaluation step.